REAL TIME LI-ION BATTERY BANK PARAMETERS ESTIMATION FOR ELECTRIC VEHICLE TRACTION SYSTEM

by

Hafiz Muhammad Usman Butt

A Thesis presented to the Faculty of the
American University of Sharjah
College of Engineering
In Partial Fulfillment
of the Requirements
for the Degree of

Master of Science in
Electrical Engineering

Sharjah, United Arab Emirates

May 2019

Approval Signatures

We, the undersigned, approve the Master's Thesis of Hafiz Muhammad Usman Butt

Thesis Title: Real Time Li-ion Battery Bank Parameters Estimation for Electric Vehicle Traction System

Signature	**Date of Signature** (dd/mm/yyyy)
_____	_____
Dr. Shayok Mukhopadhyay Assistant Professor, Department of Electrical Engineering Thesis Advisor	
_____	_____
Dr. Habibur Rehman Associate Professor, Department of Electrical Engineering Thesis Co-Advisor	
_____	_____
Dr. Rached Bin H'mida Dhaouadi Professor, Department of Electrical Engineering Thesis Committee Member	
_____	_____
Dr. Mohammad Jaradat Associate Professor, Department of Mechanical Engineering Thesis Committee Member	
_____	_____
Dr. Nasser Qaddoumi Head, Department of Electrical Engineering	
_____	_____
Dr. Lotfi Romdhane Associate Dean for Graduate Affairs and Research College of Engineering	
_____	_____
Dr. Naif Darwish Acting Dean, College of Engineering	
_____	_____
Dr. Mohamed El-Tarhuni Vice Provost for Graduate Studies	

Acknowledgement

First of all, I am highly thankful to Allah almighty for the countless blessings and strengthening me to complete this research work at a level that I did not expect. I am also forever indebted to my family members who have always supported and encouraged me.

I would like to express my sincere regards and heartfelt gratitude to my esteemed mentors Dr. Shayok Mukhopdhyay and Dr. Habibur Rehman for their continued support, constructive feedback, and valuable suggestions throughout the period of my research work at AUS. I would also like to express my wholehearted thanks to Dr. Nasser Qaddoumi and the Department of Electrical Engineering at the American University of Sharjah for providing me graduate assistantship during my master's studies.

A sincere thanks to my committee members Dr. Rached Dhaouadi and Dr. Mohammad A. Jaradat for sparing their time to provide me feedback on my thesis. Finally, I would also like to thank my friends with whom I shared exceptional moments at AUS.

Dedication

This work is dedicated to my family…

Abstract

This work focuses on accurate and efficient real-time estimation of Li-ion battery model parameters for electric vehicle (EV) traction systems. The contributions made by this thesis are: accurate estimation of Li-ion battery parameters using a two-stage adaptive optimization strategy, which minimizes the need of offline processing, and enables efficient real-time estimation of Li-ion battery model parameters for EV traction systems. In the first part of this thesis, a two-stage universal adaptive stabilizer (UAS) based optimization technique is proposed for estimation of Li-ion battery model parameters. The first stage utilizes a UAS based APE technique to acquire an initial estimate of battery parameters. The second stage utilizes one of the three different optimization techniques, i.e., *fmincon*, particle swarm optimization (PSO), and hybrid PSO to improve the accuracy of battery model parameters obtained by the APE. The parameters estimated by the APE help in reducing the search space interval required by the optimization technique, thus reducing the computation time for the optimization process. This thesis presents detailed comparison of experimental results using the proposed approach, and other well-known optimization techniques from the literature. In the second part of this thesis, a modification to the existing UAS based APE strategy is proposed. The existing UAS based APE strategy requires a small amount of prior offline experimentation and some post-processing to determine some of the battery parameters. However, the proposed modified APE strategy estimates all battery parameters in a single experimental run. Mathematical proofs, simulation and experimental results supporting the proposed modified APE strategy are also presented. In the third part of this thesis, the modified APE strategy is employed for real-time parameters estimation of a 400 V, 6.6 Ah Li-ion battery bank, which supplies power to a field-oriented control based EV drive system. Some of the distinct features of the modified APE strategy, such as simple real-time implementation, fast convergence, and minimal experimental effort, show the effectiveness of the modified APE strategy developed in this work for real-time Li-ion battery model parameters estimation of EV traction systems.

Keywords: ***Adaptive parameters estimation; Li-ion battery; particle swarm optimization; universal adaptive stabilizer.***

Table of Contents

List of Figures

List of Tables

Chapter 1. Introduction and Literature Review

Li-ion batteries have gained global attention, compared to other batteries, due to their appealing features, such as high energy density, portability, low self-discharge, and extended life cycle. Due to the above-mentioned characteristics of Li-ion batteries, they have become the premium candidate for electric vehicles (EVs), aerospace, portable electronics, renewable energy storage, biomedical applications etc.

Different types of Li-ion batteries are being used in several applications. The fundamental difference among various Li-ion batteries is the material of electrodes. Li-ion batteries with high specific energy are often employed for long runtime applications. Whereas, the Li-ion batteries of high specific power are used to supply high power loads. Lithium Cobalt Oxide ($LiCoO_2$), Lithium Nickel Manganese Cobalt Oxide ($LiNiMnCoO_2$ or NMC), and Lithium Nickel Cobalt Aluminum Oxide ($LiNiCoAlO_2$) are the kind of Li-ion batteries which have high specific energy, and, therefore, these are used in portable electronics and medical devices. However, these types of Li-ion batteries are expensive, have shorter lifespan, exhibit lower specific power, and less safe compared to Lithium Manganese Oxide ($LiMn_2O_4$), Lithium Iron Phosphate ($LiFePO_4$), and Lithium Titanate ($Li_4Ti_5O_{12}$) batteries, which are widely used for high power loads [1]. Li-ion batteries outperform nickel-cadmium, lead-acid, and nickel-metal hydride batteries due to higher energy density, lighter weight, and comparatively lesser physical volume. Scientists are modifying the existing Li-ion battery technologies and focusing on developing new chemistry to enhance the performance of Li-ion batteries. Some of the important aspects of advanced research on Li-ion batteries include adaptive parameters estimation [2, 3], battery management system [4], state-of-charge (SoC) estimation [5], and detection of terminal voltage collapse [6].

1.1. Literature Review

Accurate state of charge (SoC) estimation is critical for battery energy management and protection. SoC plays a vital role in assessing remaining battery lifetime, protection against overcharging and accidental over-discharging, fault detection and for a safe and reliable operation of a Li-ion battery [2]. SoC of a battery cannot be mea-

sured directly but needs to be estimated through online or offline methods. Some SoC estimation strategies include chemical methods where specific gravity or battery electrolyte pH is translated to SoC. In the voltage method, the open circuit voltage vs SoC curve is used to estimate the SoC. In the Coulomb counting method a simple integration of the battery current provides a measure of battery SoC. The shortcomings of voltage and Coulomb counting methods can be overcome by Kalman filtering. Adaptive nonlinear observer based SoC estimation is presented in [7]. Different algorithms for SoC estimation are reviewed in [8].

A comprehensive review of existing SoC estimation methods for electric vehicle applications is presented in [5]. The 'big cell' concept, which considers multiple series or parallel connected batteries as a big cell, is also reviewed in [5]. For accurate estimation of SoC, a neural network-based approach is employed in [9] to adaptively adjust the switching gain of a sliding-mode observer. This strategy also requires the parameters of a Li-ion battery circuit model, which are identified through an online recursive least squares approach. The online parameters identification and learning capability of a neural network provides robustness to the sliding-mode observer against battery nonlinearities. The technique to improve the accuracy of SoC using an adaptive extended Kalman filter is reported in [10]. Instead of using a conventional battery circuit model, the authors in [10] split the battery model into two sub models, i.e. separate SoC and RC voltage sub models.

As stated in [3], "Precise estimation of a battery SoC requires an accurate battery model. Electro-chemical [11] and mathematical models [12] of a battery are complex and can be computationally expensive. The battery model in [13] presents an equivalent circuit model of a battery which provides real time voltage, current dynamics, and all other essential dynamic characteristics. The battery model in [13] is utilized in this work because this model captures the effect of variation of SoC on the battery model parameters. Also as mentioned in [2], the model from [13] can incorporate effects of temperature, and number of charge-discharge cycles. Therefore, it is simple enough for easy implementation in control oriented purposes, yet it is detailed enough to capture essential dynamic characteristics. However, the method suggested in [13] requires a lot of experimental effort to acquire battery model parameters." Our earlier

work [2] proposed an adaptive methodology for the parameters estimation of the model suggested in [13], which reduces experimental effort compared to strategies available in the literature.

A recently developed sensitivity-based group-wise Li-ion battery parameters estimation strategy is reported in [14]. The term sensitivity of a parameter quantifies the significance of a parameter on the output of a Li-ion battery model. In [14], the parameters having similar sensitivities are identified and grouped together using sensitivity analysis and are then identified by using the Levenberg-Marquardt algorithm. The author in [15] proposes a generic approach to estimate the Li-ion battery model parameters by utilizing Particle Swarm Optimization (PSO) strategy. The algorithm for the Li-ion battery parameters estimation using a Butterworth filter is outlined in [16]. The estimation of SoC and temperature dependent parameters of a Li-ion battery by Gauss-Newton and PSO techniques is studied in [17]. Battery model parameters are obtained experimentally via discharge data interpolation in [18]. A multi-objective optimization strategy to estimate equivalent circuit model battery parameters is analyzed in [19]. Non-linear least squares based battery parameters identification is reported in [20]. Genetic algorithm (GA) based optimization is used in [21] for battery parameters identification. Co-evolutionary particle swarm optimization PSO has been developed in [22] for optimum battery model parameters estimation. In [22], each battery parameter is optimized separately and the acquired optimized battery parameters are utilized in sequence to get the optimal solution for rest of the parameters. The PSO strategy is used in [23] to estimate an electrochemical Li-ion battery model's parameters. A study on convergence and stability analysis of the PSO algorithm is reported in [24]. Extended Levenberg-Marquart based optimization is used [25] to estimate Li-ion electrical circuit model parameters.

An online estimation of internal series resistance of a Li-ion battery is utilized as State-of-Health indicator for electric vehicle battery operation in [26]. A simple dynamical model of Li-ion battery, based on voltage and current, is derived using a black box identification method. Using this dynamical model, a 10 seconds battery discharge test is performed for an online estimation of internal series resistance of a Li-ion battery. Recently, dual unscented Kalman filter and H_∞ Kalman filter based

approaches are proposed in [27] and [28], respectively, to overcome the limitations of Kalman Filter (KF) and Extended Kalman Filters (EKF) for accurate estimation of battery SoC. The strategies presented in [27], and [28] simultaneously identify both the battery model circuit elements and SoC. A fractional calculus theory-based intuitive and highly accurate fractional-order equivalent circuit model of Li-ion battery is presented in [29]. The fractional-order circuit model is capable of modeling many electrochemical aspects of Li-ion battery which are typically ignored by integer-order RC equivalent circuit model of Li-ion battery. The authors in [29] used a modified version of Particle Swarm Optimization algorithm for accurate estimation of equivalent circuit elements and validated their results on various operating conditions of Li-ion battery.

To reduce the complexity and computational cost for online identification of equivalent circuit elements along with SoC co-estimation of Li-ion battery, the author in [30] proposed a moving window based least squares method. The technique presented in [30] utilizes the piece-wise linear approximations of the open circuit voltage curve. The authors in [31] attempt to identify the equivalent circuit elements of a Li-ion battery model by means of voltage relaxation characteristics. Although the strategy described in [31] requires several pulse discharge and pulse charge experiments, it extracts the equivalent circuit elements with good accuracy. Two extended Kalman filters are combined, i.e., named as dual EKFs, in [32] for the simultaneous estimation of Li-ion battery parameters and SoC. However, to overcome the issue of high computational cost of dual EKFs, the concept of the dead zone is explained in [32]. The dead zone defines the duration for no adaptive estimation of parameters and SoC while the terminal voltage error stays within the user-designed error boundary.

1.2. Motivation

The strategies presented in the literature review have merits. However, the analyses of shortcomings of these strategies motivated us to utilize the existing high-gain universal adaptive stabilizer (UAS) based adaptive parameters estimation (APE) method [2] to overcome the limitations of existing Li-ion battery parameters and SoC estimation strategies. For example, the data-driven algorithms in [5] are used offline and require intensive computation. Moreover, these algorithms may not ensure convergence with

inappropriate initial parameters selection. The 'big cell' realization in [5] requires battery pack voltage and current for SoC estimation and ignores unavoidable inconsistent characteristics of batteries such as resistance, capacity, and voltage variation. The fast convergence of SoC estimation error in [9] may compromise the accuracy of estimated SoC. The method in [10] requires a prior knowledge of battery model parameters, for onboard SoC estimation in electric vehicles. Because GA is based on heuristics, and convergence for a GA based optimizer in [21] may take a very long time, and still may converge to a local optimum. The results obtained in [22] are accurate but the process is computationally time consuming. The combination of two or more strategies in [14], [17] may produce accurate estimates of Li-ion battery parameters, but this may increase computational time.

Most of the optimization based Li-ion battery parameters estimation approaches are unguided, i.e. the search space, or search interval is selected randomly. The optimization techniques in [15], [17], [22] and [23] may substantially prolong the time required to obtain the solutions. The estimation method in [26] requires an accurate knowledge of SoC and needs to be reiterated for different SoC and temperature values. Usually, model-based KF and EKF methods in [27] and [28], respectively, require prior knowledge of battery parameters via some offline method, which is normally time-consuming and may prone to error. The strategy in [29] requires precise knowledge of open circuit voltage. Moreover, the optimization based strategy in [29] may require high computational effort. In [30], the length of the moving window may affect the overall performance of the system and the accuracy of the equivalent circuit elements estimates. Some possible downsides of the strategy in [31] include offline identification and, like other techniques described earlier, rely on accurate open circuit voltage measurement. In addition, the accuracy of estimated parameters and open circuit voltage is not analyzed in [32].

In contrast to the above mentioned techniques, the APE technique described in [2] has low computational cost, captures dynamic characteristics of a battery, and ensures convergence of battery parameters estimates, yet it works offline, requires accurate and prior knowledge of open circuit voltage and battery parameters estimates. Therefore, the aim of this is the modification of existing APE [2] method for simultane-

ous real-time estimation of battery parameters, open circuit voltage, and battery series resistance, and incorporation of optimization routines for accuracy enhancement of existing APE method, while simultaneously reducing the computational time required as much as possible, compared to purely optimization based techniques.

1.3. Research Contributions

Following are the three primary contributions of this research work.

I. In the first part of this thesis, a two stage strategy for battery model parameters estimation is developed. The APE process is the first stage of the proposed battery parameters estimation technique, this helps in narrowing the search space for an optimizer i.e. the second stage of the proposed technique. This allows the optimization technique to quickly converge as compared to initializing an optimization routine with arbitrary guesses of initial conditions, and arbitrary search intervals. Compared to parameters estimation done by using APE alone, the proposed strategy minimizes the influence of initial guesses of parameters and their upper, lower bounds. This portion of the work provides detailed simulation and experimental results related to charging and discharging of batteries, and also considers three different optimization routines following the adaptive estimation process and provides a comprehensive analysis of battery parameters estimation accuracy, and the computation time required by each approach. The proposed two-stage methodology increases the accuracy of estimated battery model parameters, and battery terminal voltage estimation. It is also shown that the proposed battery model parameters estimation methodology reduces the computation time compared to using purely optimization based methods, and increases accuracy compared to the purely adaptation based method presented in [2].

II. The second contribution of this thesis is the mathematical proof of UAS based adaptive estimation strategy which estimates all equivalent circuit elements, including open circuit voltage and series resistance, of a Li-ion battery model. This mathematical proof is an extension of previous work provided in [2], where open circuit voltage and series resistance parameters were found by the voltage relax-

ation test and curve fitting, respectively. In contrast to [27, 32], the proposed modified APE strategy does not require any prior knowledge of open circuit voltage. Furthermore, this work also provides some simulation results, performed on a 4.1 V, 270 mAh Li-ion battery model, and comprehensive experimental validation on sixteen 22.2 V, 6.6 Ah Li-ion batteries to illustrate the accuracy of the proposed modified APE approach.

III. The last contribution of this thesis includes parameters estimation of a 400 V, 6.6 Ah Li-ion battery bank via modified APE strategy. The 400 V, 6.6 Ah Li-ion battery bank is developed by connecting sixteen 25 V, 6.6 Ah Li-ion batteries in series. The offline verification of estimated parameters on a 400 V battery bank allows us to implement the modified APE strategy for an induction motor driven EV traction system. The EV traction system is controlled by indirect field-orientation strategy and powered by a 400 V, 6.6 Ah Li-ion battery bank. The real-time, accurate, and simultaneous estimation of all equivalent circuit elements of a battery bank, including open circuit voltage and series resistance, in EV traction systems can be utilized for highly desired applications such as precise SoC and state-of-health (SoH) estimation, fault diagnosis and protection, temperature control, and power management.

1.4. Thesis Organization

The organization of this thesis is as follows. A two-stage UAS based optimization strategy for Li-ion battery model parameters estimation is described in Chapter 2. Chapter 3 proposes the modified APE strategy which estimates the open circuit voltage and series resistance along with the other circuit elements in a single adaptation run. Rigorous and comprehensive validation of the modified APE strategy and its real-time implementation are presented in Chapter 4. Concluding remarks and some future possibilities of research are given in Chapter 5.

Chapter 2. Universal Adaptive Stabilizer Based Optimization for Li-ion Battery Model Parameters Estimation

In this chapter, a two-stage strategy based on adaptation and optimization is developed for parameters estimation of a Li-ion battery. The aim of this strategy is to enhance the accuracy of estimated Li-ion battery parameters while consuming relatively less computational effort. The chapter begins with the background section that briefly reviews the formulation of APE strategy followed by the details of PSO algorithm. Section 2.2 describes UAS based optimization methodology for parameters estimation of a Li-ion battery. A comprehensive comparison of simulation and experimental results is provided in sections 2.3 and 2.4, respectively.

2.1. Background

This work utilizes Chen and Mora's equivalent circuit model [13] of the Li-ion battery. Subsection 2.1.1 presents Chen and Mora's equivalent circuit model of a Li-ion battery, which has been verified by rigorous experimentation in [13]. Subsection 2.1.2 presents the UAS based APE technique [2] which is used to obtain estimated values of the Chen and Mora's battery model parameters. Finally, subsection 2.1.3 presents the optimization techniques [33] that are employed to improve the accuracy of the battery model parameters estimated by UAS based APE.

2.1.1. Equivalent circuit model of a Li-ion battery. The equivalent circuit model [13] of a Li-ion battery is shown in Figure 2.1. This equivalent circuit model is easy to simulate [2], [34], [35]. The equivalent circuit parameters of this model are

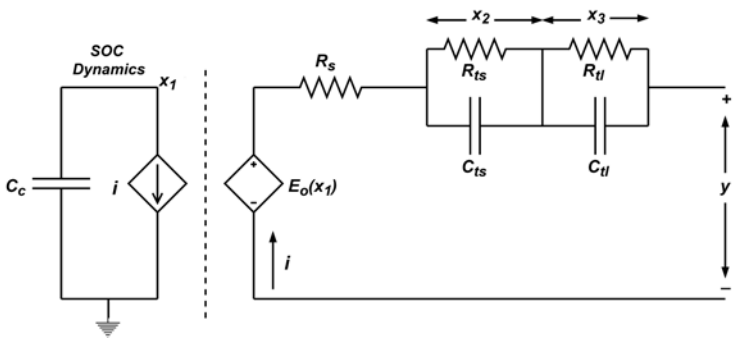

Figure 2.1: Equivalent circuit model used for Li-ion battery.

non-linear functions of battery SoC. In this model, transient response is captured by the RC network as shown in Figure 2.1. A voltage-controlled voltage source models the dependence of the open circuit voltage (OCV) on the battery SoC. The state space equations for Figure 2.1 are described by (1)-(4).

$$\dot{x}_1(t) = -\frac{1}{C_c} i(t), \;\; C_c = 3600 C f_1 f_2 f_3 \tag{1}$$

$$\dot{x}_2(t) = -\frac{x_2(t)}{R_{ts}(x_1(t)) C_{ts}(x_1(t))} + \frac{i(t)}{C_{ts}(x_1(t))} \tag{2}$$

$$\dot{x}_3(t) = -\frac{x_3(t)}{R_{tl}(x_1(t)) C_{tl}(x_1(t))} + \frac{i(t)}{C_{tl}(x_1(t))} \tag{3}$$

$$y(t) = E_o(x_1(t)) - x_2(t) - x_3(t) - i(t) R_s(x_1(t)) \tag{4}$$

State $x_1 \in [0,1]$ denotes battery SoC, x_2 and x_3 represent voltage across $R_{ts} \| C_{ts}$ and $R_{tl} \| C_{tl}$ respectively. Factors f_1, f_2 and f_3 account for temperature effects, charge-discharge cycle and self-discharge respectively which, for simplicity, are taken as 1 in this work. C_c is the Ampere-hour (Ah) capacity of a battery and $y(t)$ denotes battery terminal voltage. The SoC dependent battery equivalent circuit elements of Figure 2.1 are presented by (5)-(10).

$$E_o(x_1(t)) = -p_1 e^{-p_2 x_1(t)} + p_3 + p_4 x_1(t) - p_5 x_1^2(t) + p_6 x_1^3(t) \tag{5}$$

$$R_{ts}(x_1(t)) = p_7 e^{-p_8 x_1(t)} + p_9 \tag{6}$$

$$R_{tl}(x_1(t)) = p_{10} e^{-p_{11} x_1(t)} + p_{12} \tag{7}$$

$$C_{ts}(x_1(t)) = -p_{13} e^{-p_{14} x_1(t)} + p_{15} \tag{8}$$

$$C_{tl}(x_1(t)) = -p_{16} e^{-p_{17} x_1(t)} + p_{18} \tag{9}$$

$$R_s(x_1(t)) = p_{19} e^{-p_{20} x_1(t)} + p_{21} \tag{10}$$

Voltage relaxation tests (see [2]) are required to obtain the OCV curve for a battery. After this, curve fitting is used to obtain the parameters $p_1, \ldots, p_6$ in (5). The parameters of (5), for a 4V, 275mAh Li-ion battery obtained via curve fitting in [2] are $p_1 = 1.031, p_2 = 35, p_3 = 3.685, p_4 = 0.2156, p_5 = 0.1178, p_6 = 0.3201$. The

remaining Li-ion battery model parameters described by (6)-(9) are obtained by the APE technique (see [2]). After estimating the battery parameters $p_7, \ldots, p_{18}$ using APE method, the battery series resistance parameters p_{19}, p_{20} and p_{21} can be obtained from the $R_s(x_1(t))$ vs SoC curve using curve fitting as described in [2].

2.1.2. UAS based adaptive parameter estimation. The Mittag-Leffler (ML) function [36] is described by (11). Where $\Gamma(z+1) = z\Gamma(z), z > 0$ is the standard Gamma function. UAS strategies have employed the ML function as a Nussbaum switching function [37] because fast error convergence is observed. A Nussbaum function is a piecewise right continuous function $N(\cdot) : [k^{'}, \infty) \to \mathbb{R}$, $k_0 > k^{'}$, if it satisfies (12) and (13), [38]. The ML function is implemented as a Nussbaum switching function in MATLAB in [39] and an example is illustrated in Figure 2.2.

$$E_\alpha(z) = \sum_{k=0}^{\infty} \frac{z^k}{\Gamma(k\alpha + 1)} \tag{11}$$

$$\sup_{k>k_0} \frac{1}{k-k_0} \int_{k_0}^{k} N(\tau) d\tau = +\infty \tag{12}$$

$$\inf_{k>k_0} \frac{1}{k-k_0} \int_{k_0}^{k} N(\tau) d\tau = -\infty \tag{13}$$

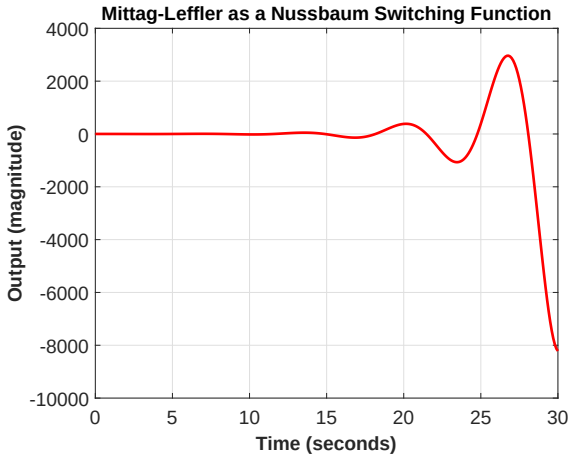

Figure 2.2: Mittag-Leffler function $E_\alpha(-\lambda t^\alpha)$ as a Nussbaum switching function for $\lambda = 1$ and $\alpha = 2.5$.

The ML function $E_\alpha(-\lambda t^\alpha)$ is a Nussbaum function if $\alpha \in (2,3]$ and $\lambda > 0$ [40]. The speed, at which the Nussbaum function increases, controls how rapidly the error between actual and estimated terminal voltage converges. In this work, we select $\lambda = 1$ and $\alpha = 2.5$. The circuit elements, described by (14)-(17), are estimated via the APE method using (19) which estimates the parameters $\widehat{p}_7, \ldots, \widehat{p}_{18}$. Where $\widehat{p}_n > 0$ for $n \in \{7, 8, \ldots, 18\}$. The adaptive equation (19) requires the steady-state upper, lower bounds and their respective confidence levels for each parameter.

$$\widehat{R}_{ts}(\widehat{x}_1(t)) = \widehat{p}_7 e^{-\widehat{p}_8 \widehat{x}_1(t)} + \widehat{p}_9 \tag{14}$$

$$\widehat{R}_{tl}(\widehat{x}_1(t)) = \widehat{p}_{10} e^{-\widehat{p}_{11} \widehat{x}_1(t)} + \widehat{p}_{12} \tag{15}$$

$$\widehat{C}_{ts}(\widehat{x}_1(t)) = -\widehat{p}_{13} e^{-\widehat{p}_{14} \widehat{x}_1(t)} + \widehat{p}_{15} \tag{16}$$

$$\widehat{C}_{tl}(\widehat{x}_1(t)) = -\widehat{p}_{16} e^{-\widehat{p}_{17} \widehat{x}_1(t)} + \widehat{p}_{18} \tag{17}$$

$$\widehat{R}_s(\widehat{x}_1(t)) = \widehat{p}_{19} e^{-\widehat{p}_{20} \widehat{x}_1(t)} + \widehat{p}_{21} \tag{18}$$

$$\dot{\widehat{p}}_n(t) = e^2(t) + \lambda_{x_n}(p_{nu} - \widehat{p}_n(t)) + \lambda_{y_n}(p_{nl} - \widehat{p}_n(t)) \tag{19}$$

The upper and lower bounds of the steady-state value of each parameter in (19) are p_{nu} and p_{nl} respectively; and λ_{xn}, λ_{yn} represent the confidence levels in upper and lower bounds respectively. The upper and lower bounds represent limits on the final steady-state value of the parameters $\widehat{p}_n$. The state space model given by (20)-(23), is a high-gain adaptive estimator used in the APE method. Where $\widehat{x}_1$ is the SoC, and is the same as x_1, $\widehat{x}_2$ and $\widehat{x}_3$ are the estimates of x_2 and x_3, and $\widehat{y}$ is the estimated battery terminal voltage.

$$\dot{\widehat{x}}_1(t) = -\frac{1}{C_c} i(t) \tag{20}$$

$$\dot{\widehat{x}}_2(t) = -\frac{\widehat{x}_2(t)}{\widehat{R}_{ts}(\widehat{x}_1(t))\widehat{C}_{ts}(\widehat{x}_1(t))} + u(t),\ \widehat{x}_2(t) > 0 \tag{21}$$

$$\dot{\widehat{x}}_3(t) = -\frac{\widehat{x}_3(t)}{\widehat{R}_{tl}(\widehat{x}_1(t))\widehat{C}_{tl}(\widehat{x}_1(t))} + u(t),\ \widehat{x}_3(t) > 0 \tag{22}$$

$$\widehat{y}(t) = \widehat{E}_o(\widehat{x}_1(t)) - \widehat{x}_2(t) - \widehat{x}_3(t) \tag{23}$$

The term $u(t)$ required by the observer equations (21)-(22) is calculated using (24)-(27). The error $e(t)$ between actual voltage $y(t)$, and estimated terminal voltage

$\widehat{y}(t)$ is given by (24). The error $e(t)$ is used in (24) to adjust the growth rate of the adaptive gain i.e. $k(t)$. The value of λ and α in (26) are taken as 1 and 2.5 respectively.

$$e(t) = y(t) - \widehat{y}(t) \tag{24}$$

$$\dot{k}(t) = e^2(t), \;\; k(t_0) = k_0 \tag{25}$$

$$N(k(t)) = E_\alpha(-\lambda k(t)^\alpha) \tag{26}$$

$$u(t) = -N(k(t))e(t) \tag{27}$$

The selection of initial guesses, upper, lower bounds with their respective confidence levels for each parameter according to the conditions described by (28)-(33) from [2] ensure the convergence of terminal voltage estimation error $e(t)$ to zero. The APE algorithm is shown in Figure 2.3. For details related to the execution of the APE process, readers are requested to see [2].

$$\widehat{p}_{13}(t_0) > \widehat{p}_{15}(t_0) > 0, \tag{28}$$

$$\lambda_{x_{15}} + \lambda_{y_{15}} > \lambda_{x_{13}} + \lambda_{y_{13}}, \tag{29}$$

$$\lambda_{x_{15}} p_{15_u} + \lambda_{y_{15}} p_{15_l} < \lambda_{x_{13}} p_{13_u} + \lambda_{y_{13}} p_{13_l}, \tag{30}$$

$$\widehat{p}_{16}(t_0) > \widehat{p}_{18}(t_0) > 0, \tag{31}$$

$$\lambda_{x_{18}} + \lambda_{y_{18}} > \lambda_{x_{16}} + \lambda_{y_{16}}, \tag{32}$$

$$\lambda_{x_{18}} p_{18_u} + \lambda_{y_{18}} p_{18_l} < \lambda_{x_{16}} p_{16_u} + \lambda_{y_{16}} p_{16_l}. \tag{33}$$

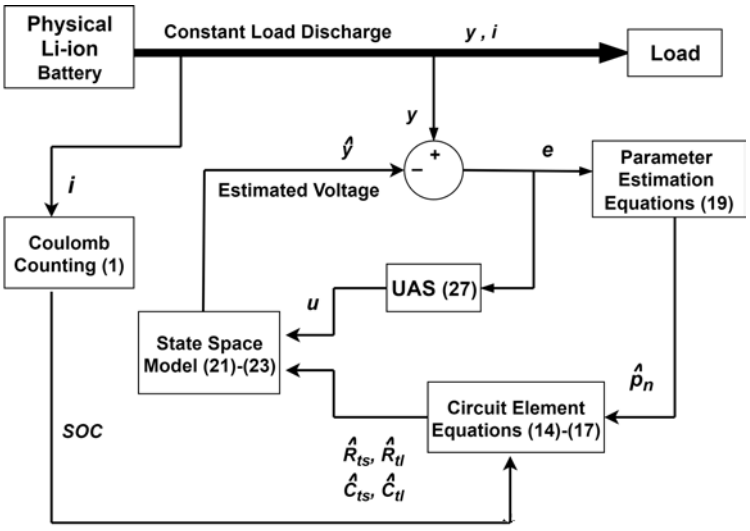

Figure 2.3: Adaptive parameter estimation methodology.

A very small positive discharge current needs to be maintained during the course of the APE process, which leads to the results as shown in (34)-(35), i.e. the products of estimated and actual battery equivalent circuit elements are equal [2].

$$\widehat{R}_{ts}(\widehat{x}_1(t))\widehat{C}_{ts}(\widehat{x}_1(t)) = R_{ts}(x_1(t))C_{ts}(x_1(t)) \tag{34}$$

$$\widehat{R}_{tl}(\widehat{x}_1(t))\widehat{C}_{tl}(\widehat{x}_1(t)) = R_{tl}(x_1(t))C_{tl}(x_1(t)) \tag{35}$$

2.1.3. Particle swarm optimization. There are several ways to solve an optimization problem. This work uses three optimization techniques, i.e. *fmincon* from MATLAB, PSO, Hybrid PSO, either alone or in combination with adaptive parameters estimation. These optimization techniques are used at the second stage of the proposed battery parameters estimation methodology. The optimization function *fmincon* is a standard and widely used function readily available in the MATLAB optimization toolbox [41]. The description of Particle Swarm Optimization (PSO) is included in this work because it produces accurate results for our work. While Hybrid PSO is the combination of *fmincon* and PSO. Next we present the basics of PSO used in this work.

Figure 2.4 shows the flowchart of PSO algorithm for optimum battery parameters estimation. Whereas, Figure 2.5 illustrates the proposed APE followed by optimization strategy for accurate Li-ion battery model parameters estimation. The details of Figure 2.5 are provided in next section. The key feature of PSO is that it is a non-gradient method which utilizes particles. For the work in this paper, the size of a particle is $1 \times n$ where $n = 15$, i.e. each element in the $1 \times n$ vector (forming a particle), represents one of the estimated Li-ion battery model parameters $\widehat{p}_7, \ldots, \widehat{p}_{21}$. The number of elements within a particle are called the decision variables, so for our $1 \times n$ vector of battery parameters a decision variable is a particular parameter i.e. $\widehat{p}_n$, $n \in \{7, \cdots, 21\}$. The upper and lower bounds for each decision variable (as stated in line-18 of Algorithm 1), swarm size S (i.e. number of particles), where $S \in \mathbb{Z}$, $S > 0$, and maximum number of iterations R also needs to be specified. In PSO terminology, a vector containing decision variables of the k^{th} particle, where $k \in \{1, \cdots, S\}$, is called the particle's position $d_k(t)$ at time t. A vector containing the values of the change in the values

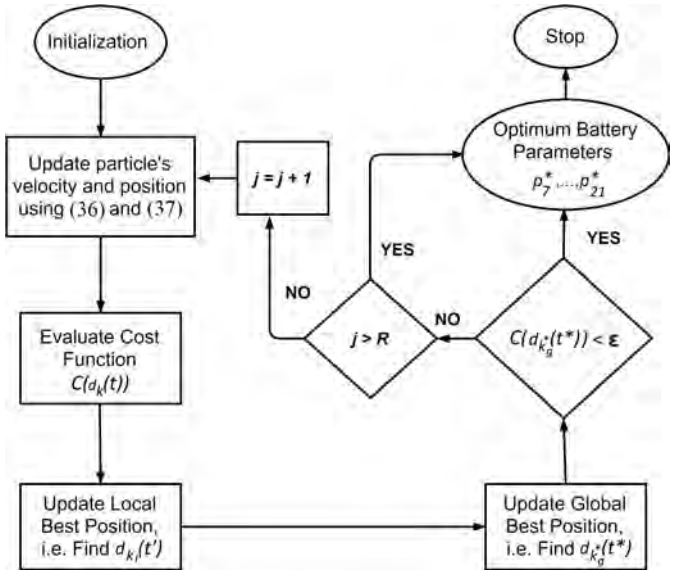

Figure 2.4: PSO algorithm for optimum battery parameters estimation.

of the decision variables of this particle per time step, is called the particle's velocity $v_k(t)$ at time t. The optimization process begins with the initialization of a particle's position, i.e. each decision variable in a particle is randomly assigned a number within the range specified by its lower bound and upper bound. Let $C(d_k(t))$ represents the cost function of the optimization problem, i.e. $C(d_k(t))$ needs to be minimized. In this work, $C(d_k(t)) = |e(t)|$, and $e(t)$ is given by (24). For all k particles, the cost function $C(d_k(t))$ is evaluated at each time step. For all $k \in \{1, \cdots, S\}$, let $d_{k_l}(t')$ be a particle having minimum cost $C(d_k(t'))$ for $t' \in [t_0, t], k_l \in \{1, \cdots, S\}$. Further let $d_{k_g^*}(t^*)$ be a particle $d_{k_l}(t')$ with minimum cost $C(d_{k_l}(t'))$ over all k_l, $t^* \in [t_0, t]$. The particle $d_{k_l}(t')$ is said to have local best position in time interval $[t_0, t]$, and particle $d_{k_g^*}(t^*)$ is said to have global best position in interval $[t_0, t]$ and across all the swarms.

The velocity of each particle is set to zero at initialization, i.e. $v_k(t_0) = 0$. Further, $C(d_{k_l}(t_0))$ and $C(d_{k_g^*}(t_0))$ are assigned a very high value. The local best position of each particle at initial time is assigned as $d_{k_l}(t_0) = d_k(t_0)$. After the initialization, the new velocity and new position of each particle is found by using (36) and (37). The vector r_1 and r_2 have size $1 \times n$ and each element of vector r_1 and r_2 is a uniformly distributed random number within the range (0,1). Here m represents particle's inertia, $m \in (0, 1]$, and a smaller value of m usually provides less oscillations around a value at which a particle's decision variable converges. The weights assigned to local and

global best positions are s_1 and s_2 respectively. The $\circ$ operator in (36) is the Hadamard product. It is used for element wise multiplication of two vectors having the same sizes, i.e. the size of each vector is $1 \times n$. The resultant vector, obtained after element wise multiplication of two same sized vectors, has the size of $1 \times n$. Thus, the element wise multiplication of vectors in (36) gives the vector $v_k(t+1)$ of size $1 \times n$. The velocity and position of the k^{th} particle are updated continuously in a loop using (36) and (37) until $C(d_{k_g^*}(t^*))$ falls below a desired small positive value, say ε, or the number of iterations j exceeds the maximum value R, as shown in Figure 2.4. Details related to the use of the PSO algorithm for estimating Li-ion battery parameters are presented in Section 2.2.

$$v_k(t+\Delta t) = m v_k(t) + s_1 r_1 \circ (d_{k_l}(t') - d_k(t)) + s_2 r_2 \circ (d_{k_g^*}(t^*) - d_k(t)) \tag{36}$$

$$d_k(t+\Delta t) = d_k(t) + v_k(t+\Delta t) \tag{37}$$

In contrast to PSO, there are also gradient based optimization techniques, e.g. MATLAB's *fmincon* function provides an implementation of such gradient based optimization techniques. The combination of PSO and *fmincon* together is known as Hybrid PSO. In Hybrid PSO, the *fmincon* algorithm is executed on the output of the PSO algorithm, after the PSO algorithm terminates, to further refine the output produced by PSO. In this work we compare the results of applying the *fmincon*, PSO, and Hybrid PSO strategies as a second stage of the proposed UAS based optimized battery parameters estimation methodology. The proposed methodology is explained in the next section.

2.2. UAS based Optimized Li-ion Battery Model Parameters Estimation Method

This section explains the proposed adaptation based optimized strategy to estimate Li-ion battery model parameters. The left half of Figure 2.5 shows the APE process. The formulation of the adaptive parameter estimation process is available in section 2.1, and details are available in [2]. The UAS based optimization process and Algorithm 1 can be briefly described as follows. The adaptive parameters estimation process requires the OCV curve, which provides the value of the estimated OCV, i.e.,

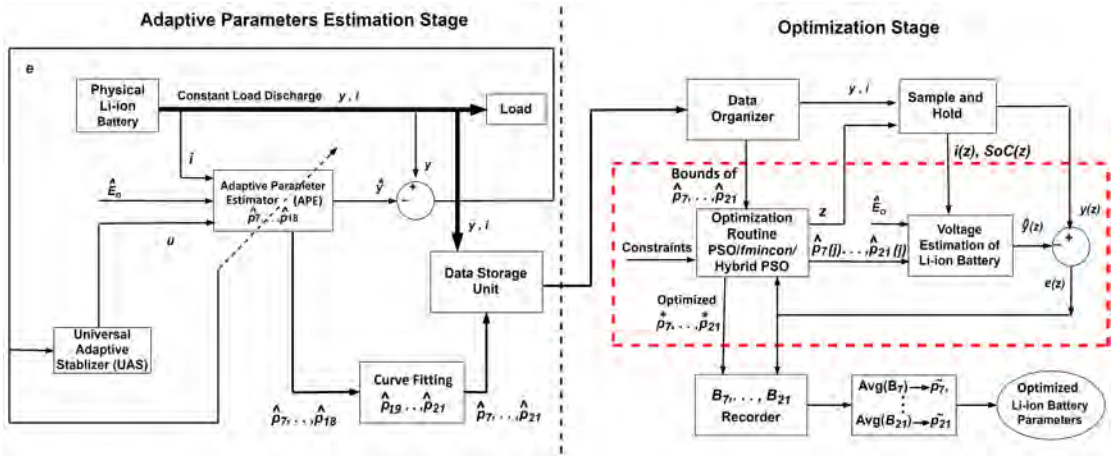

Figure 2.5: Architecture of APE followed by optimization methodology.

$\widehat{E}_0(\widehat{x}_1(t))$. This, along with the measured battery current $i(t)$, and the output $u(t)$ of the universal adaptive stabilizer, is used by the APE block to calculate the estimated battery terminal voltage $\widehat{y}(t)$. The difference between the measured battery terminal voltage $y(t)$, and $\widehat{y}(t)$ gives the terminal voltage estimation error $e(t)$. This error $e(t)$ is used to adaptively adjust values of the Li-ion battery model parameters. This process outputs parameters $\widehat{p}_7, \cdots, \widehat{p}_{18}$, which along with some further curve fitting based operations as shown in [2], produces parameters $\widehat{p}_{19}, \cdots, \widehat{p}_{21}$. The values of the battery terminal voltage $y(t)$, the battery current $i(t)$ at each time step of execution, and the values of estimated parameters $\widehat{p}_7, \cdots, \widehat{p}_{21}$ are stored in a data storage unit.

In the right half of Figure 2.5, the dotted box represents the optimization process of the battery parameters obtained via UAS based estimation. The discrete data points i.e. the voltage and current data points stored in the data storage unit, are extracted by the data organizer block and forwarded to the sample and hold unit. The data organizer block also assigns the upper and lower bounds for battery parameters $\widehat{p}_7, \cdots, \widehat{p}_{21}$ required by optimization routine. The sample and hold block simply reads the terminal voltage and current values one by one, and holds them until one iteration of the optimization routine is completed. The optimization routine block also requires some constraints e.g. the number of iterations, number of swarms, upper and lower bounds of decision variable values, and desired minimum value for the cost function. The $\min_{t\in[t_0,T],k\in\{1,\cdots,S\}} C(x_{k_g^*}(t^*))$, where $t^* = [t_0, T]$, $k_g^* \in \{1, \cdots, S\}$ optimization is then performed. Here T is the time at which battery SoC is 7%, $C(x_k(t)) = |e(t)|$, and $e(t)$

is given by (24). When the error $|e(t)|$ from cost function reaches a desired minimum value ε, the battery parameters $p_7^*, \cdots, p_{21}^*$ are recorded in arrays $B_7, \cdots, B_{21}$. When

Algorithm 1 Adaptation, and optimization based Li-ion battery parameters estimation algorithm.

Requirements: Current $i(t)$ and voltage $y(t)$ for battery discharge through a constant load resistance, where $t = [t_0, t_{end}]$ and t_{end} is the time at which battery SoC is 7%.
Data: Initial values $\widehat{p}_n(0) > 0$, $n \in \{7, \cdots, 18\}$, upper bounds p_{nu}, lower bounds p_{nl}, and their respective confidence levels λ_{x_n} and λ_{y_n} for each parameters $p_7, \ldots, p_{18}$. Battery capacity C_c (Ah) value. Maximum number of optimization iterations R, number of swarms S for PSO, and a small positive constant ε. Upper and lower limits of search space interval for optimization, i.e. $\widehat{p}_7 \pm \delta_7, \ldots, \widehat{p}_{21} \pm \delta_{21}$, where $\delta_n \in \mathbb{R}$, $n \in \{7, \cdots, 21\}$ and $\widehat{p}_7, \ldots, \widehat{p}_{21}$ obtained from APE.
Initial conditions $\widehat{x}_1(t_0) = 1, \widehat{x}_2(t_0) = \widehat{x}_3(t_0) = 0, \widehat{y}(t_0) = y(t_0)V$, and $SoC(t_0) = 1$. Initialize the iterator variables $h = 1$, $j = 1$, and $z = 1$.
Output: Optimized estimated battery model parameters $\tilde{p}_7, \ldots, \tilde{p}_{21}$.

1: **for** $t = t_0 : t_{step} : t_{end}$ **do** ▷ Adaptive parameters estimation of Li-ion battery.
2: Read discharge current $i(t)$ and voltage $y(t)$.
3: Update the error using (24).
4: Find the estimated terminal voltage error using (24), and calculate the $SoC(t)$ using equation (1).
5: Get estimated parameters from (19).
6: Find the equivalent circuit elements from (14) to (17).
7: Evaluate state estimates from (21) and (22), and find estimated terminal voltage using (23).
8: **if** $(|e(t)| < \varepsilon)$ **then**
9: Store the estimates of Li-ion battery parameters in arrays, $A_7[h] \leftarrow \widehat{p}_7(t), \cdots, A_{18}[h] \leftarrow \widehat{p}_{18}(t)$, and
10: $h \leftarrow (h+1)$.
11: **else**
12: **Continue** loop execution.
13: **end if**
14: **end for**
15: Find the mean value of all individual arrays $A_7, \cdots, A_{18}$ to get the estimates of Li-ion battery parameters $\widehat{p}_7, \ldots, \widehat{p}_{18}$.
16: Estimate $\widehat{p}_{19}$, $\widehat{p}_{20}$ and $\widehat{p}_{21}$ parameters from $\widehat{R}_s(\widehat{x}_1(t))$ vs SoC curve using curve fitting as in [2].
17: Store all the battery parameters $\widehat{p}_7, \ldots, \widehat{p}_{21}$, voltage $y(t)$, current $i(t)$, and $SoC(t)$ profiles in the data storage unit.
18: Organize the data for optimization by setting upper and lower limits of search space interval for each parameter, i.e. $\widehat{p}_7 \pm \delta_7, \ldots, \widehat{p}_{21} \pm \delta_{21}$, where $\delta_n \in \mathbb{R}$, $n \in \{7, \cdots, 21\}$, and $\widehat{p}_7, \ldots, \widehat{p}_{21}$ obtained from APE.
19: Set the constraints, such as ε, S, and R, for optimization process.

while $SoC(z) > 7\%$ **do** ▷ Optimization of Li-ion battery model parameters.
    Read constant load discharge current *i(z)*, voltage *y(z)* and *SoC(z)* at z_{th} sample.
    Run an optimization routine (*fmincon*, PSO or Hybrid PSO) to identify the best value of battery parameters in the preset search space interval, i.e. get battery parameter values that minimize $|e(z)|$.
    ▷ The optimization process described in Figure 2.4, along with (36) and (37), is used for APE with PSO (T3-II) or APE with Hybrid PSO (T3-III) techniques.
    if $(|e(z)| < \varepsilon)$ **or** $(j > R)$ **then**
        Store the estimates of Li-ion battery parameters in arrays, $B_7[z] \leftarrow p_7^*(j), \cdots, B_{21}[z] \leftarrow p_{21}^*(j)$ and
        $j \leftarrow 1$ and $z \leftarrow (z+1)$.
    else
        Continue $j \leftarrow (j+1)$.
    ▷ Increment optimization algorithm iteration number.
    end if
end while
Find the mean value of all individual arrays $B_7, \cdots, B_{21}$ to get the optimized estimates of Li-ion battery parameters $\tilde{p}_7, \ldots, \tilde{p}_{21}$.

either the number of iterations or the minimum error criteria in estimated terminal voltage is satisfied, the iterator variable j is incremented to optimize the battery parameters at the next sample of voltage and current data point. The average of recorded battery parameters in $B_7, \cdots, B_{21}$ arrays, after the optimization process, provides the optimized estimates of Li-ion battery parameters and they are named as $\tilde{p}_7, \cdots, \tilde{p}_{21}$. The implementation details of the proposed technique, whose architecture is given in Fig 2.5, has been described in the Algorithm 1. It is also worth noting that T is selected as the time at which battery SoC is 7% [2] because it enables capturing battery behavior over a sufficiently long range of battery cycle life, while making sure that batteries are not discharged to dangerously low operating SoC.

We select the sampling period of 0.01 seconds for battery voltage and current in this work, which is sufficient enough to capture the nonlinear behavior of discharge voltage especially when SoC is between seven and twenty percent. The factors influencing the computational time and accuracy of Algorithm 1 are as follows: 1. Sampling period of battery voltage and current, 2. Maximum number of optimization iterations, 3. Swarm size in optimization stage, 4. Search space interval for each decision variable in optimization stage, 5. Desired minimum value of cost function in optimization

stage. The selection of these factors requires a trade-off between more accurate estimates of Li-ion battery parameters and overall less computational time of Algorithm 1. Furthermore, the accuracy of Algorithm 1 is more sensitive to factor 4 and 5, and the computational time depends mainly on factor 1, 2, and 3.

Our two-stage adaptive-optimized strategy focuses on optimum estimation of Li-ion battery parameters while requiring reduced number of iterations, number of swarms, and search space interval needed by the optimization technique. In next section, we present a comprehensive comparison of estimates of Li-ion battery parameters and overall computational time between APE technique, our proposed algorithm, and optimization routine.

2.3. Computer Simulations for Battery Model Parameters Estimation

The parameters of a 4.1 V, 850 mAh polymer Li-ion battery are obtained by Chen and Mora in [13]. We used the same parameters as a benchmark to perform the computer simulations in this work. However, a Li-ion battery of 275 mAh capacity is employed to reduce the simulation time to almost one-third of 850 mAh Li-ion battery, which Chen and Mora utilize in their experiments. Three different techniques are used to estimate the battery parameters $\widehat{p}_7, \cdots, \widehat{p}_{21}$. In this work, these techniques will be termed as Technique 1 (T1), Technique 2 (T2), and Technique 3 (T3), and they are defined as follows.

- Technique 1 (T1): This technique utilizes one of the three optimization routines i.e. *fmincon* (T1-I), PSO (T1-II), and Hybrid PSO (T1-III). These optimization routines have a random search space interval for each parameter and number of iterations $R = 50$. A swarm size of $S = 50$ is set for PSO (T1-II) and Hybrid PSO (T1-III).
- Technique 2 (T2): This technique [2] uses Universal Adaptive Stabilizer (UAS) based Adaptive Parameters Estimation (APE) alone to acquire the set of Li-ion battery model parameters.
- Technique 3 (T3): This is our newly proposed technique which consists of a two-stage process. The first stage utilizes UAS based APE to obtain the initial values of the parameters. The second stage utilizes one of the three optimization routines

i.e. *fmincon*, PSO, and Hybrid PSO. Thus, Technique 3 employs one of the three two-stage processes, i.e. APE with *fmincon* (T3-I), APE with PSO (T3-II), and APE with Hybrid PSO (T3-III). Complete details for the implementation of the proposed technique are given in the Algorithm 1. The search space interval, as defined in Algorithm 1, for each parameter is $\widehat{p}_7 \pm \delta_7, \ldots, \widehat{p}_{21} \pm \delta_{21}$. The values of parameters $\widehat{p}_7, \ldots, \widehat{p}_{21}$ are obtained from APE (T2) while the values of δ_n is set at 10 percent of the value of a parameter estimated by the APE process, i.e. $\delta_n = 0.1\widehat{p}_n$ and $n \in \{7, \cdots, 21\}$. The number of iterations for all optimization routines are $R = 10$ and swarm sizes of $S = 10$ are selected for PSO and Hybrid PSO. Please note that the number of iterations and swarm size are deliberately set to five times lesser than T1 to illustrate the effectiveness of the proposed technique T3.

The parameters estimated using techniques T1, T2, and T3 are first assessed by comparing the estimated battery parameter values output by each of them, with the parameter values that were experimentally obtained by Chen and Mora. The simulation results of estimated parameters using techniques T1, T2, and T3, and the estimation error results are shown in Table 2.1 and Table 2.2, respectively. The computational time needed by each technique is also noted, and compared. Secondly, the values of battery circuit elements $R_{ts}, R_{tl}, C_{ts}, C_{tl}$, and R_s are calculated using the parameters $\widehat{p}_7, \ldots, \widehat{p}_{21}$. The values of these battery circuit elements are compared with the ones that are pro-

Table 2.1: Simulation results of a 4.1 V, 275 mAh Li-ion battery model parameters.

		Technique 1: $S = 50$ and $R = 50$			Technique 2	Technique 3: $S = 10$ and $R = 10$		
Parameters	Chen & Mora's model values	(T1-I) *fmincon*	(T1-II) PSO	(T1-III) Hybrid PSO	(T2) APE	(T3-I) APE with *fmincon*	(T3-II) APE with PSO	(T3-III) APE with Hybrid PSO
$\widehat{p}_7$	0.3208	9.5897	9.8156	9.7002	0.5555	0.4671	0.4269	0.4518
$\widehat{p}_8$	29.14	49.8232	52.6729	50.8992	29.9996	29.7794	28.9964	29.2309
$\widehat{p}_9$	0.0467	0.4188	0.4843	0.503	0.0552	0.0508	0.0476	0.0481
$\widehat{p}_{10}$	6.603	49.6475	49.3597	49.0668	6.2806	5.1921	5.2384	5.5205
$\widehat{p}_{11}$	155.2	399.9443	422.7023	421.5437	149.999	149.8901	150.0354	154.4826
$\widehat{p}_{12}$	0.0498	0.3937	0.4592	0.5064	0.0577	0.0516	0.05	0.0498
$\widehat{p}_{13}$	752.9	999.9688	1020.6	1016.1	760.867	759.2227	711.8321	724.5906
$\widehat{p}_{14}$	13.51	49.2998	43.0861	45.9953	10.6713	10.28	11.5074	11.715
$\widehat{p}_{15}$	703.6	2000	1816.6	1937.2	684.614	684.5661	685.6799	700.3178
$\widehat{p}_{16}$	6056	5000	5034.2	4994.2	5999.7	5999.6	6002.2	6001.6
$\widehat{p}_{17}$	27.12	199.7554	241.1454	243.94	27.5014	26.5309	27.4755	27.3444
$\widehat{p}_{18}$	4475	4000	3934.2	3907	3666.6	3666.6	3898	4089.5
$\widehat{p}_{19}$	0.1562	2.4398	4.756	4.1083	0.4963	0.2482	0.217	0.2731
$\widehat{p}_{20}$	24.37	199.6888	330.0194	327.6911	33.07	31.6387	26.9885	27.362
$\widehat{p}_{21}$	0.0745	0.1027	0.2168	0.3136	0.06546	0.0526	0.0681	0.0673

Table 2.2: Absolute average percentage error in estimated parameters.

	Technique 1: $S = 50$ and $R = 50$			Technique 2	Technique 3: $S = 10$ and $R = 10$		
Parameters	(T1-I) *fmincon*	(T1-II) PSO	(T1-III) Hybrid PSO	(T2) APE	(T3-I) APE with *fmincon*	(T3-II) APE with PSO	(T3-III) APE with Hybrid PSO
$\widehat{p}_7$	2889.31	2959.73	2923.75	73.16	45.60	33.07	40.84
$\widehat{p}_8$	70.98	80.76	74.67	2.95	2.19	0.49	0.31
$\widehat{p}_9$	796.98	937.27	977.32	18.23	8.80	1.95	3.02
$\widehat{p}_{10}$	651.89	647.53	643.10	4.88	21.37	20.67	16.39
$\widehat{p}_{11}$	157.70	172.36	171.61	3.35	3.42	3.33	0.46
$\widehat{p}_{12}$	689.93	821.35	916.05	15.77	3.53	0.32	0.08
$\widehat{p}_{13}$	32.82	35.56	34.96	1.06	0.84	5.45	3.76
$\widehat{p}_{14}$	264.91	218.92	240.45	21.01	23.91	14.82	13.29
$\widehat{p}_{15}$	184.25	158.19	175.33	2.70	2.71	2.55	0.47
$\widehat{p}_{16}$	17.44	16.87	17.53	0.93	0.93	0.89	0.90
$\widehat{p}_{17}$	636.56	789.18	799.48	1.41	2.17	1.31	0.83
$\widehat{p}_{18}$	10.61	12.08	12.69	18.06	18.06	12.89	8.61
$\widehat{p}_{19}$	1461.97	2944.81	2530.15	217.73	58.90	38.92	74.84
$\widehat{p}_{20}$	719.40	1254.20	1244.65	35.70	29.83	10.74	12.28
$\widehat{p}_{21}$	37.93	191.16	321.17	12.09	29.36	8.54	9.62

vided by Chen and Mora. Finally, the accuracy of the estimated parameters is evaluated by comparing the estimated battery terminal voltage using the above estimated battery parameters, with the battery terminal voltage given by Chen and Mora.

2.3.1. Parameters estimation accuracy comparison. The values of battery parameters $\widehat{p}_7, \ldots, \widehat{p}_{21}$ estimated by using three techniques, T1, T2, and T3 are given in Table 2.1. Whereas, Table 2.2 shows the estimation error of each parameter with respect to the benchmark parameters obtained from Chen and Mora's work [13]. The results in Table 2.1 and Table 2.2 show that the battery parameters obtained using the proposed two-stage parameters estimation methodology (T3) are more accurate compared to the parameters that are obtained either by using the optimization technique (T1) alone or by using the APE (T2) alone.

The battery parameters obtained using APE with *fmincon* (T3-I) are more accurate as compared to the ones that are obtained by using optimization techniques (T1) alone and are somewhat comparable with the ones that are obtained by using APE (T2) alone. However, the parameters obtained by the proposed technique T3-II and T3-III i.e. APE in combination with PSO and Hybrid PSO respectively are more accurate and have much lesser error with reference to the Chen and Mora's benchmark param-

eters values. In purely optimization based technique (T1), the number of iterations are $R = 50$ and the swarm size of $S = 50$ are selected. However, the parameters estimation error in Table 2.2 suggests that it requires a bigger population of particles and number of iterations to give reasonable estimates of battery model parameters.

Table 2.1 and 2.2 show that the parameters estimated by the optimization technique (T1) alone have a larger error. Therefore, the following discussion will only focus on APE (T2) and our proposed technique (T3). Table 2.1 shows a good match between the parameters obtained by the proposed technique (T3-II and T3-III), and the Chen and Mora's parameters values. We further evaluate the parameters estimation accuracy by calculating the battery equivalent circuit elements and estimating the battery terminal voltage. The equivalent circuit element values and estimated battery terminal voltage are compared with the ones given by Chen and Mora.

We also record the average simulation time (over 10 simulations of each technique), required by the three proposed techniques, i.e. T3-I, T3-II, and T3-III. These results are shown in Figure 2.6. It can be seen from Figure 2.6 that APE with PSO (T3-II), and APE with Hybrid PSO (T3-III) which give the best estimation of battery parameters have relatively larger time consumption when compared to APE (T2), APE with *fmincon* (T3-I), and the *fmincon* optimization technique (T1-I). However, the time consumption of APE with PSO (T3-II) and APE with Hybrid PSO (T3-III) is much less than the PSO (T1-II) and Hybrid PSO optimization (T1-III) techniques.

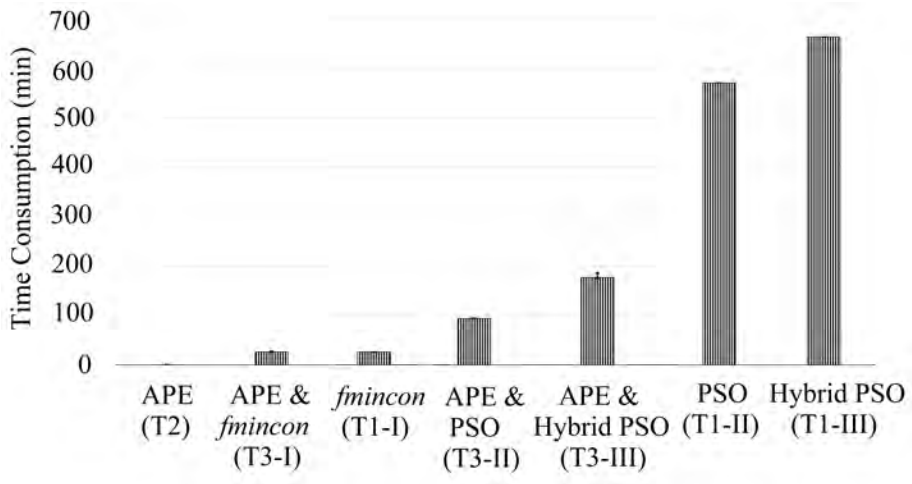

Figure 2.6: Time consumption comparison of parameters estimation strategies.

Since the accuracy of the estimated parameters using optimization techniques alone is very poor. Therefore, there will be no further assessment of optimization based technique (T1). The rest of the simulation and implementation work will focus on Technique 2 and Technique 3.

2.3.2. Battery circuit elements ($R_{ts}, R_{tl}, C_{ts}, C_{tl}, R_s$) estimation comparison.

In this section, the battery is subjected to 0.5 amperes constant resistive load and parameters $\widehat{p}_7, \ldots, \widehat{p}_{21}$ are estimated during the simulation. These parameters are then used to calculate the battery circuit elements $R_{ts}, R_{tl}, C_{ts}, C_{tl}$, and R_s. The accuracy of the circuit elements is evaluated by comparing the error between the estimated circuit elements and reference values of Chen and Mora's circuit elements. The error in the estimated circuit elements, using the APE technique (T2) alone and the proposed techniques T3-I, T3-II, and T3-III, is shown in Figure 2.7.

The estimation error percentage, during the course of simulation, in each circuit element is obtained by subtracting the Chen and Mora's circuit element value at a particular time instant, from the ones that are obtained either via technique T2 or T3 at the same time instant, and then dividing by the Chen and Mora's circuit element value at that instant. The absolute value of this estimation error in circuit elements are recorded during the simulation and the mean of this estimation error array gives the average percentage error in circuit elements estimation. Overall Figure 2.7 shows that APE with PSO (T3-II) and APE with Hybrid PSO (T3-III) have lesser circuit elements estimation error compared to APE alone (T2) and APE with *fmincon* (T3-I) technique.

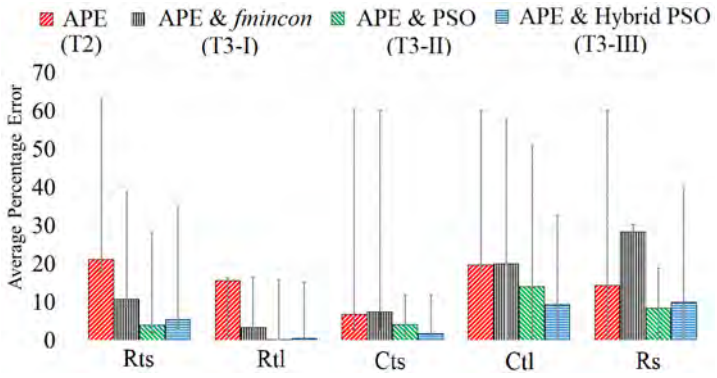

Figure 2.7: Circuit elements error analysis for technique 2 (T2) and technique 3 (T3).

2.3.3. Battery terminal voltage estimation comparison. The battery terminal voltage is estimated using four different load profiles with irregular discharging intervals. These load profiles are given in Table 2.3. The battery current in these load profiles varies from 0.5 amperes to 6 amperes while the total simulation time period changes from 150 seconds to 25 seconds as shown in Table 2.3. For all the four load profiles, the battery is discharged until the SoC reaches 7%. The results of battery terminal voltage estimation and their respective estimation error for the designed four load profiles are illustrated in Figure 2.8a to Figure 2.8d.

The voltage estimated by using Chen and Mora's parameters values, is termed as actual voltage in Figure 2.8. The voltage estimation error is obtained by subtracting the voltage estimated by Technique 2 or 3 from Chen and Mora's voltage. The terminal voltage estimation error is reduced using the battery parameters obtained from APE

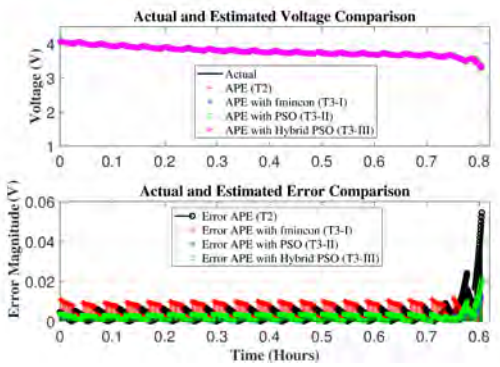

(a) Terminal voltage estimation and error calculation for load profile 1.

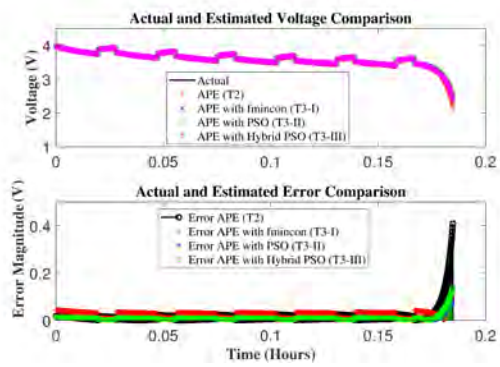

(b) Terminal voltage estimation and error calculation for load profile 2.

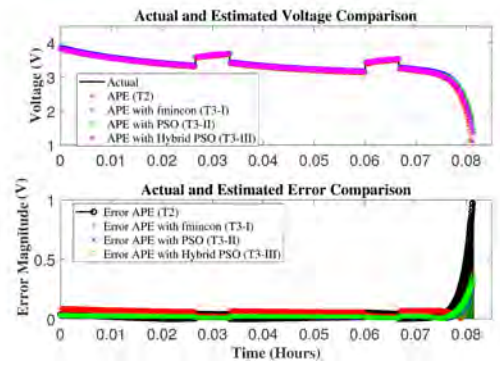

(c) Terminal voltage estimation and error calculation for load profile 3.

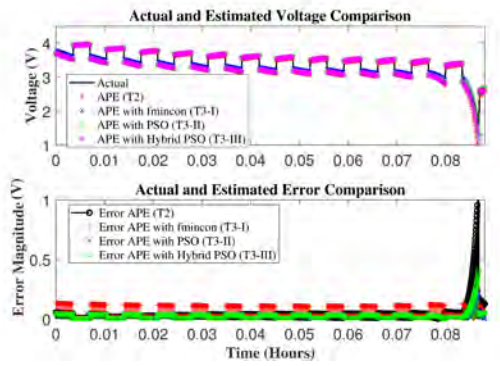

(d) Terminal voltage estimation and error calculation for load profile 4.

Figure 2.8: Terminal voltage estimation and error comparison among Chen and Mora, technique 2 (T2) and technique 3 (T3) for four load profiles.

Table 2.3: Battery discharging load profiles.

Load profiles	Magnitude A	Time period seconds	OFF time seconds	ON time seconds
Load profile 1	0.5	150	52.5	97.5
Load profile 2	2	100	30	70
Load profile 3	4	120	24	96
Load profile 4	6	25	12.5	12.5

with PSO (T3-II) and APE with Hybrid PSO (T3-III), especially in the relaxation period when the battery is not discharging and when SoC becomes less than 10%.

Under the discharging current profiles defined in Table 2.3, the $\sum_{t=t_0}^{T} e^2(t)$ and average of absolute percentage error of terminal voltages, estimated using techniques T2 and T3, are also highlighted in Figure 2.9 and Figure 2.10 respectively. The time duration for the terminal voltage error analysis is $t = [t_0, T]$, where T is the time at which the battery SoC approaches to 7%. The overall results in these figures for four designed discharging load profiles show that the $\sum_{t=t_0}^{T} e^2(t)$ and average of absolute terminal voltage error for APE (T2) and APE with *fmincon* (T3-I) are larger than APE with PSO (T3-II) and APE with Hybrid PSO (T3-III).

The only anomaly in these computer simulations is that APE with PSO (T3-II) has higher $\sum_{t=t_0}^{T} e^2(t)$ when the discharging load profile 1 is used, i.e. the battery is discharged with a low current and larger time period. This anomaly will be further evaluated in our experimental investigation.

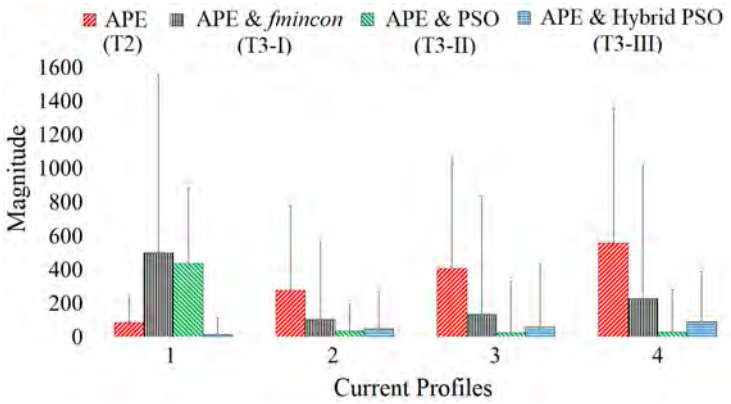

Figure 2.9: $\sum_{t=t_0}^{T} e^2(t)$ analysis for technique 2 (T2) and technique 3 (T3) for four load profiles.

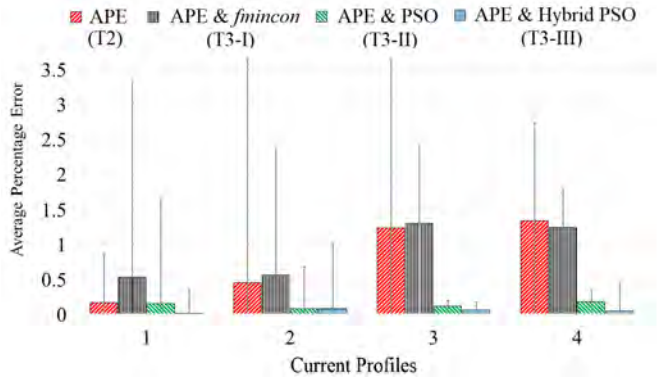

Figure 2.10: Average of absolute terminal voltage error for technique 2 (T2) and technique 3 (T3) for four load profiles.

Our simulation results for parameters estimation, battery circuit elements calculation and battery terminal voltage estimation show that proposed two-stage methodology consisting of APE with PSO (T3-II) and APE with Hybrid PSO (T3-III) perform better than the purely optimization based techniques (T1), APE (T2) and APE with *fmincon* (T3-I) techniques. Moreover, the proposed APE with PSO (T3-II), and APE with Hybrid PSO (T3-III) techniques need less computation time compared to purely optimization based techniques (T1-II), and (T1-III) to estimate battery model parameters more accurately.

2.4. Experimental Validations of The Proposed Technique

The simulation results showed very poor accuracy of the estimated parameters $\widehat{p}_7, \ldots, \widehat{p}_{21}$ when using purely optimization based technique (T1). Therefore, only Technique 2 and our proposed Technique 3 will be experimentally investigated for the accuracy assessment of the estimated parameters. The experimental setup designed for this work is shown in Figure 2.11. This setup similar to [2] includes a Thunder-Power 22.2 V, 6.6 Ah Lithium-Polymer battery $(TP6600-6SP+25)$, different type of loads for battery discharging, voltage and current sensors for the battery voltage and current measurements. A dSPACE 1103 board is used for experimentation and data acquisition. The sampling period of 0.01 seconds is selected to measure the voltage and current of Lithium-Polymer battery.

The voltage relaxation test is performed to get the OCV curve as a function of battery SoC. Curve fitting, as mentioned in the background section (II.A), is used

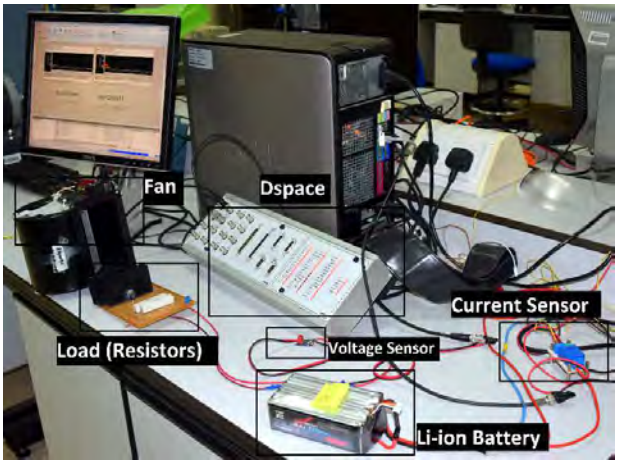

Figure 2.11: Experimental setup.

to get the OCV parameters $\widehat{p}_1,\ldots,\widehat{p}_6$ of equation (5). The values obtained for these parameters are; $p_1 = 5.112, p_2 = 40.955, p_3 = 22.195, p_4 = 1.9215, p_5 = 1.759, p_6 = 3.0435$, which are same as shared in our earlier work [2]. The major focus of this work is estimation and accuracy assessment of the remaining battery parameters $\widehat{p}_7,\ldots,\widehat{p}_{21}$.

Subsection 2.4.1 presents the experimental estimation of the battery model parameters $\widehat{p}_7,\ldots,\widehat{p}_{21}$. Subsection 2.4.2 assess the accuracy of estimated battery parameters by comparing the estimated and measured voltage for sixteen discharging load profiles. Finally, subsection 2.4.3 evaluates the parameters estimation accuracy again by comparing the estimated and measured voltage for charging process of sixteen individual batteries.

2.4.1. Experimental estimation of battery model parameters. In this section, the battery model parameters $\widehat{p}_7,\ldots,\widehat{p}_{21}$ are estimated using the APE (T2) and our proposed two-stage parameters estimation technique (T3). The fully charged Lithium-Polymer battery is connected with the 50 Ω resistive load to discharge the battery with a small load current of about 0.4 amperes. The slow battery discharging during APE process ensures the convergence of product of estimated resistances and capacitances to the product of actual resistances and capacitances, as proved in our earlier work [2]. Therefore, it will provide accurate estimate of battery model circuit elements $R_{ts}, R_{tl}, C_{ts}, C_{tl}$, and R_s which will ensure an accurate estimation of battery terminal voltage. The battery terminal voltage and discharging current profiles are shown in Figure 2.12. It took about

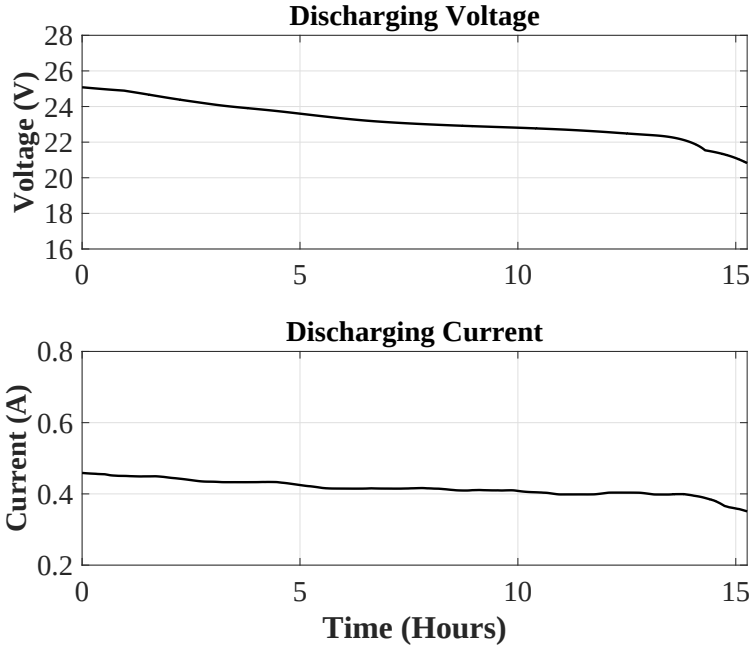

Figure 2.12: Discharging voltage and current profiles of Lithium-Polymer battery connected with 50 Ω resistor.

15 hours to discharge the battery upto 7% of its rated capacity with a load resistance of 50 Ω. Each voltage and current data contains 5,493,994 number of samples and are utilized in Algorithm 1 to estimate Lithium-Polymer battery parameters. Algorithm 1 is the combination of APE algorithm (Line 1 to 16) and optimization algorithm (Line 17 to 29). APE algorithm, detailed in section (2.2), uses UAS, adaptive equation (19), and curve fitting to estimate the Lithium-Polymer battery parameters. The estimated parameters, using APE technique (T2), are recorded in column 2 of Table 2.4.

Next, the parameters obtained by the APE technique (T2) are utilized to design the search space interval of $\widehat{p}_7, \ldots, \widehat{p}_{21}$ parameters for optimization. The parameters obtained by APE (T2) are optimized at the second stage of Algorithm 1. The search space interval of the optimization techniques (T3-I) to (T3-III) for each parameter is designed by setting the upper and lower bounds, δ_n. The value of δ_n is set at 10 percent of the value of parameters estimated by the APE process, i.e. $\delta_n = 0.1\widehat{p}_n$ and $n \in \{7, \cdots, 21\}$. Thus the search space interval of the estimated parameters are defined as $\widehat{p}_7 \pm \delta_7, \ldots, \widehat{p}_{21} \pm \delta_{21}$. Furthermore, at the second stage of proposed technique (T3), the number of iterations $R = 10$ for (T3-I) to (T3-III) and a swarm size of $S = 10$ for (T3-II) and (T3-III) are selected. The estimated parameters using APE with *fmincon*

Table 2.4: Experimental parameters estimation of 22.2 V, 6.6 Ah Lithium-Polymer battery.

	Technique 2	Technique 3: $S = 10$ and $R = 10$		
Parameters	(T2) APE values	(T3-I) APE with *fmincon*	(T3-II) APE with PSO	(T3-III) APE with Hybrid PSO
$\widehat{p}_7$	0.5505	0.5493	0.5525	0.5436
$\widehat{p}_8$	30.0475	29.9866	30.0538	29.7022
$\widehat{p}_9$	0.0551	0.0549	0.0536	0.0538
$\widehat{p}_{10}$	6.2585	6.0380	6.2454	5.9850
$\widehat{p}_{11}$	30	29.8603	30.0176	29.5146
$\widehat{p}_{12}$	0.0551	0.0549	0.0545	0.0536
$\widehat{p}_{13}$	760.2266	760.2144	754.6998	754.6072
$\widehat{p}_{14}$	10.7686	10.0683	10.0012	9.3990
$\widehat{p}_{15}$	685.7457	685.7182	674.5923	674.6247
$\widehat{p}_{16}$	6036.4	6036.7	5991.9	5995.3
$\widehat{p}_{17}$	27.5422	27.2466	27.4837	26.8348
$\widehat{p}_{18}$	3696	3696	3649.5	3650
$\widehat{p}_{19}$	0.0439	0.0449	0.0450	0.0447
$\widehat{p}_{20}$	59.07	58.8419	60.0453	58.8088
$\widehat{p}_{21}$	0.2246	0.2078	0.1186	0.1527

(T3-I), APE with Particle Swarm Optimization (T3-II) and APE with Hybrid PSO (T3-III) are tabulated in column 3, 4, and 5 of Table 2.4 respectively. The optimization techniques are employed to improve the accuracy of the parameters that are originally obtained by using APE (T2). Therefore, the acquired parameters accuracy is assessed in the following subsection 2.4.2 and 2.4.3.

2.4.2. Parameters estimation accuracy assessment via battery discharging tests. This section evaluates the accuracy of the estimated parameters obtained by APE (T2) and our proposed technique (T3) via battery discharging. The estimated parameters are used to calculate the values of battery circuit elements $R_{ts}, R_{tl}, C_{ts}, C_{tl}, R_s$ which are then used to estimate the battery terminal voltage. Thus, the accuracy of estimated parameters is evaluated by comparing the estimated and measured battery voltage. The 22.2 V, 6.6 Ah Lithium-Polymer battery is connected with resistive load and the battery is discharged until the SoC approaches 7%. Sixteen different rigorous load profiles are designed for battery discharging and data for estimated and measured

voltages are acquired. These sixteen discharging load profiles are separated in the form of five groups. Group 1 constantly discharge the battery, Group 2 discharges the battery with the periodic ON and OFF intervals while Group 3 to 5 discharge the battery with random ON and OFF intervals. The details of these sixteen discharging load profiles are given below.

- Group 1 (G1), 4 Tests: The battery is subjected to a constant discharging using four resistive loads of 50 Ω, 25 Ω, 11.11 Ω and 7.5 Ω.
- Group 2 (G2), 4 Tests: In this group the battery is periodically discharged and relaxed with different loads. The four load profiles designed in this group are:
  - The battery is discharged for 15 minutes followed by relaxation time of 15 minutes using two load resistors, 25 Ω and 11.11 Ω.
  - The battery is discharged for 1 minutes followed by relaxation time of 1 minutes using two load resistors, 25 Ω and 11.11 Ω.
- Group 3 (G3), 3 Tests: The discharging tests in this group are conducted with randomly varying ON and OFF time in contrast to Group 2 periodic ON and OFF time. The experiments are performed with three values of resistor loads, i.e. 25 Ω, 11.11 Ω and 7.5 Ω.
- Group 4 (G4), 2 Tests: These tests are also performed with randomly varying ON and OFF time using light bulbs as a load. The following two load profiles are designed.
  - Parallel combination of two 24 V, 60 W DC bulbs
  - Parallel combination of three 24 V, 60 W DC bulbs
- Group 5 (G5), 3 Tests: This group contains the last three load profiles of our rigorous testing. The tests are again conducted with randomly varying ON and OFF time. Three load profiles are designed using parallel combination of three 24 V, 60 W DC bulbs. The number of bulbs in parallel combination is randomly varied from one bulb to three bulbs.

The Lithium-Polymer battery is discharged under the aforementioned 16 load profiles that are separated in five groups. The terminal voltage estimation errors, for all the sixteen discharging load profiles, are recorded in an array, for APE technique (T2) and for the developed two-stage technique (T3). As a sample, the estimated and

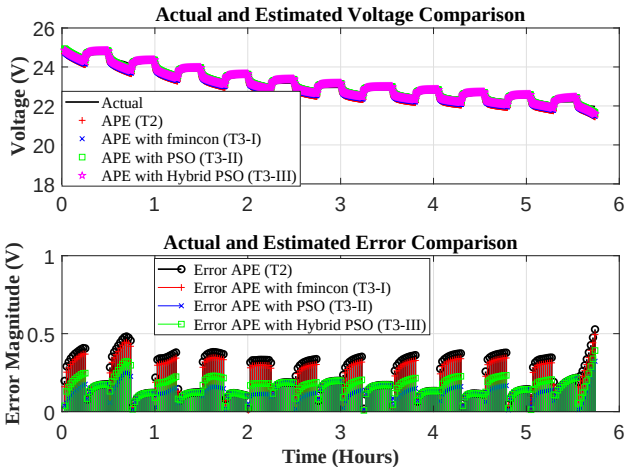

Figure 2.13: Terminal voltage estimation and error comparison for resistive load of 11.11 Ω with 15 minutes ON and OFF times.

measured terminal voltage along with the absolute voltage estimation error for two of the sixteen discharging load profiles are shown in Figure 2.13 and Figure 2.14. Figure 2.13 shows that voltage error profiles of APE (T2) and APE with *fmincon* (T3-I) techniques are about the same. However, APE with PSO (T3-II) and APE with Hybrid PSO (T3-III) show a significant drop in the voltage estimation error magnitude. In Figure 2.14, the voltage estimation error is investigated when the battery is subjected to a random and relatively higher discharging current. The significant reduction in error profile magnitude is noticed in Figure 2.14 when APE with PSO (T3-II) and APE with Hybrid PSO (T3-III) techniques are employed. Thus, the reduction in the terminal voltage estimation error for (T3-II) and (T3-III) techniques verifies the accuracy of the estimated parameters.

Sixteen terminal voltage estimation error arrays are obtained from sixteen discharging load profiles. Due to the different discharging interval of each load profile,

Table 2.5: Terminal voltage estimation error statistics while discharging the battery with sixteen different load profiles using technique 2 (T2) and technique 3 (T3).

Parameters estimation methods	Mean of error (V)	Median of error (V)	Mode of error (V)	Standard deviation of error (V)
APE (T2)	0.0211	0.027	-0.055	0.5026
APE with fmincon (T3-I)	0.0022	0.0234	-0.083	0.489
APE with PSO (T3-II)	-0.0973	-0.0252	0.0278	0.4316
APE with Hybrid PSO (T3-III)	-0.0604	-0.0023	0.138	0.4496

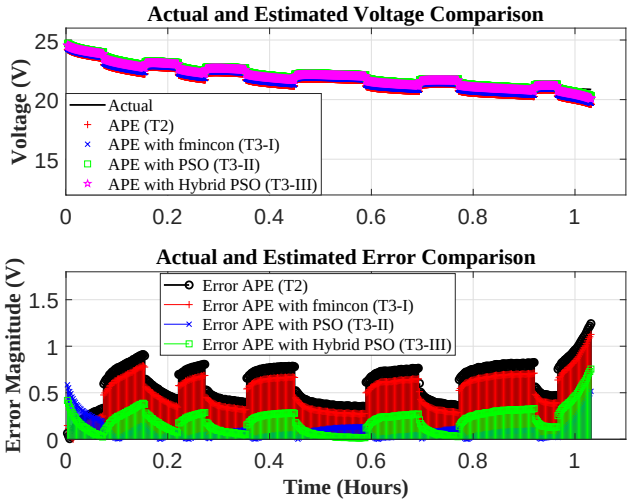

Figure 2.14: Terminal voltage estimation and error comparison for randomly varying load with random ON and OFF times drawing 5 A and 7.5 A.

each array has different number of samples. To perform the overall error analysis, all the sixteen terminal voltage estimation error arrays are stacked to form a large array. Such four large terminal voltage estimation error arrays, i.e. one array for technique T2 and one for each of the techniques T3-I, T3-II and T3-III, are formed. The total number of samples in each large terminal voltage estimation error array are 2.75e7. The mean, median, mode and standard deviation for each of these four terminal voltage estimation error arrays are described in Table 2.5. The extensive investigation for the overall terminal voltage estimation error arrays was carried out by further showing their histogram and cumulative distribution graphs in Figure 2.15 and Figure 2.16 respectively. Where the red vertical lines in Figure 2.16 indicate the $\pm$ 4.5% terminal voltage estimation error i.e. $\pm$ 1 V. The following observations can be made from the data presented in Table 2.5, Figure 2.15 and Figure 2.16.

- In Table 2.5, the standard deviation values imply that the terminal voltage estimation error is less dispersed and settled around the small mode value for APE with PSO (T3-II) and APE with Hybrid PSO (T3-III) techniques.
- Figure 2.15 shows that more than 95% of terminal voltage error lies within $\pm$ 1 V for T2 and all T3 techniques. Also, the low standard deviation of terminal voltage estimation error, settled around mode value, for T3-II and T3-III techniques can be visualized from histogram analysis in Figure 2.15.

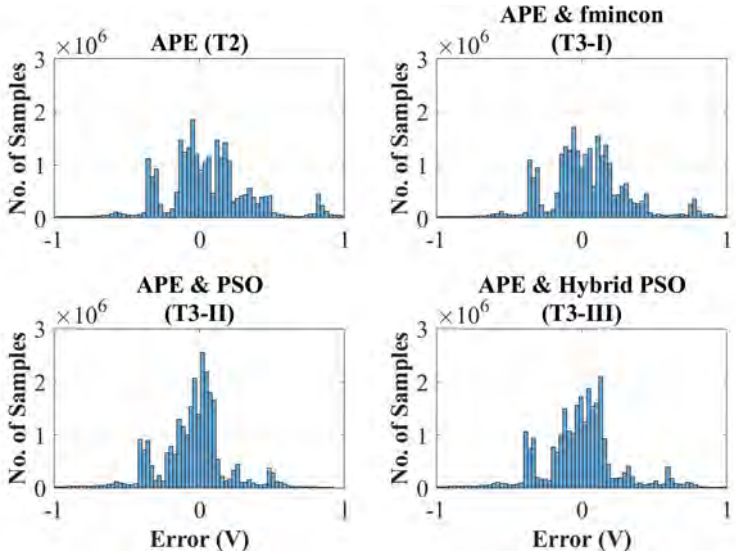

Figure 2.15: Histogram of terminal voltage estimation error for technique 2 (T2) and technique 3 (T3) under sixteen different discharging profiles.

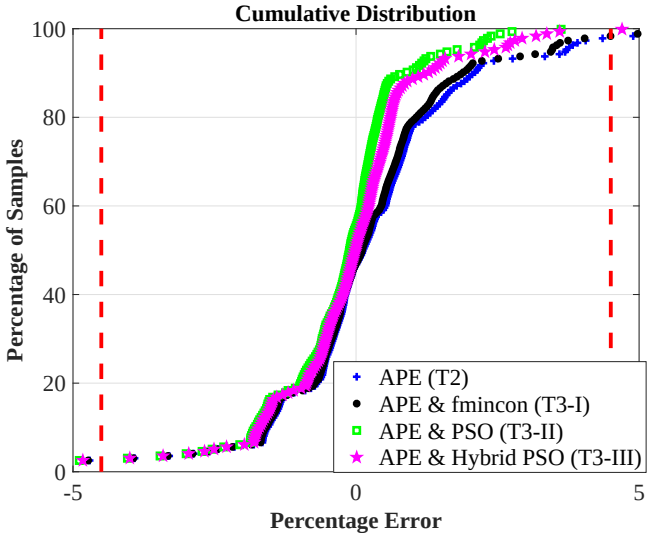

Figure 2.16: Cumulative distribution of terminal voltage estimation error for techique 2 (T2) and technique (T3) under sixteen different discharging profiles.

- Figure 2.16 shows that the voltage estimation error data that lies within $\pm$ 1 V ($\pm$ 4.5% range) is: 95.43% for APE (T2), 95.78% for APE with *fmincon* (T3-I), 97.29% for APE with PSO (T3-II), and 97.08% for APE with Hybrid PSO (T3-III). Furthermore, the voltage estimation error data that lies within $\pm$ 0.5 V ($\pm$ 2.25% range) is: 86.90% for APE (T2), 87.33% for APE with *fmincon* (T3-I), 91.74% for APE with PSO (T3-II), and 89.12% for APE with Hybrid PSO (T3-III).

Thus the statistical analysis presented in Table 2.5, Figure 2.15 and Figure 2.16 for battery discharging shows that battery parameters estimated using APE with PSO (T3-II) and APE with Hybrid PSO (T3-III) are more accurate as compared to APE (T2) and APE with *fmincon* (T3-I) techniques.

2.4.3. Parameters estimation accuracy assessment via battery charging tests. In this section, we charged sixteen individual batteries with a constant current of 2.5 amperes using the Thunder-Power charger (TP820CD). The estimated and measured voltage of the battery using Technique 2 and Technique 3 are compared to assess the accuracy of the estimated battery parameters. The voltage estimation error is recorded for each battery during the charging process. As a sample, detailed data collected for one battery during the charging process is shown in Figure 2.17. The error magnitude plot shows that APE (T2) and APE with *fmincon* (T3-I) techniques have higher terminal voltage estimation errors compared to APE with PSO (T3-II) and APE with Hybrid PSO (T3-III) techniques.

For all the sixteen batteries, four terminal voltage estimation error arrays using T2, T3-I, T3-II, T3-III techniques, similar to the battery discharging case, are formed. Each array includes the terminal voltage estimation error of all the sixteen individual

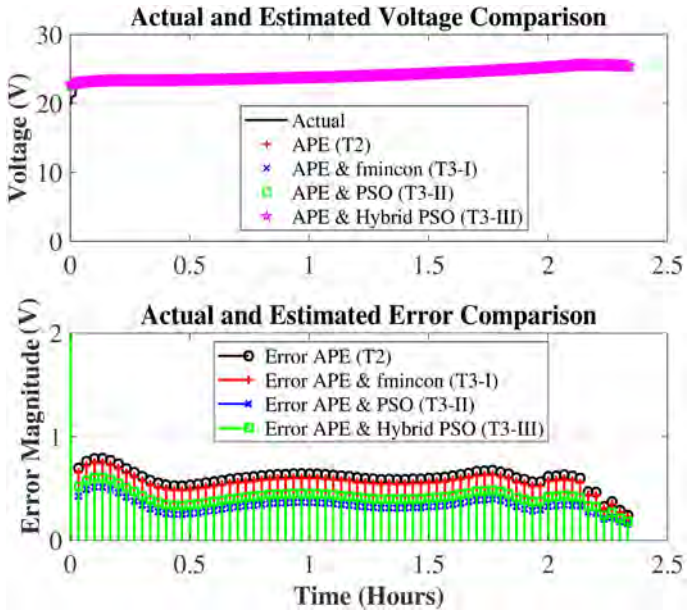

Figure 2.17: Terminal voltage estimation and error comparison while charging the 22.2 V, 6.6 Ah Li-Polymer battery, technique 2 (T2) and technique 3 (T3).

batteries. The total number of samples collected in each array during the batteries charging are 1.258e7. The statistical error analysis of these four error arrays is provided in Table 2.6. The terminal voltage estimation error, of all the sixteen individual batteries, is further analyzed by performing the histogram and cumulative distribution as shown in Figure 2.18 and Figure 2.19 respectively. The data presented in Table 2.6, Figure 2.18 and Figure 2.19 can be analyzed as follows:

- Table 2.6 shows that mean, median, mode and standard deviation values for APE with PSO (T3-II) and APE with Hybrid PSO (T3-III) are relatively lower than APE (T2) and APE with *fmincon* (T3-I) techniques.
- Figure 2.18 shows that more than 94% of terminal voltage error lies within $\pm$ 1 V for T2 and all T3 techniques. Also, the voltage error is less dispersed and settled around a small mode value, for T3-II and T3-III techniques.
- Figure 2.19 shows that the voltage estimation error data that lies within $\pm$ 1 V ($\pm$ 4.5% range) is: 94.34% for APE (T2), 95.55% for APE with *fmincon* (T3-I), 99.35% for APE with PSO (T3-II), and 98.26% for APE with Hybrid PSO (T3-III). Furthermore, the voltage estimation error data that lies within $\pm$ 0.6 V (2.7% range) for different techniques is: 38.32% for APE (T2), 50.72% for APE with *fmincon* (T3-I), 89.01% for APE with PSO (T3-II), and 81.98% for APE with Hybrid PSO (T3-III).

The study of terminal voltage estimation error while charging sixteen individual batteries with a constant 2.5 amperes current shows that the proposed APE with PSO (T3-II) and APE with Hybrid PSO (T3-III) techniques estimate the battery model parameters more accurately compared to APE (T2) and optimization techniques (T1) alone.

Table 2.6: Terminal voltage estimation error statistics while charging sixteen different batteries with a constant 2.5 amperes for technique 2 (T2) and technique 3 (T3).

Parameters estimation methods	Mean of error (V)	Median of error (V)	Mode of error (V)	Standard deviation of error (V)
APE (T2)	-0.6509	-0.6396	-0.641	0.3847
APE with fmincon (T3-I)	-0.6110	-0.5969	-0.589	0.3828
APE with PSO (T3-II)	-0.3879	-0.3699	-0.308	0.3787
APE with Hybrid PSO (T3-III)	-0.4723	-0.4538	-0.4895	0.3824

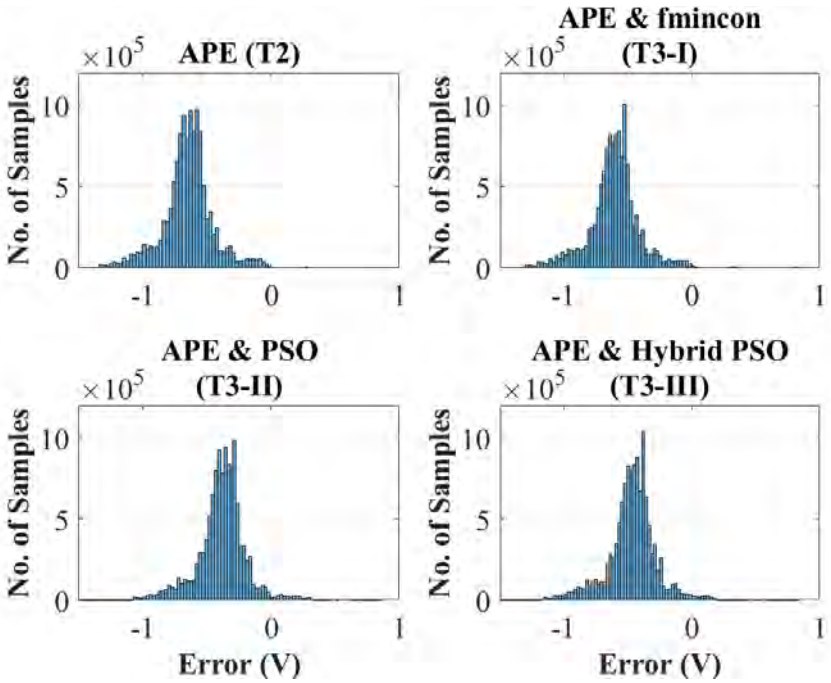

Figure 2.18: Histogram of terminal voltage estimation error for technique 2 (T2) and technique 3 (T3) while charging sixteen individual batteries with a constant 2.5 A current.

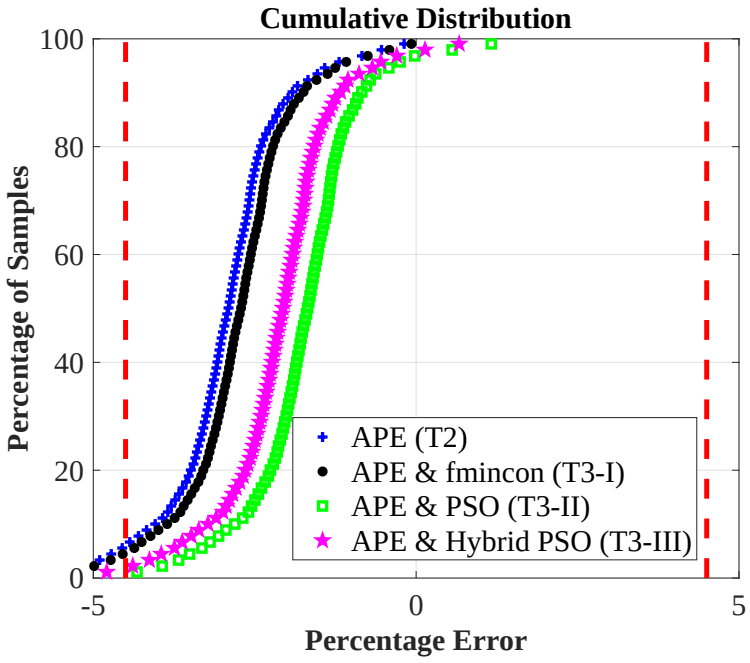

Figure 2.19: Cumulative distribution of terminal voltage estimation error for technique 2 (T2) and technique 3 (T3) while charging sixteen individual batteries with a constant 2.5 A current.

Chapter 3. Real-Time Parameters Estimation of a Li-ion Battery Model via Universal Adaptive Stabilizer

In this chapter, a modification of the UAS based APE strategy is presented. The existing UAS based APE strategy reported in [2, 3] requires a prior knowledge of open circuit voltage (OCV), and curve fitting at the end for series resistance estimation. Therefore, the modified APE strategy proposes high-gain UAS based adaptive estimators for OCV and series resistance estimation and incorporates them into previously developed APE strategy. Because this modified strategy estimates all the equivalent circuit elements of a Li-ion battery model at once, and does not require any prior knowledge of OCV, or post processing for series resistance, so it can be used for real-time implementation. Development of such a real-time methodology is a motivation for the modification of the APE strategy proposed in this work.

This chapter begins by presenting Chen and Mora's model, but this time we also introduce two additional states, one related to the OCV, the other related to the series resistance. Section 3.2 presents the formulation of the proposed modified APE strategy. The mathematical proof of the proposed modified APE strategy is given in Section 3.3. Section 3.4 provides a comparison of simulation results against well-established results from [13] on a 4.1 V, 270 mAh Li-ion battery.

3.1. Li-ion Battery Equivalent Circuit Model- With Introduction of Two Additional States

Chen and Mora's model [13], as presented earlier in equations (1)-(4), is shown again in Figure 3.1. The difference is that this time we include two additional states i.e. x_1 which is the OCV, and x_4 which is the series resistance R_s itself.

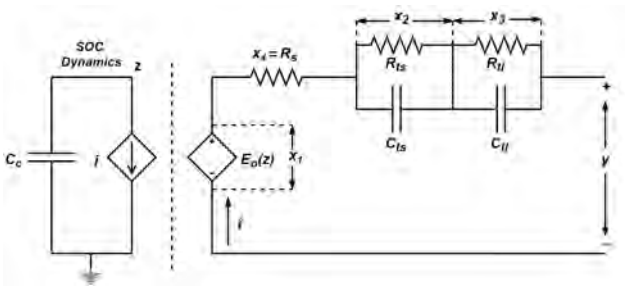

Figure 3.1: Li-ion battery equivalent circuit model-with additional states.

$$E_o(z) = -r_1 e^{-r_2 z} + r_3 + r_4 z - r_5 z^2 + r_6 z^3 = x_1(z) \tag{38}$$

$$R_{ts}(z) = r_7 e^{-r_8 z} + r_9 \tag{39}$$

$$R_{tl}(z) = r_{10} e^{-r_{11} z} + r_{12} \tag{40}$$

$$C_{ts}(z) = -r_{13} e^{-r_{14} z} + r_{15} \tag{41}$$

$$C_{tl}(z) = -r_{16} e^{-r_{17} z} + r_{18} \tag{42}$$

$$R_s(z) = r_{19} e^{-r_{20} z} + r_{21} = x_4(z). \tag{43}$$

For convenience we present the equations representing the battery circuit elements in terms of parameters r_1 to r_{21}, as displayed in (38)-(43) above. Unlike SoC and battery parameters representations in Chapter 2, here the battery SoC is denoted by $z \in [0,1]$, and the battery parameters are represented by r_n, $n \in \{1,2,\cdots,21\}$. Whereas the open circuit voltage (OCV), and the voltage across $R_{ts}||C_{ts}$, $R_{tl}||C_{tl}$, and R_s are represented by the states x_1, x_2, x_3, and x_4 respectively. The term C_c and $y(t)$ simply denote the battery capacity in ampere-hour (Ah) and battery terminal voltage. The factors f_1, f_2, $f_3 \in [0,1]$ are to represent the temperature effects, charge-discharge cycles, and self discharge. The equations for battery open circuit voltage x_1 in (45), battery series resistance x_4 in (48), and equivalent circuit elements $R_{ts}, R_{tl}, C_{ts}, C_{tl}$ in (38)-(43) are derived from Chen and Mora's work [13]. Further the battery dynamics are now given by (44)-(49).

$$\dot{z}(t) = -\frac{1}{C_c} i(t), \;\; C_c = 3600 C f_1 f_2 f_3 \tag{44}$$

$$\dot{x}_1(t) = \frac{\partial x_1(z)}{\partial z(t)} \dot{z}(t) = -\left(r_1 r_2 e^{-r_2 z} + r_4 - 2 r_5 z + 3 r_6 z^2 \right) \frac{i(t)}{C_c} \tag{45}$$

$$\dot{x}_2(t) = -\frac{x_2(t)}{R_{ts}(z) C_{ts}(z)} + \frac{i(t)}{C_{ts}(z)} \tag{46}$$

$$\dot{x}_3(t) = -\frac{x_3(t)}{R_{tl}(z) C_{tl}(z)} + \frac{i(t)}{C_{tl}(z)} \tag{47}$$

$$\dot{x}_4(t) = \frac{\partial x_4(z(t))}{\partial z(t)} \dot{z}(t) = \left(r_{19} r_{20} e^{-r_{20} z} \right) \frac{i(t)}{C_c} \tag{48}$$

$$y(t) = x_1(z) - x_2(t) - x_3(t) - i(t) x_4(t). \tag{49}$$

In the following section, we will formulate the UAS observer-based Li-ion battery model parameters estimator for estimating Li-ion battery model parameters, i.e. $r_1, \cdots, r_{21}$.

3.2. Modified Adaptive Parameters Estimation Methodology for a Li-on Battery Model

This section first provides the formulation details and algorithm for the proposed modified UAS based APE strategy. Whereas, the second subsection presents the operation through a flowchart of our proposed methodology.

3.2.1. Modified UAS based battery parameters estimation methodology.

A high gain adaptive estimator for a Li-ion battery model, based on (44)-(49), is described by (50)-(55).

$$\dot{\widehat{z}}(t) = -\frac{1}{C_c} i(t), \;\; C_c = 3600 C f_1 f_2 f_3 \tag{50}$$

$$\dot{\widehat{x}}_1(t) = \frac{\partial \widehat{x}_1(\widehat{z})}{\partial \widehat{z}(t)} \dot{\widehat{z}}(t) - u(t) = -\left(\widehat{r}_1 \widehat{r}_2 e^{-\widehat{r}_2 \widehat{z}} + \widehat{r}_4 - 2\widehat{r}_5 \widehat{z} + 3\widehat{r}_6 \widehat{z}^2 \right) \frac{i(t)}{C_c} - u(t), \;\; \widehat{x}_1(t) \geq 0 \tag{51}$$

$$\dot{\widehat{x}}_2(t) = -\frac{\widehat{x}_2(t)}{\widehat{R}_{ts}(\widehat{z}) \widehat{C}_{ts}(\widehat{z})} + \frac{i(t)}{\widehat{C}_{ts}(z)} + u(t), \;\; \widehat{x}_2(t) \geq 0 \tag{52}$$

$$\dot{\widehat{x}}_3(t) = -\frac{\widehat{x}_3(t)}{\widehat{R}_{tl}(\widehat{z}) \widehat{C}_{tl}(\widehat{z})} + \frac{i(t)}{\widehat{C}_{tl}(z)} + u(t), \;\; \widehat{x}_3(t) \geq 0 \tag{53}$$

$$\dot{\widehat{x}}_4(t) = \frac{\partial \widehat{x}_4(\widehat{z}(t))}{\partial \widehat{z}(t)} \dot{\widehat{z}}(t) + u(t) = \left(\widehat{r}_{19} \widehat{r}_{20} e^{-\widehat{r}_{20} \widehat{z}} \right) \frac{i(t)}{C_c} + u(t), \;\; \widehat{x}_4(t) \geq 0 \tag{54}$$

$$\widehat{y}(t) = \widehat{x}_1(t) - \widehat{x}_2(t) - \widehat{x}_3(t) - i(t) \widehat{x}_4(t) \tag{55}$$

Here $i(t)$ is the actual battery current and $\widehat{z}(t)$ is the same as $z(t)$ in (44). The states $\widehat{x}_1$, $\widehat{x}_2$, $\widehat{x}_3$, and $\widehat{x}_4$ denote the estimates of OCV, voltage across $\widehat{R}_{ts}||\widehat{C}_{ts}$, $\widehat{R}_{tl}||\widehat{C}_{tl}$, and estimated series resistance, respectively. For simplicity, the values of f_1, f_2, f_3 are taken 1 in this work and the their effects will be considered in future work. The estimated voltage is represented by $\widehat{y}(t)$, whereas the estimated circuit elements are given by (56)-(61).

$$\widehat{E}_o(\widehat{z}) = -\widehat{r}_1 e^{-\widehat{r}_2\widehat{z}} + \widehat{r}_3 + \widehat{r}_4\widehat{z} - \widehat{r}_5\widehat{z}^2 + \widehat{r}_6\widehat{z}^3 = \widehat{x}_1(\widehat{z}) \tag{56}$$

$$\widehat{R}_{ts}(\widehat{z}) = \widehat{r}_7 e^{-\widehat{r}_8\widehat{z}} + \widehat{r}_9 \tag{57}$$

$$\widehat{R}_{tl}(\widehat{z}) = \widehat{r}_{10} e^{-\widehat{r}_{11}\widehat{z}} + \widehat{r}_{12} \tag{58}$$

$$\widehat{C}_{ts}(\widehat{z}) = -\widehat{r}_{13} e^{-\widehat{r}_{14}\widehat{z}} + \widehat{r}_{15} \tag{59}$$

$$\widehat{C}_{tl}(\widehat{z}) = -\widehat{r}_{16} e^{-\widehat{r}_{17}\widehat{z}} + \widehat{r}_{18} \tag{60}$$

$$\widehat{R}_s(\widehat{z}) = \widehat{r}_{19} e^{-\widehat{r}_{20}\widehat{z}} + \widehat{r}_{21} = \widehat{x}_4(\widehat{z}). \tag{61}$$

The control input $u(t)$ of the UAS based-observer, as described in chapter 2, is designed by employing (62)-(65).

$$e(t) = y(t) - \widehat{y}(t), \tag{62}$$

$$\dot{k}(t) = e^2(t), \;\; k(t_0) = k_0 \tag{63}$$

$$N(k(t)) = E_\alpha(-\lambda k(t)^\alpha), \tag{64}$$

$$u(t) = -N(k(t))e(t). \tag{65}$$

The adaptive equation for battery parameters estimation, recalled from [2, 3] and chapter 2, is given by (66).

$$\dot{\widehat{r}}_n(t) = e^2(t) + \lambda_{x_n}(r_{n_u} - \widehat{r}_n(t)) + \lambda_{y_n}(r_{n_l} - \widehat{r}_n(t)). \tag{66}$$

The adaptive equation (66) requires an upper bound r_{n_u} and a lower bounds r_{n_l} for each estimated parameter $\widehat{r}_n(t)$, $n \in \{1,2,\cdots,21\}\backslash\{3,21\}$, and user's confidence levels on the upper and lower bounds, i.e. λ_{x_n} and λ_{y_n} respectively. It is shown in *Lemma 3.3* that the non-negative real values of r_{n_u}, r_{n_l}, λ_{x_n}, and λ_{y_n} leads to $\widehat{r}(t) > 0$, for $t > t_0$. The flowchart of proposed modified APE method for Li-ion battery parameters estimation is shown in Figure 3.2. Note that the UAS based parameters estimation method, explained above, is capable of estimating the battery parameters $n \in \{1,2,\cdots,21\}\backslash\{3,21\}$. The estimates of $\widehat{r}_3$ and $\widehat{r}_{21}$ can be obtained, during or after the adaptation process, by applying the least squares estimation or curve fitting tech-

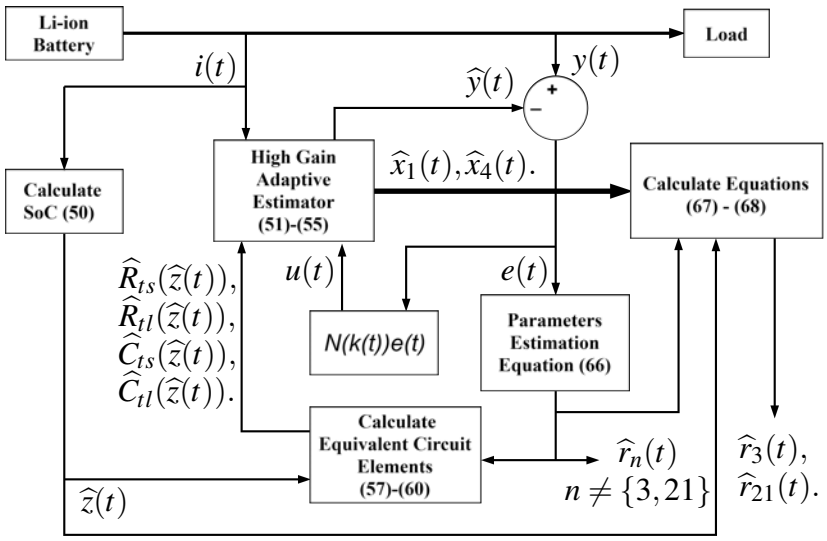

Figure 3.2: Flowchart of modified UAS based adaptive parameters estimation of a Li-ion battery model.

niques, etc., on (56) and (61) respectively. However, this work uses a direct approach to estimate $\widehat{r}_3$ and $\widehat{r}_{21}$, during the adaptation process. Our approach to estimate $\widehat{r}_3$ and $\widehat{r}_{21}$ is based on the results of *Theorem 3.2*. In *Theorem 3.2*, where it is shown that $\widehat{x}_1(t) \to x_1(t)$ and $\widehat{x}_4(t) \to x_4(t)$ as $t \to \infty$, and convergence of $\widehat{r}_n \to r_n$, where $n \in \{1, 2, \cdots, 21\} \backslash \{3, 21\}$ as $t \to \infty$ respectively. Thus, $\widehat{x}_1(t) \to x_1(t)$ and $\widehat{x}_4(t) \to x_4(t)$ at $t \to \infty$ lets us write the equations (56) and (61) into (67) and (68) form to estimate $\widehat{r}_3$ and $\widehat{r}_{21}$ respectively.

$$\widehat{r}_3 = x_1(t) + \widehat{r}_1 e^{-\widehat{r}_2 \widehat{z}} - \widehat{r}_4 \widehat{z} + \widehat{r}_5 \widehat{z}^2 - \widehat{r}_6 \widehat{z}^3, \tag{67}$$

$$\widehat{r}_{21} = x_4(t) - \widehat{r}_{19} e^{-\widehat{r}_{20} \widehat{z}}. \tag{68}$$

The steps to implement the modified UAS based adaptation methodology for battery model parameters estimation are described in Algorithm 2. In the following subsection, the flowchart for algorithm 2 is presented and transcribed.

3.2.2. Proposed modified algorithm for Li-ion battery parameters estimation. This section provides the details of our proposed modified UAS based adaptation algorithm to estimate Li-ion battery parameters. The flowchart of the algorithm 2 is shown in Figure (3.2). The UAS based adaptation process begins with the measurement of current and voltage of a Li-ion battery. A small positive current needs to

Algorithm 2 Modified UAS based algorithm for real-time adaptive parameters estimation of a Li-ion battery.

Requirements: Data acquisition circuit to measure the terminal voltage $y(t)$ and current $i(t)$ of a Li-ion battery.

Data: Initial values $\widehat{r}_n(0)$, upper bounds r_{n_u}, lower bounds r_{n_l}, confidence levels λ_{x_n}, and λ_{y_n} for $n \in \{1,2,\cdots,21\}\backslash\{3,21\}$. Satisfying *Lemma 3.1*. Initial states $\widehat{x}_1(0) = E_o(0)$, $\widehat{x}_2(0) = 0$, $\widehat{x}_3(0) = 0$, $\widehat{x}_4(0) = 0$, and $\widehat{y}(0) = y(0)$. A small positive tracking error bound ε. Battery capacity value C_c(Ah).

Output: Estimated Li-ion battery model parameters $\widehat{r}_1(t), \widehat{r}_2(t), \cdots, \widehat{r}_{21}(t)$.

for $t = t_0 : t_{step} : t_{end}$ **do**
  Read battery terminal voltage $y(t)$ and current $i(t)$.
  Update the error $e(t)$ using (62).
  Estimate battery SoC value $\widehat{z}(t)$ using (50).
  Evaluate (66) for $\widehat{r}_n(t)$ estimation, where $n \in \{1,2,\cdots,21\}\backslash\{3,21\}$.
  Calculate equivalent circuit element $\widehat{R}_{ts}(\widehat{z})$, $\widehat{R}_{tl}(\widehat{z})$, $\widehat{C}_{ts}(\widehat{z})$, $\widehat{C}_{tl}(\widehat{z})$ using (57)-(60).
  Find $u(t)$ using (65).
  Estimate the states $\widehat{x}_1(\widehat{t})$, $\widehat{x}_2(t)$, $\widehat{x}_3(t)$, $\widehat{x}_4(\widehat{t})$ using (51)-(54).
  Estimate the terminal voltage $\widehat{y}(t)$ using (55).
  Update the error $e(t)$ using (62).
  if $(|e(t)| < \varepsilon)$ **then**
    if $\left[\widehat{r}_{14}(t) > -\dfrac{1}{\widehat{z}(t)} \ln\left(\dfrac{\widehat{r}_{15}(t)}{\widehat{r}_{13}(t)}\right)\right]$ **and** $\left[\widehat{r}_{17}(t) > -\dfrac{1}{\widehat{z}(t)} \ln\left(\dfrac{\widehat{r}_{18}(t)}{\widehat{r}_{16}(t)}\right)\right]$ **then**
      Solve (67) and (68) to get $\widehat{r}_3(t)$ and $\widehat{r}_{21}(t)$.
      Return $\left[\widehat{r}_1(t), \widehat{r}_2(t), \cdots, \widehat{r}_{21}(t)\right]$.
    else
      Continue loop execution.
    end if
  else
    Continue loop execution.
  end if
end for

be maintained during the adaptation, as per Theorem 3.2, for accurate results. The error between actual and estimated terminal voltages is used by UAS and the adaptive estimation equation in (66) to identify $\widehat{r}_n(t)$, where $n \in \{1,2,\cdots,21\}\backslash\{3,21\}$. These estimated parameters are employed to calculate the equivalent circuit elements. Next, the equivalent circuit elements' estimates together with the output of UAS and current are input to high gain adaptive estimator. The adaptation process ends with the evaluation of state estimates, i.e. $\widehat{x}_1(\widehat{t})$, $\widehat{x}_2(t)$, $\widehat{x}_3(t)$, $\widehat{x}_4(\widehat{t})$, of a Li-ion battery model followed by the error update. When the error magnitude goes below the user's defined threshold

during the adaptation, the estimated states approach to actual states of a Li-ion battery model, as per Theorem 3.2. Thereafter, the convergence of estimated states to their actual values lets us use equation (67) and (68) for identification of $\widehat{r}_3(t)$ and $\widehat{r}_{21}(t)$. In the following section, we provide mathematical justification of our proposed modified UAS based adaptation strategy for a Li-ion battery model parameters estimation.

3.3. Mathematical Justification

In this section, the convergence of terminal voltage estimation error $e(t)$ to zero is proved. The proof of $e(t) \to 0$ as $t \to \infty$ lets us derive the following results: $\widehat{x}_1(t) \to x_1(t)$, $\widehat{R}_{ts}(\widehat{z})\widehat{C}_{ts}(\widehat{z}) \to R_{ts}(z)C_{ts}(z)$, $\widehat{R}_{tl}(\widehat{z})\widehat{C}_{tl}(\widehat{z}) \to R_{tl}(z)C_{tl}(z)$, and $\widehat{x}_4(t) \to x_4(t)$ as $t \to \infty$. Afterward, the analysis of the above results leads to the conclusion that the Li-ion battery model parameters can be estimated using the proposed method. Before proving the above mentioned statements, some results for $\lambda_{x_n}, \lambda_{y_n}, r_{n_u}$, and r_{n_l} selection needs to be established in *Lemma 3.1*.

Lemma 3.1. *Suppose $\lambda_{x_n}, \lambda_{y_n}, r_{n_u}$, and r_{n_l} are the positive real numbers for $n = \{13, 15, 16, 18\}$, and $\widehat{z}(t) \in (0, 1]$, then the following conditions hold for all $t > t_0$.*

- ***If*** $\widehat{r}_{13}(t_0) > \widehat{r}_{15}(t_0) > 0$, $\lambda_{x_{15}} + \lambda_{y_{15}} > \lambda_{x_{13}} + \lambda_{y_{13}}$, $\lambda_{x_{15}}\widehat{r}_{15_u} + \lambda_{y_{15}}\widehat{r}_{15_l} < \lambda_{x_{13}}\widehat{r}_{13_u} + \lambda_{y_{13}}\widehat{r}_{13_l}$, *and* $\widehat{r}_{14}(t) > -\dfrac{1}{\widehat{z}(t)} \ln\left(\dfrac{\widehat{r}_{15}(t)}{\widehat{r}_{13}(t)}\right)$, ***then*** $\widehat{C}_{ts}(\widehat{z}(t)) > 0$.
- ***If*** $\widehat{r}_{16}(t_0) > \widehat{r}_{18}(t_0) > 0$, $\lambda_{x_{18}} + \lambda_{y_{18}} > \lambda_{x_{16}} + \lambda_{y_{16}}$, $\lambda_{x_{18}}\widehat{r}_{18_u} + \lambda_{y_{18}}\widehat{r}_{18_l} < \lambda_{x_{16}}\widehat{r}_{16_u} + \lambda_{y_{16}}\widehat{r}_{16_l}$, *and* $\widehat{r}_{17}(t) > -\dfrac{1}{\widehat{z}(t)} \ln\left(\dfrac{\widehat{r}_{18}(t)}{\widehat{r}_{16}(t)}\right)$ ***then*** $\widehat{C}_{tl}(\widehat{z}(t)) > 0$.

The detailed proof of *Lemma 3.1* is available in [2]. The conditions established in *Lemma 3.1* are utilized in the following theorem to prove the convergence of terminal voltage error $e(t)$ to zero and, thereafter, the convergence of estimated circuit elements to actual circuit elements of a Li-ion battery.

Theorem 3.2. *Suppose that conditions needed for Lemma 3.1 to hold are satisfied.* ***If*** *the Li-ion battery discharge current $i(t)$, $t > 0$, is a small positive value* ***then*** *we get the following as $t \to \infty$.*

- $\widehat{x}_1(t) = x_1(t)$,
- $\widehat{R}_{ts}(\widehat{z})\widehat{C}_{ts}(\widehat{z}) = R_{ts}(\widehat{z})C_{ts}(\widehat{z})$,
- $\widehat{R}_{tl}(\widehat{z})\widehat{C}_{tl}(\widehat{z}) = R_{tl}(\widehat{z})C_{tl}(\widehat{z})$,

- $\widehat{x}_4(t) = x_4(t)$.

Proof. Suppose the assumptions mentioned above are satisfied. Take the time derivative of (62) to get

$$\dot{e}(t) = \dot{y}(t) - \dot{\widehat{y}}(t), \tag{69}$$

Addition and subtraction of $e(t)$ to R.H.S of (69), and recognizing that $e(t) = y(t) - \widehat{y}(t)$ provides

$$\dot{e}(t) = -e(t) + y(t) - \widehat{y}(t) + \dot{y}(t) - \dot{\widehat{y}}(t). \tag{70}$$

Now, substitution of $-\widehat{y}(t)$ and $\dot{\widehat{y}}(t)$ from (55) in (70) provides

$$\begin{aligned} \dot{e}(t) = &- e(t) + y(t) + \dot{y}(t) - \widehat{x}_1(\widehat{z}(t)) + \widehat{x}_2(t) + \widehat{x}_3(t) + i(t)\widehat{x}_4(\widehat{z}(t)) \\ &- \dot{\widehat{x}}_1(\widehat{z}(t)) + \dot{\widehat{x}}_2(t) + \dot{\widehat{x}}_3(t) + \frac{di(t)}{dt}\widehat{x}_4(\widehat{z}(t)) + i(t)\dot{\widehat{x}}_4(\widehat{z}(t)), \end{aligned} \tag{71}$$

Using (52) and (53) in (71) gives

$$\begin{aligned} \dot{e}(t) = &- e(t) + y(t) + \dot{y}(t) - \widehat{x}_1(\widehat{z}(t)) + \widehat{x}_2(t) + \widehat{x}_3(t) + i(t)\widehat{x}_4(\widehat{z}(t)) - \dot{\widehat{x}}_1(\widehat{z}(t)) \\ &- \frac{\widehat{x}_2(t)}{\widehat{R}_{ts}(\widehat{z}(t))\widehat{C}_{ts}(\widehat{z}(t))} - \frac{\widehat{x}_3(t)}{\widehat{R}_{tl}(\widehat{z}(t))\widehat{C}_{tl}(\widehat{z}(t))} + \frac{i(t)}{\widehat{C}_{ts}(\widehat{z}(t))} + \frac{i(t)}{\widehat{C}_{tl}(\widehat{z}(t))} + 2u(t) \\ &+ \frac{di(t)}{dt}\widehat{x}_4(\widehat{z}(t)) + i(t)\dot{\widehat{x}}_4(\widehat{z}(t)), \end{aligned} \tag{72}$$

Re-arrangement of (72) yields the following

$$\begin{aligned} \dot{e}(t) = &- e(t) + y(t) + \dot{y}(t) + \widehat{x}_2(t)\left(1 - \frac{1}{\widehat{R}_{ts}(\widehat{z}(t))\widehat{C}_{ts}(\widehat{z}(t))}\right) + \widehat{x}_3(t)\left(1 - \frac{1}{\widehat{R}_{tl}(\widehat{z}(t))\widehat{C}_{tl}(\widehat{z}(t))}\right) \\ &- \widehat{x}_1(\widehat{z}(t)) + i(t)\widehat{x}_4(\widehat{z}(t)) - \dot{\widehat{x}}_1(\widehat{z}(t)) + i(t)\left(\frac{1}{\widehat{C}_{ts}(\widehat{z}(t))} + \frac{1}{\widehat{C}_{tl}(\widehat{z}(t))}\right) \\ &+ \frac{di(t)}{dt}\widehat{x}_4(\widehat{z}(t)) + i(t)\dot{\widehat{x}}_4(\widehat{z}(t)) + 2u(t). \end{aligned} \tag{73}$$

Since by definition of (57) and (58), $\widehat{R}_{ts}(\widehat{z}(t)) > 0$, $\widehat{R}_{tl}(\widehat{z}(t)) > 0$ for all $t > t_0$. Also by Lemma 3.1, we know that $\widehat{C}_{ts}(\widehat{z}(t)) > 0$ and $\widehat{C}_{tl}(\widehat{z}(t)) > 0$ for all $t > t_0$. Therefore,

$\widehat{R}_{ts}(\widehat{z}(t))\widehat{C}_{ts}(\widehat{z}(t)) > 0$ and $\widehat{R}_{tl}(\widehat{z}(t))\widehat{C}_{tl}(\widehat{z}(t)) > 0$.

$$\text{which implies } 1 - \frac{1}{\widehat{R}_{ts}(\widehat{z}(t))\widehat{C}_{ts}(\widehat{z}(t))} < 1, \tag{74}$$

From (52), $\widehat{x}_2(t) \geq 0$, Thus,

$$\widehat{x}_2(t)\left(1 - \frac{1}{\widehat{R}_{ts}(\widehat{z}(t))\widehat{C}_{ts}(\widehat{z}(t))}\right) \leq \widehat{x}_2(t), \tag{75}$$

Similarly using $\widehat{x}_3(t) \geq 0$ from (53) provides

$$\widehat{x}_3(t)\left(1 - \frac{1}{\widehat{R}_{tl}(\widehat{z}(t))\widehat{C}_{tl}(\widehat{z}(t))}\right) \leq \widehat{x}_3(t), \tag{76}$$

From (75) and (76) we get

$$\widehat{x}_2(t) + \widehat{x}_3(t) \geq x_2(t)\left(1 - \frac{1}{\widehat{R}_{ts}(\widehat{z}(t))\widehat{C}_{ts}(\widehat{z}(t))}\right) + \widehat{x}_3(t)\left(1 - \frac{1}{\widehat{R}_{tl}(\widehat{z}(t))\widehat{C}_{tl}(\widehat{z}(t))}\right). \tag{77}$$

Using (77) in (73) and re-arrangement of terms provides the following

$$\begin{aligned}\dot{e}(t) \leq & -e(t) + y(t) + \dot{y}(t) - \widehat{x}_1(\widehat{z}(t)) + \widehat{x}_2(t) + \widehat{x}_3(t) + i(t)\widehat{x}_4(\widehat{z}(t)) - \dot{\widehat{x}}_1(\widehat{z}(t)) \\ & + \frac{di(t)}{dt}\widehat{x}_4(\widehat{z}(t)) + i(t)\dot{\widehat{x}}_4(\widehat{z}(t)) + i(t)\left(\frac{1}{\widehat{C}_{ts}(\widehat{z}(t))} + \frac{1}{\widehat{C}_{tl}(\widehat{z}(t))}\right) + 2u(t),\end{aligned} \tag{78}$$

Simplification of (78) using (55) and (62) gives

$$\begin{aligned}\dot{e}(t) \leq & -y(t) + \widehat{y}(t) + y(t) + \dot{y}(t) - \widehat{y}(t) - \dot{\widehat{x}}_1(\widehat{z}(t)) + \frac{di(t)}{dt}\widehat{x}_4(\widehat{z}(t)) + i(t)\dot{\widehat{x}}_4(\widehat{z}(t)) \\ & + i(t)\left(\frac{1}{\widehat{C}_{ts}(\widehat{z}(t))} + \frac{1}{\widehat{C}_{tl}(\widehat{z}(t))}\right) + 2u(t),\end{aligned} \tag{79}$$

$$\dot{e}(t) \leq \dot{y}(t) - \dot{\widehat{x}}_1(\widehat{z}(t)) + \frac{di(t)}{dt}\widehat{x}_4(\widehat{z}(t)) + i(t)\dot{\widehat{x}}_4(\widehat{z}(t)) + i(t)\left(\frac{1}{\widehat{C}_{ts}(\widehat{z}(t))} + \frac{1}{\widehat{C}_{tl}(\widehat{z}(t))}\right) + 2u(t). \tag{80}$$

Using (51) and (54) in (80) gives

$$\begin{aligned}\dot{e}(t) \leq & \dot{y}(t) - \frac{\partial \widehat{x}_1(\widehat{z}(t))}{\partial \widehat{z}(t)}\dot{\widehat{z}}(t) + \frac{di(t)}{dt}\widehat{x}_4(\widehat{z}(t)) + i(t)\frac{\partial \widehat{x}_4(\widehat{z}(t))}{\partial \widehat{z}(t)}\dot{\widehat{z}}(t) + i(t)u(t) \\ & + i(t)\left(\frac{1}{\widehat{C}_{ts}(\widehat{z}(t))} + \frac{1}{\widehat{C}_{tl}(\widehat{z}(t))}\right) + 3u(t).\end{aligned} \tag{81}$$

Following this, the proof of error $e(t)$ convergence to zero is derived from the equation (81). We will consider two cases of error, i.e. $e(t)$ can be either positive or negative, and each case produces a particular form. This particular form in both cases lets us show that $e(t) \to 0$ as $t \to \infty$. Prior to considering the case of positive or negative error, some inequalities are required to be established.

Consider the following inequality related to $e(t)$ and the first term of R.H.S of (81),

$$\begin{aligned}\left(e(t) - \dot{y}(t)\right)^2 &\geq 0, \\ \frac{1}{2}e^2(t) + \frac{1}{2}\dot{y}^2(t) &\geq e(t)\dot{y}(t).\end{aligned} \tag{82}$$

The inequality related to $e(t)$ and the second term of R.H.S of (81) is as follows,

$$\begin{aligned}\left(e(t) + \frac{\partial \widehat{x}_1(\widehat{z}(t))}{\partial \widehat{z}(t)}\dot{\widehat{z}}(t)\right)^2 &\geq 0, \\ \frac{1}{2}e^2(t) + \frac{1}{2}\left(\frac{\partial \widehat{x}_1(\widehat{z}(t))}{\partial \widehat{z}(t)}\dot{\widehat{z}}(t)\right)^2 &\geq -e(t)\frac{\partial \widehat{x}_1(\widehat{z}(t))}{\partial \widehat{z}(t)}\dot{\widehat{z}}(t).\end{aligned} \tag{83}$$

The inequality related to $e(t)$ and the third term of R.H.S of (81) is given as,

$$\begin{aligned}\left(e(t) - \frac{di(t)}{dt}\widehat{x}_4(\widehat{z}(t))\right)^2 &\geq 0, \\ \frac{1}{2}e^2(t) + \frac{1}{2}\left(\frac{di(t)}{dt}\right)^2\widehat{x}_4^2(\widehat{z}(t)) &\geq e(t)\frac{di(t)}{dt}\widehat{x}_4(\widehat{z}(t)).\end{aligned} \tag{84}$$

The inequality related to $e(t)$ and the fourth term of R.H.S of (81) is as follows,

$$\begin{aligned}\left(e(t) - i(t)\frac{\partial \widehat{x}_4(\widehat{z}(t))}{\partial \widehat{z}(t)}\dot{\widehat{z}}(t)\right)^2 &\geq 0, \\ \frac{1}{2}e^2(t) + \frac{1}{2}i^2(t)\left(\frac{\partial \widehat{x}_4(\widehat{z}(t))}{\partial \widehat{z}(t)}\dot{\widehat{z}}(t)\right)^2 &\geq e(t)i(t)\frac{\partial \widehat{x}_4(\widehat{z}(t))}{\partial \widehat{z}(t)}\dot{\widehat{z}}(t).\end{aligned} \tag{85}$$

The inequality related to $e(t)$ and the sixth term of R.H.S of (81) is given below,

$$\left(e(t)-i(t)\left(\frac{1}{\widehat{C}_{ts}(\widehat{z}(t))}+\frac{1}{\widehat{C}_{tl}(\widehat{z}(t))}\right)\right)^2\geq 0,$$

$$\frac{1}{2}e^2(t)+\frac{1}{2}i^2(t)\left(\frac{1}{\widehat{C}_{ts}(\widehat{z}(t))}+\frac{1}{\widehat{C}_{tl}(\widehat{z}(t))}\right)^2\geq e(t)i(t)\left(\frac{1}{\widehat{C}_{ts}(\widehat{z}(t))}+\frac{1}{\widehat{C}_{tl}(\widehat{z}(t))}\right). \quad (86)$$

From (82), (83), (84), (85), and (86), we get (87)

$$\frac{5}{2}e^2(t)+\frac{1}{2}\dot{y}^2(t)+\frac{1}{2}\left(\frac{\partial\widehat{x}_1(\widehat{z}(t))}{\partial\widehat{z}(t)}\dot{\widehat{z}}(t)\right)^2+\frac{1}{2}\left(\frac{di(t)}{dt}\right)^2\widehat{x}_4^2(\widehat{z}(t))+\frac{1}{2}i^2(t)\left(\frac{\partial\widehat{x}_4(\widehat{z}(t))}{\partial\widehat{z}(t)}\dot{\widehat{z}}(t)\right)^2$$
$$+\frac{1}{2}i^2(t)\left(\frac{1}{\widehat{C}_{ts}(\widehat{z}(t))}+\frac{1}{\widehat{C}_{tl}(\widehat{z}(t))}\right)^2\geq e(t)\dot{y}(t)-e(t)\frac{\partial\widehat{x}_1(\widehat{z}(t))}{\partial\widehat{z}(t)}\dot{\widehat{z}}(t)+e(t)\frac{di(t)}{dt}\widehat{x}_4(\widehat{z}(t))$$
$$+e(t)i(t)\frac{\partial\widehat{x}_4(\widehat{z}(t))}{\partial\widehat{z}(t)}\dot{\widehat{z}}(t)+e(t)i(t)\left(\frac{1}{\widehat{C}_{ts}(\widehat{z}(t))}+\frac{1}{\widehat{C}_{tl}(\widehat{z}(t))}\right). \quad (87)$$

Similarly, consider the following inequalities related to $e(t)$ and the first term of R.H.S of (81),

$$-\left(e(t)+\dot{y}(t)\right)^2\leq 0,$$
$$-\frac{1}{2}e^2(t)-\frac{1}{2}\dot{y}^2(t)\leq e(t)\dot{y}(t). \quad (88)$$

The inequality related to $e(t)$ and the second term of R.H.S of (81) is as follows,

$$-\left(e(t)-\frac{\partial\widehat{x}_1(\widehat{z}(t))}{\partial\widehat{z}(t)}\dot{\widehat{z}}(t)\right)^2\leq 0,$$
$$-\frac{1}{2}e^2(t)-\frac{1}{2}\left(\frac{\partial\widehat{x}_1(\widehat{z}(t))}{\partial\widehat{z}(t)}\dot{\widehat{z}}(t)\right)^2\leq -e(t)\frac{\partial\widehat{x}_1(\widehat{z}(t))}{\partial\widehat{z}(t)}\dot{\widehat{z}}(t). \quad (89)$$

The inequality related to $e(t)$ and the third term of R.H.S of (81) is given as,

$$-\left(e(t)+\frac{di(t)}{dt}\widehat{x}_4(\widehat{z}(t))\right)^2\leq 0,$$
$$-\frac{1}{2}e^2(t)-\frac{1}{2}\left(\frac{di(t)}{dt}\right)^2\widehat{x}_4^2(\widehat{z}(t))\leq e(t)\frac{di(t)}{dt}\widehat{x}_4(\widehat{z}(t)). \quad (90)$$

The inequality related to $e(t)$ and the fourth term of R.H.S of (81) is as follows,

$$-\left(e(t)+i(t)\frac{\partial\widehat{x}_4(\widehat{z}(t))}{\partial\widehat{z}(t)}\dot{\widehat{z}}(t)\right)^2\leq 0,$$

$$-\frac{1}{2}e^2(t)-\frac{1}{2}i^2(t)\left(\frac{\partial\widehat{x}_4(\widehat{z}(t))}{\partial\widehat{z}(t)}\dot{\widehat{z}}(t)\right)^2\leq e(t)i(t)\frac{\partial\widehat{x}_4(\widehat{z}(t))}{\partial\widehat{z}(t)}\dot{\widehat{z}}(t). \tag{91}$$

The inequality related to $e(t)$ and the sixth term of R.H.S of (81) is given below,

$$\begin{aligned}&-\left(e(t)+i(t)\left(\frac{1}{\widehat{C}_{ts}(\widehat{z}(t))}+\frac{1}{\widehat{C}_{tl}(\widehat{z}(t))}\right)\right)^2\leq 0,\\ &-\frac{1}{2}e^2(t)-\frac{1}{2}i^2(t)\left(\frac{1}{\widehat{C}_{ts}(\widehat{z}(t))}+\frac{1}{\widehat{C}_{tl}(\widehat{z}(t))}\right)^2\leq e(t)i(t)\left(\frac{1}{\widehat{C}_{ts}(\widehat{z}(t))}+\frac{1}{\widehat{C}_{tl}(\widehat{z}(t))}\right).\end{aligned} \tag{92}$$

From (88), (89), (90), (91), and (92), we get (93).

$$\begin{aligned}-\frac{5}{2}e^2(t)-\frac{1}{2}\dot{y}^2(t)-\frac{1}{2}\left(\frac{\partial\widehat{x}_1(\widehat{z}(t))}{\partial\widehat{z}(t)}\dot{\widehat{z}}(t)\right)^2-\frac{1}{2}\left(\frac{di(t)}{dt}\right)^2\widehat{x}_4^2(\widehat{z}(t))-\frac{1}{2}i^2(t)\left(\frac{\partial\widehat{x}_4(\widehat{z}(t))}{\partial\widehat{z}(t)}\dot{\widehat{z}}(t)\right)^2\\ -\frac{1}{2}i^2(t)\left(\frac{1}{\widehat{C}_{ts}(\widehat{z}(t))}+\frac{1}{\widehat{C}_{tl}(\widehat{z}(t))}\right)^2\leq e(t)\dot{y}(t)-e(t)\frac{\partial\widehat{x}_1(\widehat{z}(t))}{\partial\widehat{z}(t)}\dot{\widehat{z}}(t)+e(t)\frac{di(t)}{dt}\widehat{x}_4(\widehat{z}(t))\\ +e(t)i(t)\frac{\partial\widehat{x}_4(\widehat{z}(t))}{\partial\widehat{z}(t)}\dot{\widehat{z}}(t)+e(t)i(t)\left(\frac{1}{\widehat{C}_{ts}(\widehat{z}(t))}+\frac{1}{\widehat{C}_{tl}(\widehat{z}(t))}\right).\end{aligned} \tag{93}$$

In the following part, we will consider (81) with two cases of error, i.e. error being positive and negative, and utilize (87) and (93) for the positive and negative error cases respectively to show the convergence of error $e(t)$.

Case. 1. Consider $e(t)>0$, at some instant $t>t_0$. Multiplying (81) by $e(t)$ and using (65) gives

$$\begin{aligned}e(t)\dot{e}(t)\leq&e(t)\dot{y}(t)-e(t)\frac{\partial\widehat{x}_1(\widehat{z}(t))}{\partial\widehat{z}(t)}\dot{\widehat{z}}(t)+e(t)\frac{di(t)}{dt}\widehat{x}_4(\widehat{z}(t))+e(t)i(t)\frac{\partial\widehat{x}_4(\widehat{z}(t))}{\partial\widehat{z}(t)}\dot{\widehat{z}}(t)\\ &+e(t)i(t)\left(\frac{1}{\widehat{C}_{ts}(\widehat{z}(t))}+\frac{1}{\widehat{C}_{tl}(\widehat{z}(t))}\right)-(3+i(t))N(k(t))e^2(t),\end{aligned} \tag{94}$$

Now use (87) in (94) to get the following

$$\begin{aligned}e(t)\dot{e}(t)\leq&\frac{5}{2}e^2(t)+\frac{1}{2}\dot{y}^2(t)+\frac{1}{2}\left(\frac{\partial\widehat{x}_1(\widehat{z}(t))}{\partial\widehat{z}(t)}\dot{\widehat{z}}(t)\right)^2+\frac{1}{2}\left(\frac{di(t)}{dt}\right)^2\widehat{x}_4^2(\widehat{z}(t))\\ &+\frac{1}{2}i^2(t)\left(\frac{\partial\widehat{x}_4(\widehat{z}(t))}{\partial\widehat{z}(t)}\dot{\widehat{z}}(t)\right)^2+\frac{1}{2}i^2(t)\left(\frac{1}{\widehat{C}_{ts}(\widehat{z}(t))}+\frac{1}{\widehat{C}_{tl}(\widehat{z}(t))}\right)^2\\ &-(3+i(t))N(k(t))e^2(t).\end{aligned} \tag{95}$$

Since $\frac{d}{dt}\left(\frac{1}{2}e^2(t)\right) = e(t)\dot{e}(t)$, thus integrating (95) from t_0 to t, and using (63) provides

$$\begin{aligned}\frac{1}{2}e^2(t) \leq & \frac{5}{2}(k(t)-k(t_0)) + \frac{1}{2}\int_{t_0}^{t}\dot{y}^2(\tau)d\tau + \frac{1}{2}\int_{t_0}^{t}\left(\frac{\partial \widehat{x}_1(\widehat{z}(\tau))}{\partial \widehat{z}(\tau)}\dot{\widehat{z}}(\tau)\right)^2 d\tau \\ & + \frac{1}{2}\int_{t_0}^{t}\left(\frac{di(\tau)}{d\tau}\right)^2 \widehat{x}_4^2(\widehat{z}(\tau))d\tau + \frac{1}{2}\int_{t_0}^{t} i^2(\tau)\left(\frac{\partial \widehat{x}_4(\widehat{z}(\tau))}{\partial \widehat{z}(\tau)}\dot{\widehat{z}}(\tau)\right)^2 d\tau \\ & + \frac{1}{2}\int_{t_0}^{t} i^2(\tau)\left(\frac{1}{\widehat{C}_{ts}(\widehat{z}(\tau))} + \frac{1}{\widehat{C}_{tl}(\widehat{z}(\tau))}\right)^2 d\tau - 3\int_{t_0}^{t} N(k(\tau))\dot{k}(\tau)d\tau \\ & - \int_{t_0}^{t} i(\tau)N(k(\tau))\dot{k}(\tau)d\tau,\end{aligned} \tag{96}$$

Let $\widetilde{k}(t) = k(t) - k(t_0)$. Dividing (96) by $\widetilde{k}(t)$ and recognizing that $\dot{\widehat{z}}(t) = -\dfrac{i(t)}{C_c}$, $\int_{t_0}^{t} N(k(\tau))\dot{k}(\tau)d\tau = \int_{k(t_0)}^{k(t)} N(k)dk$ and $\int_{t_0}^{t} i(\tau)N(k(\tau))\dot{k}(\tau)d\tau = i(t)\int_{k(t_0)}^{k(t)} N(k)dk$ gives

$$\begin{aligned}\frac{e^2(t)}{2\widetilde{k}(t)} \leq & \frac{5}{2} + \frac{1}{2\widetilde{k}(t)}\int_{t_0}^{t}\dot{y}^2(\tau)d\tau + \frac{1}{2\widetilde{k}(t)}\int_{t_0}^{t}\left(\frac{i(\tau)}{C_c}\frac{\partial \widehat{x}_1(\widehat{z}(\tau))}{\partial \widehat{z}(\tau)}\right)^2 d\tau \\ & + \frac{1}{2\widetilde{k}(t)}\int_{t_0}^{t}\left(\frac{di(\tau)}{d\tau}\right)^2 \widehat{x}_4^2(\widehat{z}(\tau))d\tau + \frac{1}{2\widetilde{k}(t)}\int_{t_0}^{t}\left(\frac{i^2(\tau)}{C_c}\frac{\partial \widehat{x}_4(\widehat{z}(\tau))}{\partial \widehat{z}(\tau)}\right)^2 d\tau \\ & + \frac{1}{2\widetilde{k}(t)}\int_{t_0}^{t} i^2(\tau)\left(\frac{1}{\widehat{C}_{ts}(\widehat{z}(\tau))} + \frac{1}{\widehat{C}_{tl}(\widehat{z}(\tau))}\right)^2 d\tau - \frac{3}{\widetilde{k}(t)}\int_{k(t_0)}^{k(t)} N(k)dk \\ & - \frac{i(t)}{\widetilde{k}(t)}\int_{k(t_0)}^{k(t)} N(k)dk.\end{aligned} \tag{97}$$

The equation (97) is the result established for $e(t) > 0$ case. Now, the Case 2, i.e. for $e(t) < 0$, is considered and an inequality having a form similar to (97) will be derived. The results of both Case 1 and Case 2 will be discussed together after establishing the required equation for Case 2.

Case. 2. Consider $e(t) < 0$, at some instant $t > t_0$. Multiplying (81) by $e(t)$ and using (65) gives

$$\begin{aligned}e(t)\dot{e}(t) \geq & e(t)\dot{y}(t) - e(t)\frac{\partial \widehat{x}_1(\widehat{z}(t))}{\partial \widehat{z}(t)}\dot{\widehat{z}}(t) + e(t)\frac{di(t)}{dt}\widehat{x}_4(\widehat{z}(t)) + e(t)i(t)\frac{\partial \widehat{x}_4(\widehat{z}(t))}{\partial \widehat{z}(t)}\dot{\widehat{z}}(t) \\ & + e(t)i(t)\left(\frac{1}{\widehat{C}_{ts}(\widehat{z}(t))} + \frac{1}{\widehat{C}_{tl}(\widehat{z}(t))}\right) - (3 + i(t))N(k(t))e^2(t),\end{aligned} \tag{98}$$

Now use (93) in (98) to get the following

$$\begin{aligned} e(t)\dot{e}(t) \geq & -\frac{5}{2}e^2(t) - \frac{1}{2}\dot{y}^2(t) - \frac{1}{2}\left(\frac{\partial \widehat{x}_1(\widehat{z}(t))}{\partial \widehat{z}(t)}\dot{\widehat{z}}(t)\right)^2 - \frac{1}{2}\left(\frac{di(t)}{dt}\right)^2 \widehat{x}_4^2(\widehat{z}(t)) \\ & - \frac{1}{2}i^2(t)\left(\frac{\partial \widehat{x}_4(\widehat{z}(t))}{\partial \widehat{z}(t)}\dot{\widehat{z}}(t)\right)^2 - \frac{1}{2}i^2(t)\left(\frac{1}{\widehat{C}_{ts}(\widehat{z}(t))} - \frac{1}{\widehat{C}_{tl}(\widehat{z}(t))}\right)^2 \\ & - (3+i(t))N(k(t))e^2(t). \end{aligned} \tag{99}$$

Since $\frac{d}{dt}\left(\frac{1}{2}e^2(t)\right) = e(t)\dot{e}(t)$, thus integrating (99) from t_0 to t, and using (63) provides

$$\begin{aligned} \frac{1}{2}e^2(t) \geq & -\frac{5}{2}(k(t)-k(t_0)) - \frac{1}{2}\int_{t_0}^{t}\dot{y}^2(\tau)d\tau - \frac{1}{2}\int_{t_0}^{t}\left(\frac{\partial \widehat{x}_1(\widehat{z}(\tau))}{\partial \widehat{z}(\tau)}\dot{\widehat{z}}(\tau)\right)^2 d\tau \\ & - \frac{1}{2}\int_{t_0}^{t}\left(\frac{di(\tau)}{d\tau}\right)^2 \widehat{x}_4^2(\widehat{z}(\tau))d\tau - \frac{1}{2}\int_{t_0}^{t} i^2(\tau)\left(\frac{\partial \widehat{x}_4(\widehat{z}(\tau))}{\partial \widehat{z}(\tau)}\dot{\widehat{z}}(\tau)\right)^2 d\tau \\ & - \frac{1}{2}\int_{t_0}^{t} i^2(\tau)\left(\frac{1}{\widehat{C}_{ts}(\widehat{z}(\tau))} - \frac{1}{\widehat{C}_{tl}(\widehat{z}(\tau))}\right)^2 d\tau - 3\int_{t_0}^{t} N(k(\tau))\dot{k}(\tau)d\tau \\ & - \int_{t_0}^{t} i(\tau)N(k(\tau))\dot{k}(\tau)d\tau, \end{aligned} \tag{100}$$

Let $\widetilde{k}(t) = k(t) - k(t_0)$. Dividing (100) by $\widetilde{k}(t)$ and recognizing that $\dot{\widehat{z}}(t) = -\frac{i(t)}{C_c}$, $\int_{t_0}^{t} N(k(\tau))\dot{k}(\tau)d\tau = \int_{k(t_0)}^{k(t)} N(k)dk$ and $\int_{t_0}^{t} i(\tau)N(k(\tau))\dot{k}(\tau)d\tau = i(t)\int_{k(t_0)}^{k(t)} N(k)dk$ gives us

$$\begin{aligned} \frac{e^2(t)}{2\widetilde{k}(t)} \geq & -\frac{5}{2} - \frac{1}{2\widetilde{k}(t)}\int_{t_0}^{t}\dot{y}^2(\tau)d\tau - \frac{1}{2\widetilde{k}(t)}\int_{t_0}^{t}\left(\frac{i(\tau)}{C_c}\frac{\partial \widehat{x}_1(\widehat{z}(\tau))}{\partial \widehat{z}(\tau)}\right)^2 d\tau \\ & - \frac{1}{2\widetilde{k}(t)}\int_{t_0}^{t}\left(\frac{di(\tau)}{d\tau}\right)^2 \widehat{x}_4^2(\widehat{z}(\tau))d\tau - \frac{1}{2\widetilde{k}(t)}\int_{t_0}^{t}\left(\frac{i^2(\tau)}{C_c}\frac{\partial \widehat{x}_4(\widehat{z}(\tau))}{\partial \widehat{z}(\tau)}\right)^2 d\tau \\ & - \frac{1}{2\widetilde{k}(t)}\int_{t_0}^{t} i^2(\tau)\left(\frac{1}{\widehat{C}_{ts}(\widehat{z}(\tau))} - \frac{1}{\widehat{C}_{tl}(\widehat{z}(\tau))}\right)^2 d\tau - \frac{3}{\widetilde{k}(t)}\int_{k(t_0)}^{k(t)} N(k)dk \\ & - \frac{i(t)}{\widetilde{k}(t)}\int_{k(t_0)}^{k(t)} N(k)dk, \end{aligned} \tag{101}$$

Notice that the (101) and (97) have similar form. The differences between them are the sign of inequalities and the terms on R.H.S of (101) are negative. The reciprocal of (101) provides the following

$$\begin{aligned}\frac{2\widetilde{k}(t)}{e^2(t)} \leq \Big[&-\frac{5}{2} - \frac{1}{2\widetilde{k}(t)}\int_{t_0}^{t}\dot{y}^2(\tau)d\tau - \frac{1}{2\widetilde{k}(t)}\int_{t_0}^{t}\left(\frac{i(\tau)}{C_c}\frac{\partial\widehat{x}_1(\widehat{z}(\tau))}{\partial\widehat{z}(\tau)}\right)^2 d\tau \\ &- \frac{1}{2\widetilde{k}(t)}\int_{t_0}^{t}\left(\frac{di(\tau)}{d\tau}\right)^2\widehat{x}_4^2(\widehat{z}(\tau))d\tau - \frac{1}{2\widetilde{k}(t)}\int_{t_0}^{t}\left(\frac{i^2(\tau)}{C_c}\frac{\partial\widehat{x}_4(\widehat{z}(\tau))}{\partial\widehat{z}(\tau)}\right)^2 d\tau \\ &- \frac{1}{2\widetilde{k}(t)}\int_{t_0}^{t} i^2(\tau)\left(\frac{1}{\widehat{C}_{ts}(\widehat{z}(\tau))} - \frac{1}{\widehat{C}_{tl}(\widehat{z}(\tau))}\right)^2 d\tau - \frac{3}{\widetilde{k}(t)}\int_{k(t_0)}^{k(t)} N(k)dk \\ &- \frac{i(t)}{\widetilde{k}(t)}\int_{k(t_0)}^{k(t)} N(k)dk\Big]^{-1}.\end{aligned} \tag{102}$$

The battery can be discharged for a certain interval of time, say $T > t_0$. After $t > T$, the following occurs: $i(t) = 0$, $y(t) = 0$, $z(t) = 0$. Therefore, as $t \to \infty$, $\dot{y}(t) = 0$, and $\frac{d(i)}{dt} = 0$. Thus, from these facts, we can conclude that the terms $\int_{t_0}^{t}\dot{y}^2(\tau)d\tau$, $\int_{t_0}^{t}\left(\frac{i(\tau)}{C_c}\frac{\partial\widehat{x}_1(\widehat{z}(\tau))}{\partial\widehat{z}(\tau)}\right)^2 d\tau$, $\int_{t_0}^{t}\left(\frac{di(\tau)}{d\tau}\right)^2\widehat{x}_4^2(\widehat{z}(\tau))d\tau$, $\int_{t_0}^{t}\left(\frac{i^2(\tau)}{C_c}\frac{\partial\widehat{x}_4(\widehat{z}(\tau))}{\partial\widehat{z}(\tau)}\right)^2 d\tau$, and $\frac{1}{2}\int_{t_0}^{t} i^2(\tau)\times\left(\frac{1}{\widehat{C}_{ts}(\widehat{z}(\tau))} - \frac{1}{\widehat{C}_{tl}(\widehat{z}(\tau))}\right)^2 d\tau$ are bounded in (97) and (102) as $t \to \infty$. Now suppose that $k(t) \to \infty$ as $t \to \infty$, then the above discussion lets us write as $t \to \infty$ for (97),

$$\lim_{t\to\infty}\frac{e^2(t)}{2\widetilde{k}(t)} \leq \frac{5}{2} - \frac{3}{\widetilde{k}(t)}\int_{k(t_0)}^{k(t)} N(k)dk - \frac{i(t)}{\widetilde{k}(t)}\int_{k(t_0)}^{k(t)} N(k)dk, \tag{103}$$

And from (102), we can write the following

$$\lim_{t\to\infty}\frac{2\widetilde{k}(t)}{e^2(t)} \leq \frac{1}{-\frac{5}{2} - \frac{3}{\widetilde{k}(t)}\int_{k(t_0)}^{k(t)} N(k)dk - \frac{i(t)}{\widetilde{k}(t)}\int_{k(t_0)}^{k(t)} N(k)dk}. \tag{104}$$

Now if $k(t) \to \infty$ as $t \to \infty$ then by the definition of a Nussbaum function in (12), the term $+\frac{1}{k(t)-k(t_0)}\int_{k(t_0)}^{k(t)} N(k)dk$, in (103) and (104), can take values approaching $+\infty$, and therefore this will violate the positiveness of the LHS of (103) and (104). By this contradiction, the assumption that $k(t) \to \infty$ is false and therefore $k(t)$ is bounded. However $\dot{k}(t)$ is an increasing function by definition and $k(t)$ is bounded, this implies that $k(t) \to k_\infty$ as $t \to \infty$ which further implies that $\dot{k}(t) \to 0$ as $t \to \infty$, i.e. $e^2(t) \to 0$ as $t \to \infty$ or $e(t) \to 0$ as $t \to \infty$, i.e. $y(t) \to \widehat{y}(t)$ as $t \to \infty$. Consider now that $y(t) \to \widehat{y}(t)$, which implies that

$$E_o(z(t)) - x_2(t) - x_3(t) - i(t)R_s(z(t)) = \widehat{x}_1(\widehat{z}(t)) - \widehat{x}_2(t) - \widehat{x}_3(t) - i(t)\widehat{x}_4(\widehat{z}(t)), \tag{105}$$

$$\begin{bmatrix} 1 & -1 & -1 & -1 \end{bmatrix} \left(\begin{bmatrix} E_o(z(t)) \\ x_2(t) \\ x_3(t) \\ i(t)R_s(z(t)) \end{bmatrix} - \begin{bmatrix} \widehat{x}_1(\widehat{z}(t)) \\ \widehat{x}_2(t) \\ \widehat{x}_2(t) \\ i(t)\widehat{x}_4(\widehat{z}(t)) \end{bmatrix} \right) = 0 \tag{106}$$

The above implies that $\widehat{x}_1(\widehat{z}(t)) = E_o(z(t))$, and $\widehat{x}_4(\widehat{z}(t)) = R_s(z(t))$. Equation (106) also implies $\widehat{x}_2(t) = x_2(t)$, and $\widehat{x}_3(t) = x_3(t)$, which means that $\dot{\widehat{x}}_2(t) = \dot{x}_2(t)$, and $\dot{\widehat{x}}_3(t) = \dot{x}_3(t)$. Let us consider $\dot{\widehat{x}}_2(t) = \dot{x}_2(t)$, the following can be written using (46) and (52)

$$-\frac{\widehat{x}_2(t)}{\widehat{R}_{ts}(\widehat{z}(t))\widehat{C}_{ts}(\widehat{z}(t))} + u(t) = -\frac{x_2(t)}{R_{ts}(z(t))C_{ts}(z(t))} + \frac{i(t)}{C_{ts}(z(t))} \tag{107}$$

Since it is proved above that $e(t) \to 0$ as $t \to \infty$, $u(t) = -N(k(t))e(t)$, $i(t)$ are infinitesimally small, and $\widehat{x}_2(t) = x_2(t)$, therefore (107) provides

$$\widehat{R}_{ts}(\widehat{z}(t))\widehat{C}_{ts}(\widehat{z}(t)) = R_{ts}(z(t))C_{ts}(z(t)) \tag{108}$$

Considering $\dot{\widehat{x}}_3(t) = \dot{x}_3(t)$ and following the exact same arguments as above, it is similarly possible to conclude that $\widehat{R}_{tl}(\widehat{z}(t))\widehat{C}_{tl}(\widehat{z}(t)) = R_{tl}(z(t))C_{tl}(z(t))$. This completes the proof. □

Remark 1. The results proved in *Theorem 3.2* hold valid provided that the battery discharging current remains small, i.e. $i(t) \to 0$ as $t \to \infty$ and the conditions in *Lemma 3.1* are satisfied. Next, we will show the convergence of Li-ion battery model parameters $\widehat{r}_n(t)$ as $t \to \infty$, where $n \in \{1, 2, \cdots, 21\} \backslash \{3, 21\}$.

Lemma 3.3. *Suppose $\lambda_{xn}, \lambda_{yn}, r_{nu}$ and r_{nl} are the positive real numbers for $n \in \{1, 2, \cdots, 21\} \backslash \{3, 21\}$. **If** the conditions required for Theorem 3.2 are satisfied, **then** $\widehat{r}_n(t)$ converges to some constant r_∞ as $t \to \infty$.*

Proof. The solution of (66) with $e^2(t) + \lambda_{xn} r_{nu} + \lambda_{yn} r_{nl}$ as an input is as follows

$$\begin{aligned} \widehat{r}_n(t) = \widehat{r}_n(t_0) e^{-(\lambda_{xn}+\lambda_{yn})t} + \left((\lambda_{xn} r_{nu} + \lambda_{yn} r_{nl}) \times \int_{t_0}^{t} e^{-(\lambda_{xn}+\lambda_{yn})\tau} d\tau \right) \\ + \int_{t_0}^{t} e^2(t-\tau) e^{-(\lambda_{xn}+\lambda_{yn})\tau} d\tau \end{aligned} \tag{109}$$

Because $e^{-(\lambda_{xn}+\lambda_{yn})t} \to 0$ as $t \to \infty$, and from *Theorem 3.2*, $e(t) \to 0$ as $t \to \infty$. So $e^{-(\lambda_{xn}+\lambda_{yn})t}$ and $e^2(t)$ remain positive and approach to zero as $t \to \infty$. Thus, on the R.H.S of (109), the first term will go to zero, the second and third terms will be bounded and approach to a constant term as $t \to \infty$. Hence, $\widehat{r}_n(t)$ converges as $t \to \infty$ for $n \in \{1,2,\cdots,21\}\backslash\{3,21\}$. □

3.3.1. Accuracy analysis of some estimated Li-ion battery model parameters. In this section, we will first demonstrate that the parameters of $\widehat{x}_1(\widehat{z}(t))$, and $\widehat{x}_4(\widehat{z}(t))$ converges to their actual values based on the results derived in *Theorem 3.2*. Afterward, the accuracy analysis of $R_{ts}(\widehat{z}(t))$, and $R_{tl}(\widehat{z}(t))$ will lead us to show the convergence of these circuit elements parameters to their actual values. As per the results derived in *Theorem 3.2*, $\widehat{x}_1(\widehat{z}(t)) = x_1(z(t))$, and $\widehat{x}_4(\widehat{z}(t)) = x_4(z(t))$ as $t \to \infty$. Using (38), (43), (56), and (61), the above two results can be written as follows

$$-\widehat{r}_1 e^{-\widehat{r}_2\widehat{z}} + \widehat{r}_3 + \widehat{r}_4\widehat{z} - \widehat{r}_5\widehat{z}^2 + \widehat{r}_6\widehat{z}^3 = -r_1 e^{-r_2 z} + r_3 + r_4 z - r_5 z^2 + r_6 z^3, \tag{110}$$

$$\widehat{r}_{19} e^{-\widehat{r}_{20}\widehat{z}} + \widehat{r}_{21} = r_{19} e^{-r_{20} z} + r_{21}. \tag{111}$$

Since $\widehat{z}(t) = z(t)$, thus the equation (110) can be rewritten as

$$\begin{bmatrix} (-\widehat{r}_1 e^{-\widehat{r}_2\widehat{z}} + r_1 e^{-r_2 z}) & (\widehat{r}_3 - r_3) & (\widehat{r}_4 - r_4) & (-\widehat{r}_5 + r_5) & (\widehat{r}_6 - r_6) \end{bmatrix} \begin{bmatrix} 1 \\ 1 \\ z(t) \\ z^2(t) \\ z^3(t) \end{bmatrix} = 0, \tag{112}$$

Similarly, the equation (111) can be represented by the following

$$\begin{bmatrix} (\widehat{r}_{19} e^{-\widehat{r}_{20}\widehat{z}} - r_{19} e^{-r_{20} z}) & (\widehat{r}_{21} - r_{21}) \end{bmatrix} \begin{bmatrix} 1 \\ 1 \end{bmatrix} = 0. \tag{113}$$

At $\widehat{z}(t) \to 0$ as $t \to \infty$, and $\widehat{z}(t) \neq 0$ as $t \to \infty$, the equation (112) implies that $\widehat{r}_1 \to r_1$, $\widehat{r}_3 \to r_3$, $\widehat{r}_4 \to r_4$, $\widehat{r}_5 \to r_5$, and $\widehat{r}_6 \to r_6$. Using $\widehat{r}_1 \to r_1$ in $\widehat{r}_1 e^{-\widehat{r}_2\widehat{z}} = r_1 e^{-r_2 z}$

provides $\widehat{r}_2 \to r_2$. Similarly, using the same argument, we can infer from (113) that $\widehat{r}_{19} \to r_{19}$, $\widehat{r}_{20} \to r_{20}$ and $\widehat{r}_{21} \to r_{21}$. Now consider $\widehat{C}_{ts}(\widehat{z}(t)) = C_{ts}(z(t)) + \Delta$, where Δ is the estimation error due to inappropriate selection of parameters such as $\lambda_{xn}, \lambda_{yn}, r_{nu}$ and r_{nl} for $n \in \{1,2,\cdots,21\}\backslash\{3,21\}$, and violation of condition $i(t) \to \infty$. Since $\widehat{z}(t) = z(t)$, and $\widehat{R}_{ts}(z(t))\widehat{C}_{ts}(z(t)) = R_{ts}(z(t))C_{ts}(z(t))$, from *Theorem 3.2*, leads to the following

$$\widehat{R}_{ts}(z(t)) = \frac{R_{ts}(z(t))C_{ts}(z(t))}{C_{ts}(z(t)) + \Delta} = \frac{R_{ts}(z(t))}{1 + \dfrac{\Delta}{C_{ts}(z(t))}}. \tag{114}$$

Because the value of $C_{ts}(z(t))$ ranges in the order of hundred or thousand Farads, the magnitude of Δ is expected to be much smaller than the magnitude of $C_{ts}(z(t))$. The above assumption results in $\widehat{R}_{ts}(z(t)) \to R_{ts}(z(t))$ from (114). Now using (39) and (57), we can write the following

$$\begin{bmatrix} (\widehat{r}_7 e^{-\widehat{r}_8 \widehat{z}} - r_7 e^{-r_7 z}) & (\widehat{r}_9 - r_9) \end{bmatrix} \begin{bmatrix} 1 \\ 1 \end{bmatrix} = 0. \tag{115}$$

Recalling the same argument that is described earlier for the convergence of estimated parameters, it is possible to present that $\widehat{r}_7 \to r_7$, $\widehat{r}_8 \to r_8$, and $\widehat{r}_9 \to r_9$.

Similarly, by considering $\widehat{R}_{tl}(z(t))\widehat{C}_{tl}(z(t)) = R_{tl}(z(t))C_{tl}(z(t))$ from *Theorem 3.2*, we can conclude that $\widehat{R}_{tl}(z(t)) \to R_{tl}(z(t))$ and $\widehat{r}_{10} \to r_{10}$, $\widehat{r}_{11} \to r_{11}$, and $\widehat{r}_{12} \to r_{12}$. The accuracy analysis shows the convergence of *fifteen* parameters to their actual values except the parameters of C_{ts} and C_{tl}, which are due to the aforementioned reasons. The results derived in this section will be discussed and validated through simulation in the next section.

3.4. Simulation Results

The mathematical proof for the convergence of Li-ion battery model circuit elements and parameters to their actual values is supported by the MATLAB simulation results. The experimentally determined Li-ion battery model parameters by Chen and Mora in [13] are used to validate the accuracy of estimated circuit elements and their parameters. We use the same 4.1 V, 850 mAh Li-ion battery model, that was utilized in

[13], for adaptive estimation process. However, to reduce the simulation time to almost one-third, the battery capacity of 270 mAh is selected in the simulation. Note that the battery parameters obtained in [13] are constant and independent of battery SoC, battery capacity, charging and discharging current, and battery temperature. Since these parameters influence the shape of voltage vs. time profile, therefore the reduction of battery capacity does not change the battery dynamics. The parameters adaptation process begins with the appropriate choice of some constraints. These constraints include the selection of upper and lower bounds and their respective confidence levels for each parameter, described in Table 3.1, and initial values of state variables, provided in algorithm 2. Note that selection of upper and lower bounds and their respective confidence levels for each parameter does not require a strenuous effort from a user who has some knowledge and experience of Li-ion batteries. Whereas, the selection rules for initial values of state variables have already been provided in algorithm 2. Since the accurate convergence of estimated battery parameters and state variables also depends upon the magnitude of the current, as per Theorem 3.2. Therefore, the battery discharge current needs to be kept very small during the adaptation process.

Algorithm 2 is run in MATLAB for real-time parameters estimation of a Li-ion battery, and the results are provided in Table 3.1. Note that each estimated parameter was recorded in a separate array during the adaptation process, i.e. the estimated parameters results were recorded in *twenty-one* arrays. We took an average of each array which gave us average estimated parameter values that are tabulated in Table 3.1. It can be inferred from Table 3.1 results that the estimation error is less than 5% for most of the estimated parameters. Note that appropriate selection of upper and lower bounds can further reduce the estimation error of all parameters. The estimated parameters are then employed to calculate circuit elements variation with SoC. During the adaptation process, the estimates of circuit elements are illustrated in Figure 3.3 and Figure 3.4. The Chen and Mora's results are classified as *actual values* in the simulation results. In Figure 3.3 and Figure 3.4, the adaptation of each circuit element along with the corresponding estimation error is shown. Excluding R_{ts}, all the circuit elements converged within 10% estimation error. As mentioned above, the estimation error of R_{ts} and other circuit elements can be further improved by fixing the upper and lower bounds prop-

Table 3.1: Simulation results of a 4.1 V, 270 mAh Li-ion battery model parameters.

Parameter	Upper bound (r_{nu})	Lower bound (r_{nl})	λ_{x_n}	λ_{y_n}	Initial value	Estimated value	Desired value	Estimation error (%)
$\widehat{r}_1$	4	0.1	20	65	100	1.0176	1.031	1.3
$\widehat{r}_2$	50	25	50	70	2000	35.4167	35	1.2
$\widehat{r}_3$	–	–	–	–	–	3.6855	3.685	0.014
$\widehat{r}_4$	0.5	0.1	30	70	50	0.22	0.2156	2.04
$\widehat{r}_5$	0.5	0.01	20	70	30	0.1189	0.1178	0.934
$\widehat{r}_6$	0.5	0.1	60	50	200	0.3182	0.3201	0.594
$\widehat{r}_7$	1	0.1	50	50	180	0.3002	0.3208	6.42
$\widehat{r}_8$	50	10	50	50	1700	30	29.14	2.95
$\widehat{r}_9$	0.1	0.01	50	50	240	0.055	0.04669	17.79
$\widehat{r}_{10}$	10	1	70	50	3600	6.2533	6.603	5.3
$\widehat{r}_{11}$	200	100	50	50	9300	149.9	155.2	3.41
$\widehat{r}_{12}$	0.1	0.01	50	50	264	0.0553	0.04984	10.95
$\widehat{r}_{13}$	1000	500	60	55	50000	760.869	752.9	1.06
$\widehat{r}_{14}$	30	1	5	10	1000	10.6672	13.51	21.04
$\widehat{r}_{15}$	800	500	80	50	50000	684.62	703.6	2.69
$\widehat{r}_{16}$	7000	5000	10	10	50000	6000	6056	0.92
$\widehat{r}_{17}$	50	5	50	50	1000	27.5	27.12	1.40
$\widehat{r}_{18}$	5000	3000	50	50	50000	4500	4475	0.558
$\widehat{r}_{19}$	0.5	0.01	20	50	60	0.15	0.1562	3.97
$\widehat{r}_{20}$	50	15	30	80	1200	24.5455	24.37	0.72
$\widehat{r}_{21}$	–	–	–	–	–	0.0826	0.07446	10.93

erly. It is worth to notice that estimation error of circuit elements is higher when SoC approaches to zero. It is explained in [6] that below certain SoC level, Li-ion battery becomes unstable and causes the estimated parameters to diverge from their actual values. Therefore, we estimated the battery parameters until the SoC approaches 7% value. Whereas, the results in Figure 3.3 are displayed till SoC approaches 1%. Furthermore, the comparison of actual and estimated terminal voltages during the adaptation process is shown in Figure 3.5. In Figure 3.5, the estimated terminal voltage converged to the actual voltage with very low estimation error i.e. about 10e-4. The zoomed in view of Figure 3.5 is shown in Figure 3.6, which shows the quick convergence of estimated terminal voltage to the actual 4.1 V, 275 mAh Li-ion battery terminal voltage during the adaptation process.

To validate the estimated parameters results against the parameters obtained by Chen and Mora in [13], we construct two 4.1 V, 275 mAh Li-ion battery models. The first model contains the parameters estimated via our proposed method, whereas the

second model holds the parameters provided by Chen and Mora in [13]. Each battery model is subjected to a random discharge current as shown in Figure 3.7a, and their terminal and open circuit voltages are compared in Figure 3.7c and Figure 3.7d respectively. The low estimation error in both terminal and open circuit voltage profiles in Figure 3.7c and Figure 3.7d show the accuracy of our proposed battery model parameters estimation strategy. Since the battery model parameters can be utilized for accurate

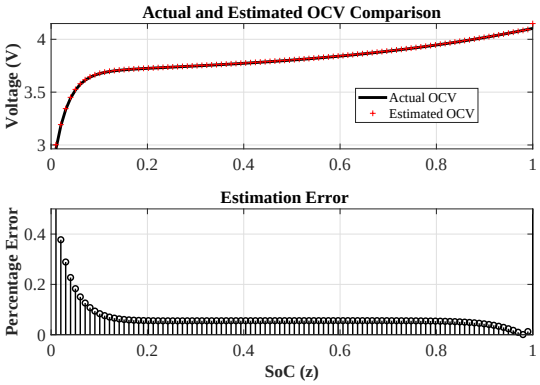

(a) Open circuit voltage E_o vs SoC.

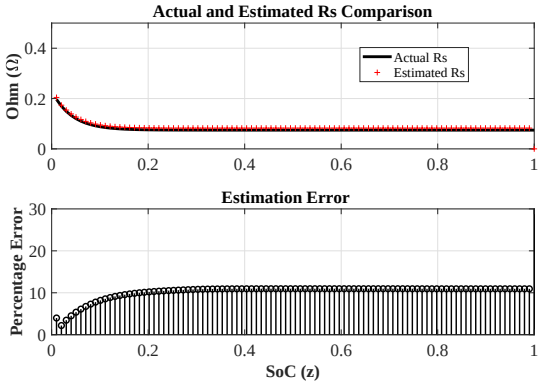

(b) Series resistance R_s vs SoC.

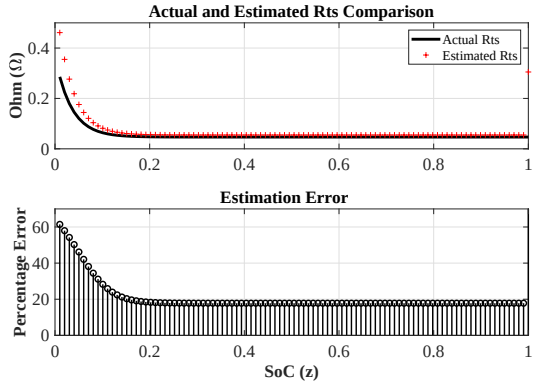

(c) Short term resistance R_{ts} vs SoC.

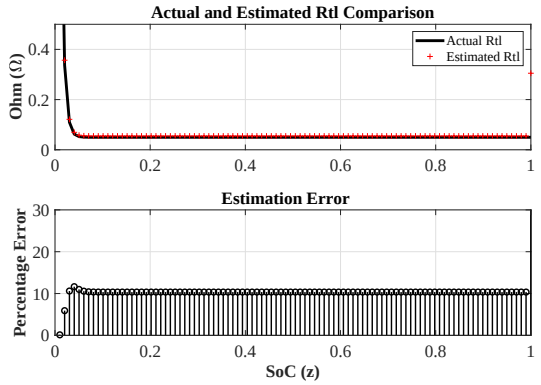

(d) Long term resistance R_{tl} vs SoC.

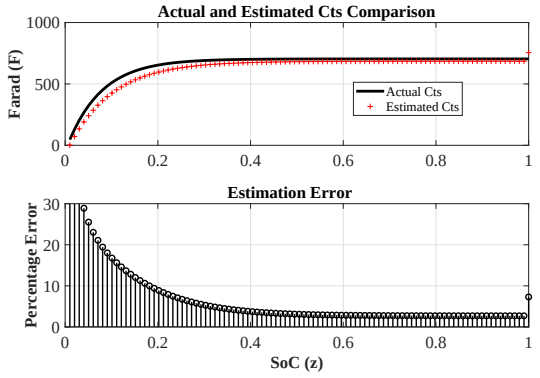

(e) Short term capacitance C_{ts} vs SoC.

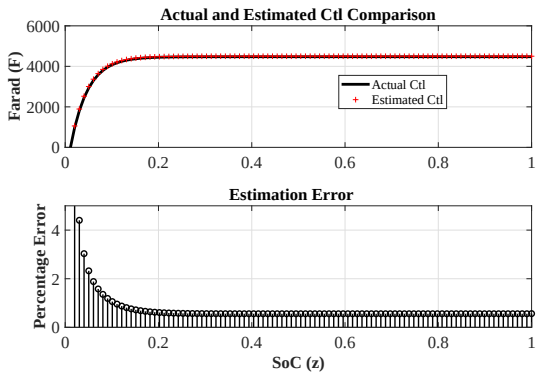

(f) Long term capacitance C_{tl} vs SoC.

Figure 3.3: Comparison of actual and estimated circuit elements of a Li-ion battery model during adaptive estimation process.

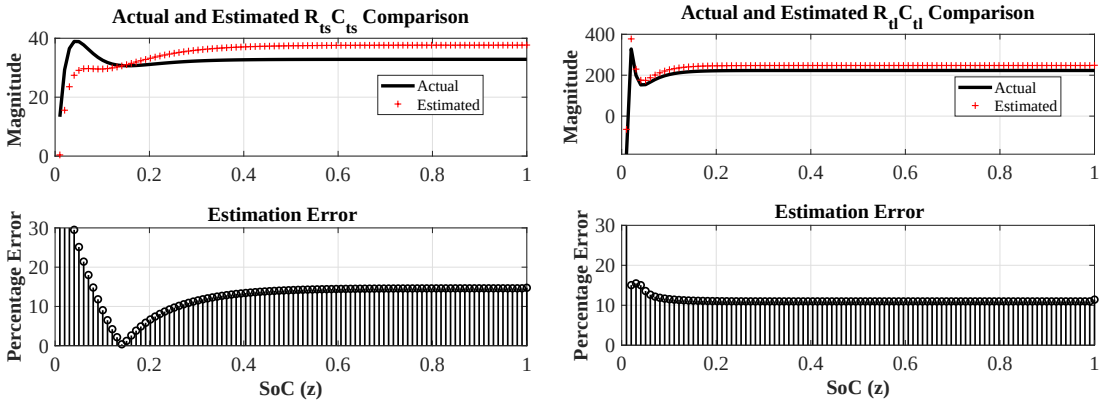

(a) $R_{ts}C_{ts}$ vs SoC. (b) $R_{tl}C_{tl}$ vs SoC.

Figure 3.4: Comparison of actual and estimated $R_{ts}C_{ts}$ and $R_{tl}C_{tl}$ during adaptive estimation process.

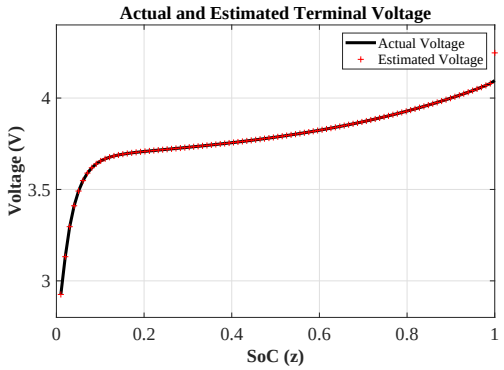

Figure 3.5: Li-ion battery terminal voltage vs SoC.

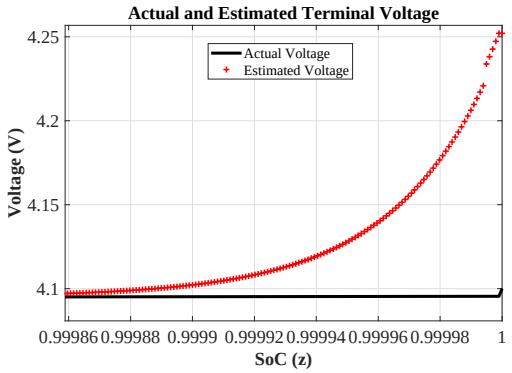

Figure 3.6: Zoomed in view of Figure 3.5.

calculation of SoC. Therefore, we used the estimated parameters to determine the SoC when the battery is subjected to a random discharge current of Figure 3.7a. As explained in [2], the SoC was estimated via interpolation method using open circuit voltage vs. SoC information of adaptive process. The estimated SoC in Figure 3.7b is compared

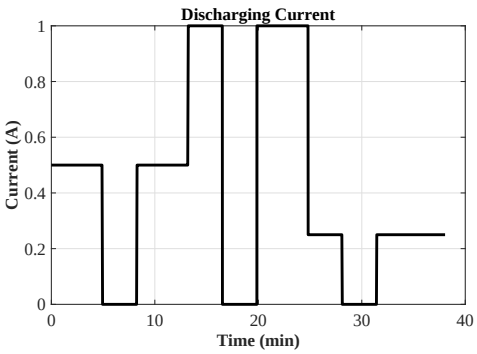

(a) Variable current drawn from Li-ion battery.

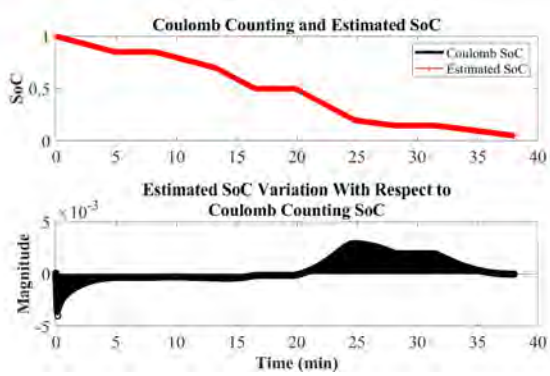

(b) Analysis of estimated SoC using interpolation via proposed technique with Coulomb counting method.

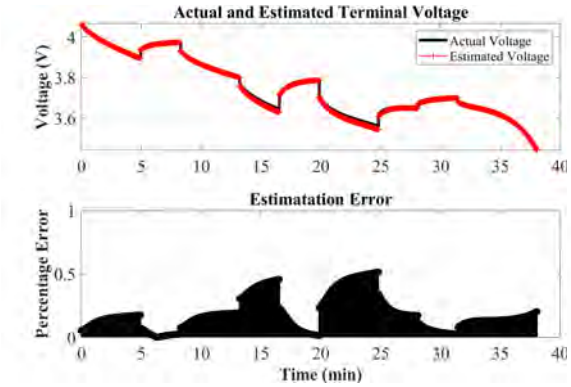

(c) Comparison of actual and estimated terminal voltage.

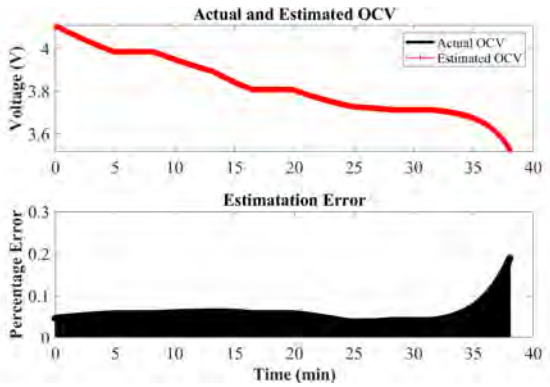

(d) Comparison of actual and estimated open circuit voltage.

.

Figure 3.7: Validation of estimated terminal voltage and OCV of Li-ion battery, and comparison of estimated SoC with Coulomb counting SOC when the battery is subjected to variable load.

with the conventional Coulomb counting method and thus reveals the deviation of estimated SoC from Coulomb counting. This deviation is observed when a small current is drawn from the battery, i.e. after 25 seconds in Figure 3.7b. Due to the division by the battery Ah capacity value in equation (44), Coulomb counting method does not capture small details of SoC when a low current is drawn from a battery, so the proposed methodology of parameters estimation can help improve the SOC estimation accuracy by using the OCV curve, whose parameters can be found using the work presented in this thesis.

Chapter 4. Experimental Validation and Real-Time Implementation of UAS Based Modified APE Method

In the first part of this chapter, the modified APE strategy is rigorously verified experimentally on a 22.2 V, 6.6 Ah Li-ion battery. The results of modified APE strategy are comprehensively compared with the existing APE results and with measured terminal voltage of a Li-ion battery. Also, the comparative study is further enhanced by investigating the histogram and cumulative distribution of terminal voltage estimation error for sixteen different discharging protocols and sixteen constant current charging protocols.

The second part of this chapter describes the real-time implementation of the proposed modified APE strategy on a 400 V, 6.6 Ah Li-ion battery bank, which powers an indirect field-oriented control based EV traction system. The validation of real-time estimated parameters against the offline experimentations shows the suitability of the proposed modified APE strategy for real-time parameters estimation of a Li-ion battery either at pack level or bank level.

4.1. Experimental Validation on a 22.2 V, 6.6 Ah Lithium-Polymer Battery

The results of modified APE strategy are compared in offline mode with the existing and experimentally verified APE technique. A fully charged 22.2 V, 6.6Ah TP6600 6S, 25C Lipo battery is connected with a resistive load of 50 ohms, which allows a small discharging current of about 0.4 amps. Note that a small discharging current ensures the convergence of estimated equivalent circuit elements to their actual values, as per mathematical proof provided in section 3.3. It took about 15 hours to discharge the battery upto 7% of its rated capacity. The voltage and current data during Lipo battery discharging is recorded via voltage and current sensors, respectively. The discharging current and voltage profiles of the above 22.2 V, 6.6 Ah Lipo battery are shown in Figure 4.1.

Algorithm 2 i.e. the proposed modified APE strategy is run in MATLAB with all the conditions, provided in section 3.3, to estimate the parameters of a 22.2 V, 66 Ah Lipo battery. The sampling time of the discharging voltage and current is set to 0.01

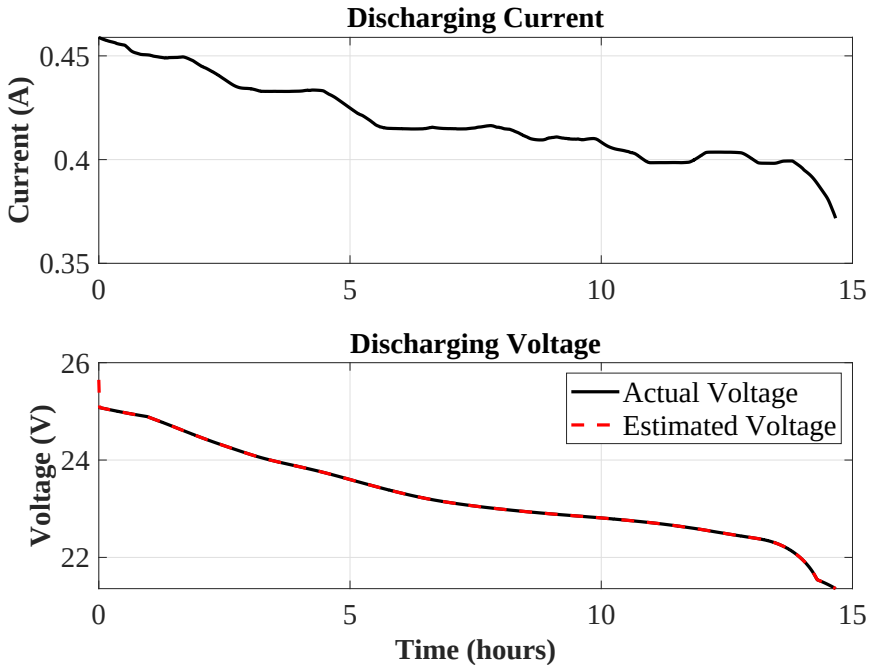

Figure 4.1: Lithium-Polymer battery discharging current and voltage profiles during adaptation process.

seconds. Once the terminal voltage estimation error goes below the user defined error bound, battery parameters is recorded separately in 21 separate arrays. The average value of each individual array represents the estimated battery parameter value, i.e. $\widehat{r}_1, \cdots, \widehat{r}_{21}$, at the end of the estimation process.

Note that the battery parameters of interest to this work are constants independent of SoC, and they control the shape of the terminal voltage vs time curve. The results of estimated parameters obtained from the modified APE strategy are provided in Table 4.1, and are compared with the results of the existing APE technique shared in [2]. Note that in Table 4.1, certain values related to parameters $\widehat{r}_3$ and $\widehat{r}_{21}$ are shown by dashes. This is because $\widehat{r}_3$ and $\widehat{r}_{21}$ disappear from the observer equations used in the modified APE strategy. So, parameters $\widehat{r}_3$ and $\widehat{r}_{21}$ are not estimated adaptively, but are estimated using equations (67)-(68). Also, the aim of modifying the existing APE strategy is to reduce the experimental effort required as in [2] for offline open circuit voltage and series resistance estimation, without compromising the accuracy of the existing APE technique for parameters estimation of a Li-ion battery. Next, the results of modified APE strategy are comprehensively compared with the existing APE technique against sixteen different discharging load protocols and sixteen constant charging pro-

Table 4.1: Experimental results of a 22 V, 6.6 Ah Li-ion battery model parameters.

Parameter	Upper bound (r_{nu})	Lower bound (r_{nl})	λ_{x_n}	λ_{y_n}	Initial value	Estimated value	Estimated value provided in [2]	Estimation error (%)
$\widehat{r}_1$	6	4	50	50	100	5	5.112	2.19
$\widehat{r}_2$	50	30	50	50	2000	40	40.955	2.33
$\widehat{r}_3$	–	–	–	–	–	22.1782	22.195	0.07
$\widehat{r}_4$	3	1	50	50	50	2	1.9215	4.08
$\widehat{r}_5$	2.5	1	50	50	30	1.75	1.759	0.51
$\widehat{r}_6$	4	2	50	50	200	3	3.0435	1.43
$\widehat{r}_7$	1	0.1	50	50	180	0.5505	0.5505	0
$\widehat{r}_8$	50	10	50	50	1700	30	30.0475	0.16
$\widehat{r}_9$	0.1	0.01	50	50	240	0.055	0.0551	0.18
$\widehat{r}_{10}$	10	1	70	50	3600	6.2557	6.2585	0.04
$\widehat{r}_{11}$	50	10	50	50	9300	30	30	0
$\widehat{r}_{12}$	0.1	0.01	50	50	264	0.0555	0.0551	0.73
$\widehat{r}_{13}$	1000	500	60	55	50000	760.8691	760.2266	0.08
$\widehat{r}_{14}$	15	5	70	50	1000	10.8334	10.7686	0.60
$\widehat{r}_{15}$	800	500	80	50	50000	684.615	685.7457	0.16
$\widehat{r}_{16}$	7000	5000	10	10	50000	6000	6036.4	0.60
$\widehat{r}_{17}$	50	5	50	50	1000	27.5	27.5422	0.15
$\widehat{r}_{18}$	5000	3000	10	20	50000	3667	3696	0.78
$\widehat{r}_{19}$	0.1	0.01	50	50	60	0.0551	0.0439	25.5
$\widehat{r}_{20}$	70	50	50	50	1200	60	59.07	1.57
$\widehat{r}_{21}$	–	–	–	–	–	0.2408	0.2246	7.21

tocols. The detailed description of discharging load protocols are given in section 4 of chapter 2.

4.1.1. Estimated parameters accuracy assessment via battery dischraging tests. The estimated terminal voltage is recorded by subjecting the estimated Li-ion battery model to sixteen different discharging load profiles successively. As a sample, the estimated and measured terminal voltages along with the absolute voltage estimation error for two of the sixteen discharging load profiles are shown in Figure 4.2 and Figure 4.3. The voltage estimation error in Figure 4.2 and Figure 4.3 shows that the modified APE strategy produces similar results compared to APE technique. The terminal voltage estimation error data, for all sixteen discharging profiles, is stacked together to form a single large error array of 2.75e7 samples. The statistical analysis of terminal voltage estimation error array is performed to quantify the accuracy of modified APE strategy against the existing APE technique. The mean, median, mode, and standard deviation analysis of the error array for modified APE and existing APE strategies are provided

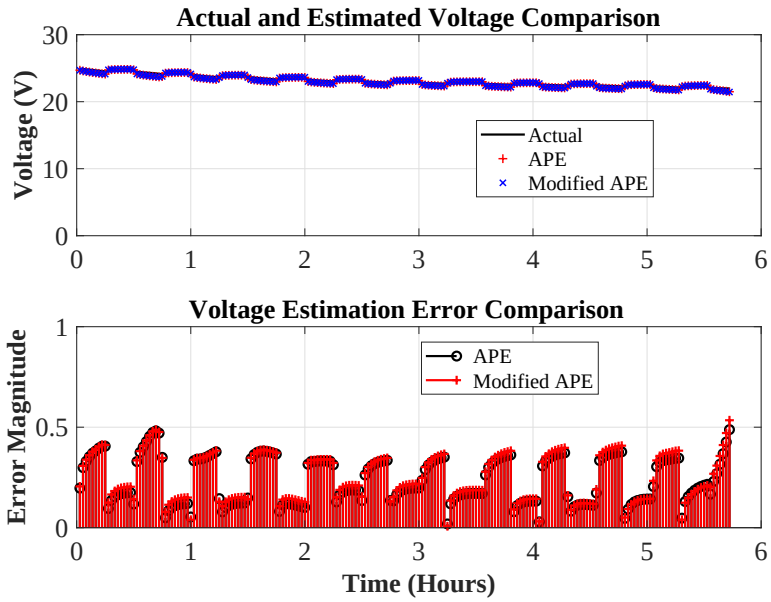

Figure 4.2: Terminal voltage estimation and absolute error $|e(t)|$ comparison for resistive load of 11.11 Ω with 15 minutes ON and 15 minutes OFF times.

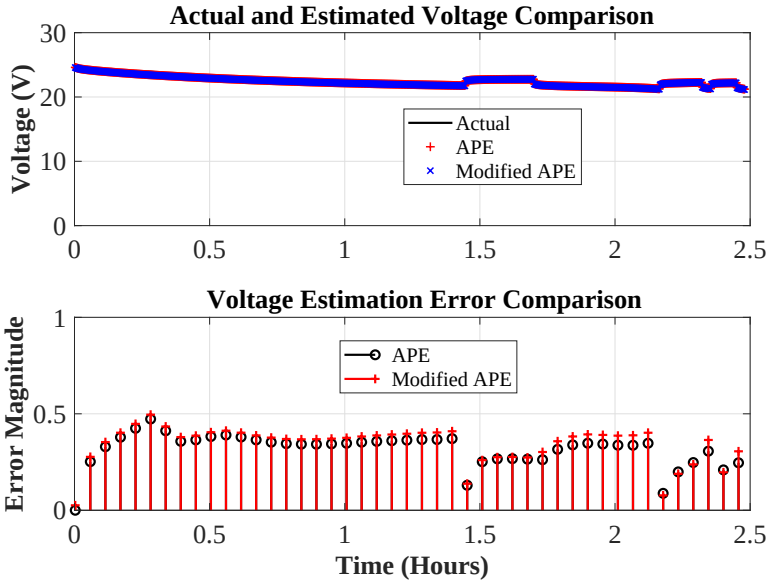

Figure 4.3: Terminal voltage estimation and absolute error $|e(t)|$ comparison for resistive load of 7.5 Ω with random time period.

in Table 4.2. The mean and standard deviation values for both techniques of interest are very similar, while the median and mode values of modified APE strategy slightly deviate from that of existing APE technique.

An extensive investigation of the overall terminal voltage estimation error array is carried out by further showing its histogram and cumulative distribution graphs

Table 4.2: Terminal voltage estimation error statistics while discharging the battery with sixteen different load profiles for APE and modified APE.

Parameters estimation methods	Mean of error (V)	Median of error (V)	Mode of error (V)	Standard deviation of error (V)
APE	0.0211	0.027	-0.4038	0.5026
Modified APE	0.0218	0.0143	-0.347	0.5139

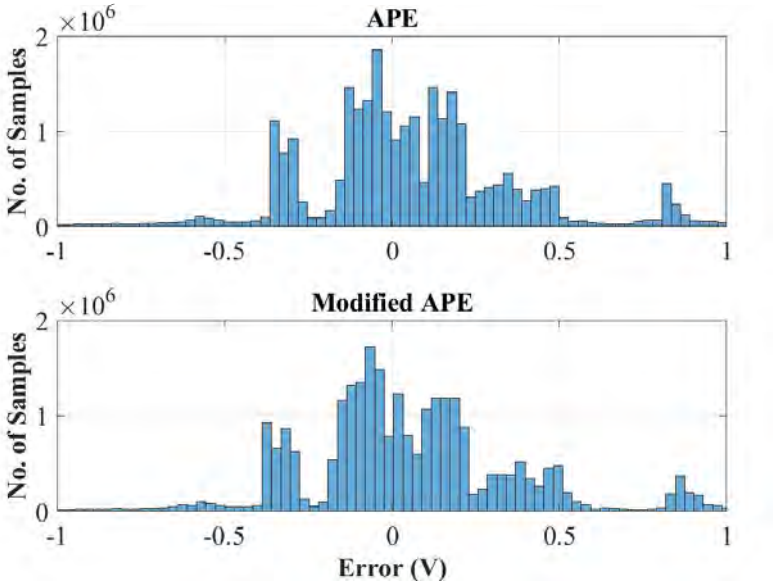

Figure 4.4: Histogram of terminal voltage estimation error for APE and modified APE under sixteen different discharging profiles.

in Figure 4.4 and Figure 4.5 respectively. Where, the red vertical lines in Figure 4.5 indicate the $\pm$ 4.5% terminal voltage estimation error limits, i.e. $\pm$ 1 V. Figure 4.4 and Figure 4.5 show no significant deviation of modified APE results compared to the existing APE technique. As mentioned in chapter 2, the accuracy of modified APE and existing APE strategies can be further enhanced by subsequent incorporation of optimization strategies.

4.1.2. Estimated parameters accuracy assessment via battery charging tests.

The estimated parameters obtained from modified APE strategy are further assessed against the results of existing APE technique over sixteen constant current charging protocols. The actual Lipo battery is charged with a constant current of 2.5 amperes using the Thunder-Power charger (TP820CD). As a sample, the estimated and measured

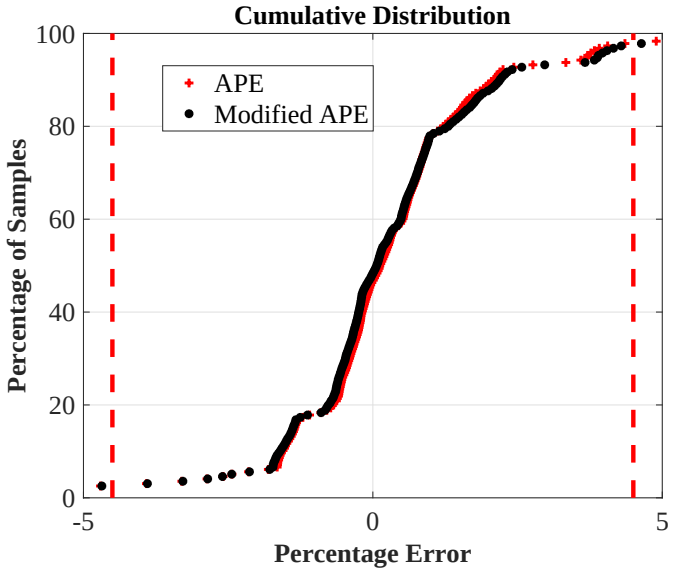

Figure 4.5: Cumulative distribution of terminal voltage estimation error for APE and modified APE under sixteen different discharging profiles.

terminal voltages along with the absolute voltage estimation error for a single test is shown in Figure 4.6. The statistical analysis, similar to discharging load protocols, is performed to compare the terminal voltage estimation errors of both the modified and existing APE strategies. The total number of samples collected in terminal voltage estimation array while charging the batteries are 1.258e7. The histogram and cumulative

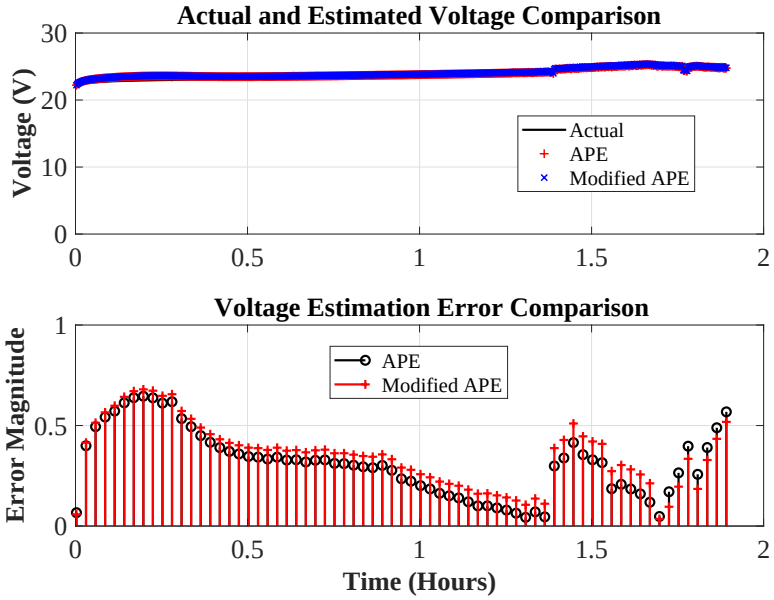

Figure 4.6: Terminal voltage estimation and absolute error $|e(t)|$ comparison while charging the 22.2 V, 6.6 Ah Li-Polymer battery.

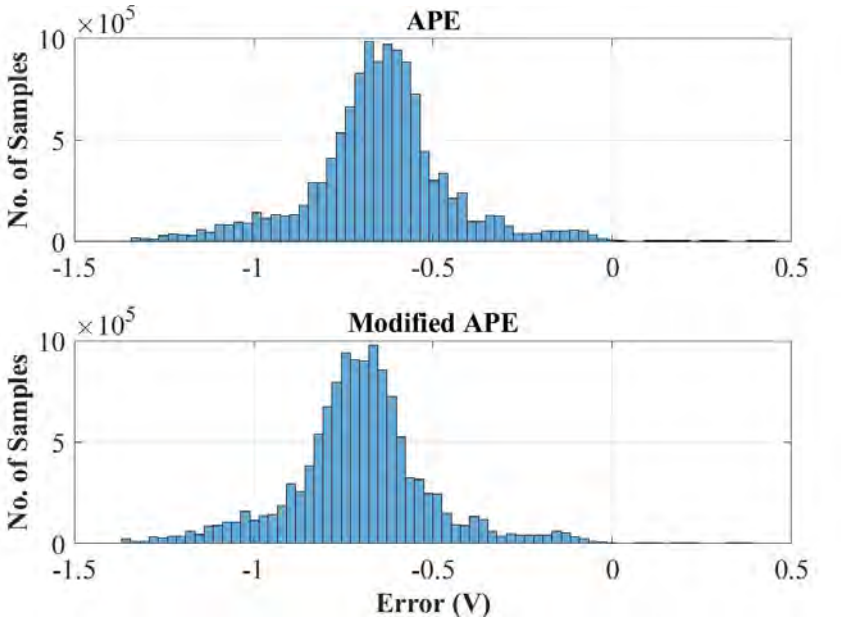

Figure 4.7: Histogram of terminal voltage estimation error for APE and modified APE techniques while charging sixteen individual batteries with a constant 2.5 A current.

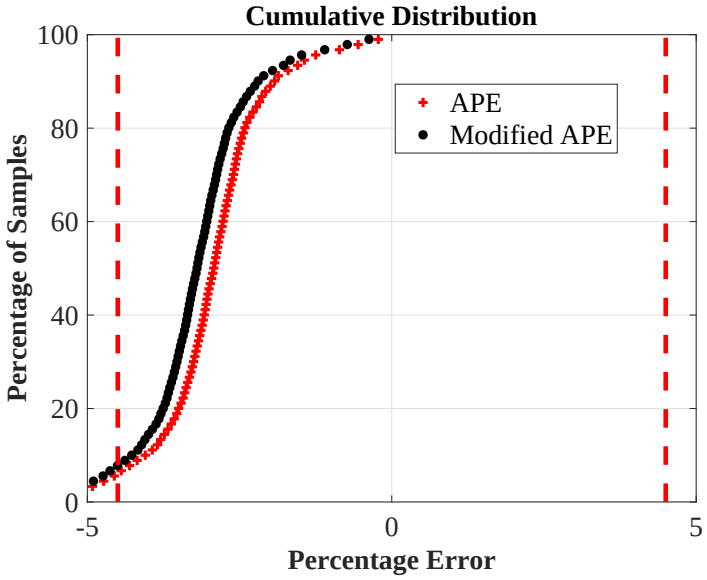

Figure 4.8: Cumulative distribution of terminal voltage estimation error for APE and modified APE techniques while charging sixteen individual batteries with a constant 2.5 A current.

distribution graphs of terminal voltage estimation error are shown Figure 4.7 and Figure 4.8, respectively, for both the existing and modified APE strategies. Moreover, the statistical analysis of terminal voltage estimation error is provided in Table 4.3. The statistical analysis along with histogram and cumulative distribution graphs show that

Table 4.3: Terminal voltage estimation error statistics while charging sixteen different batteries with a constant 2.5 Amperes for APE and modified APE.

Parameters estimation Methods	Mean of error (V)	Median of error (V)	Mode of error (V)	Standard deviation of error (V)
APE	-0.6518	-0.6451	-2.1223	0.2271
Modified APE	-0.7080	-0.7059	-2.1470	0.2231

the modified APE strategy produces results similar to APE technique while charging a Lipo battery.

In the next section, the modified APE strategy is employed for real-time parameters estimation of a 400 V, 6.6 Ah, Li-ion battery bank. The Li-ion battery bank is utilized to power an indirect field-oriented control based electric vehicle (EV) traction system. The real-time estimated parameters are also validated against the offline results on a 400 V, 6.6 Ah Li-ion battery bank.

4.2. Real-time Parameters Estimation of a 400 V, 6.6 Ah Lithium-Polymer Battery Bank

In this section, the modified APE strategy is implemented and validated on a 400 V, 6.6 Ah Lithium-Polymer battery bank for electric vehicle (EV) traction system, which is controlled by indirect field-oriented strategy. The picture of a complete prototype EV traction testbench is shown in Figure 4.9. Starting from the right side, a 400 V, 6.6 Ah Li-ion battery bank is connected to a three-phase IGBT inverter. The induction motor (IM) is powered and controlled by the three-phase inverter and the dynamometer is employed to load the prototype EV traction system. The computer system on the left side allows the control and real-time monitoring of the EV traction testbench. The dSPACE 1103 control board is responsible for performing several real-time tasks such as control of three-phase PWM inverter, voltage and current measurements of Li-ion battery bank and IM, implementation of indirect FOC algorithm for IM drive and modified APE strategy for real-time parameters estimation of Li-ion battery bank. Due to accurate and high-speed Input/Output operation, dSPACE real-time processor board has become a primary choice for prototype automotive and drive applications. The detailed specifications of the prototype EV traction testbench are provided in Table 4.4.

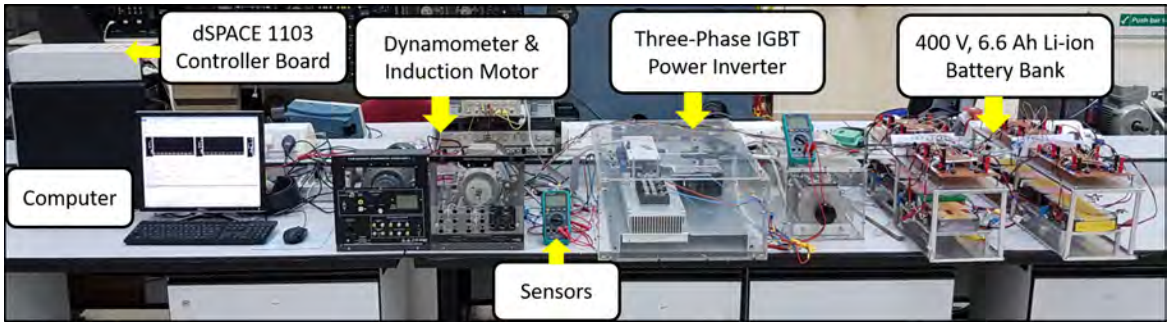

Figure 4.9: Li-ion battery bank powered EV traction system.

Table 4.4: Prototype EV traction system specifications.

Induction motor parameters	
Nominal voltage	400 V-Y, 50 Hz
Nominal current	1.37 A
Nominal power	0.55 kW
Nominal efficiency	78.1%
Nominal power Factor	0.74
Nominal speed	1440 RPM
Nominal torque	3.65 Nm
Poles pairs	2
Stator resistance (R_s)	17.36 Ω
Rotor resistance (R_r)	6.3 Ω
Stator inductance (L_{ls})	0.12185 H
Rotor inductance (L_{lr})	0.03614 H
Mutual inductance (L_m)	0.87097 H
Drive system specifications	
Inverter rating	500 V, 10 A
Controller board	dSPACE 1103
Sampling time	0.1 ms
Encoder resolution	1024 pulses per revolution
Voltage sensor	(LEM LV-25 P) 500 V
Current sensor	(LEM LA-25 NP) 25 A
Li-Ion battery bank specifications	
Battery model (Lithium-Polymer)	TP6600-6SP+25
Number of batteries	16
Battery bank capacity	6.6 Ah
Nominal voltage of each battery	22.2 V
Maximum voltage of each battery	25.2 V
Maximum battery bank voltage	403.2 V
Maximum charging current of each battery	33 A

4.2.1. Experimental estimation of battery bank parameters. The real-time adaptive parameters estimation of a 400 V, 6.6 Ah Li-ion battery bank is performed by executing algorithm 2 with all the required conditions described in section 3.2. The Li-ion battery bank powers an indirect field-orientation based EV traction system. The no-load operation of an induction motor in EV traction system draws around 0.2 amperes current and, thus, satisfies one of the essential conditions, i.e. the low discharge current requirement, of UAS based parameters estimation method. The estimated parameters at no-load operation of an induction motor in EV traction system are presented in Table 4.5. Note that in Table 4.5, certain values related to parameters $\widehat{r}_3$ and $\widehat{r}_{21}$ are shown by dashes. This is because $\widehat{r}_3$ and $\widehat{r}_{21}$ disappear from the observer equations used in the modified APE strategy. So, parameters $\widehat{r}_3$ and $\widehat{r}_{21}$ are not estimated adaptively, but are estimated using equations (67)-(68). The battery parameters estimated at no-load condition can be employed for SoC and SoH estimation, open circuit voltage and series resistance estimation, and fault detection in a battery management system during any loading condition of EV traction system.

4.2.2. Accuracy assessment of estimated parameters via battery bank discharging test. The effectiveness of modified APE strategy is further quantified by

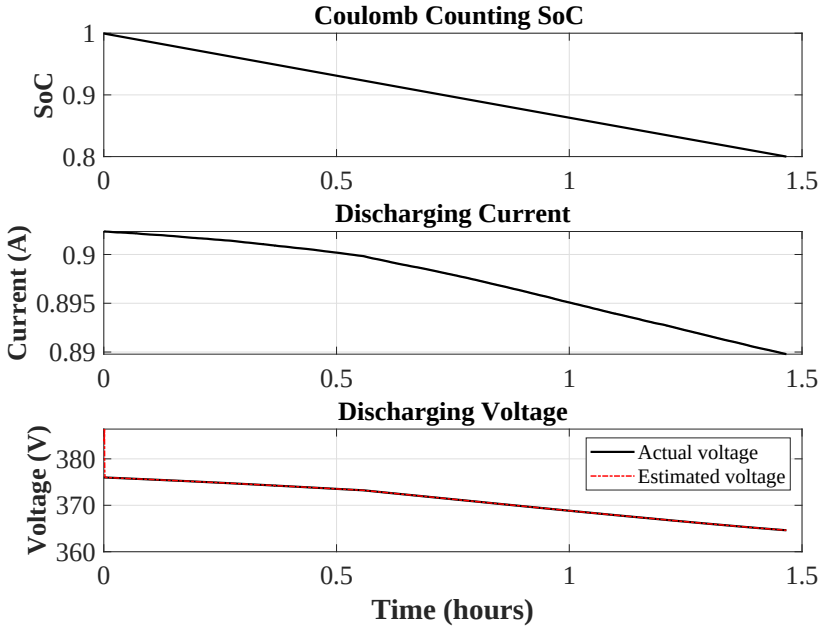

Figure 4.10: Lithium-Polymer battery bank discharging SoC, current, and voltage profiles during adaptation process.

investigating the estimated parameters obtained through offline experimentation. For that purpose, the 400 V, 6.6 Ah Li-ion battery bank is discharged through a 384 ohms, 600 W resistive load. The battery bank discharge current and voltage profiles along with the estimated terminal voltage during the adaptation process are shown in Figure 4.10. The detailed procedure of modified APE strategy has been described in Section 3.2, and the results of estimated battery bank parameters are given in Table 4.5. The real-time estimated parameters of a 400 V, 6.6 Ah Li-ion battery bank model are quantified against the parameters obtained through offline mode. The estimation error in Table 4.5 shows the accuracy of real-time parameters. The accuracy of offline estimated parameters is assessed by analyzing the estimated terminal voltage against an offline and fast periodic measured discharging voltage profile at 230 ohms, 1000 W load. The time period of discharging profile is two minutes with 50% duty cycle. The measured and estimated terminal voltage along with the estimation error are illustrated in Figure 4.11. The terminal voltage estimation error in Figure 4.11 is around 1% which signifies the potential of modified APE strategy.

Table 4.5: Experimental results of a 400 V, 6.6 Ah Li-ion battery bank model parameters.

Parameter	Upper bound (r_{nu})	Lower bound (r_{nl})	λ_{x_n}	λ_{y_n}	Initial value	Estimated value (Real-time)	Estimated value (Offline)	Estimation error (%)
$\widehat{r}_1$	150	45	50	50	100	97.5	97.51	0.01
$\widehat{r}_2$	50	20	50	50	2000	35	35.01	0.03
$\widehat{r}_3$	–	–	–	–	–	356.865	357.236	0.1
$\widehat{r}_4$	7.5	1.5	50	50	100	4.5	5.2	13.4
$\widehat{r}_5$	20	2	50	50	230	11	11.01	0.1
$\widehat{r}_6$	50	25	50	50	400	37.5	37.55	0.13
$\widehat{r}_7$	1	0.1	50	50	180	0.6125	0.5643	8.54
$\widehat{r}_8$	50	10	50	50	1700	30	30.01	0.03
$\widehat{r}_9$	0.1	0.01	50	50	240	0.0568	0.069	17.68
$\widehat{r}_{10}$	10	1	70	50	3600	6.4074	6.262	2.32
$\widehat{r}_{11}$	200	100	50	50	9300	150	150	0
$\widehat{r}_{12}$	0.1	0.01	50	50	264	0.0694	0.0693	0.14
$\widehat{r}_{13}$	1000	500	60	55	50000	760.8586	760.882	0.003
$\widehat{r}_{14}$	15	5	70	50	1000	10.8367	10.845	0.07
$\widehat{r}_{15}$	800	500	80	50	50000	684.6064	684.626	0.16
$\widehat{r}_{16}$	7000	5000	10	10	50000	5998.5	6000	0.025
$\widehat{r}_{17}$	50	5	50	50	1000	27.507	27.514	0.025
$\widehat{r}_{18}$	5000	3000	10	20	50000	3666	3666.71	0.02
$\widehat{r}_{19}$	25	5	50	50	100	15	15.014	0.1
$\widehat{r}_{20}$	40	15	50	50	1200	27.505	27.514	0.033
$\widehat{r}_{21}$	–	–	–	–	–	5.01	5.428	7.7

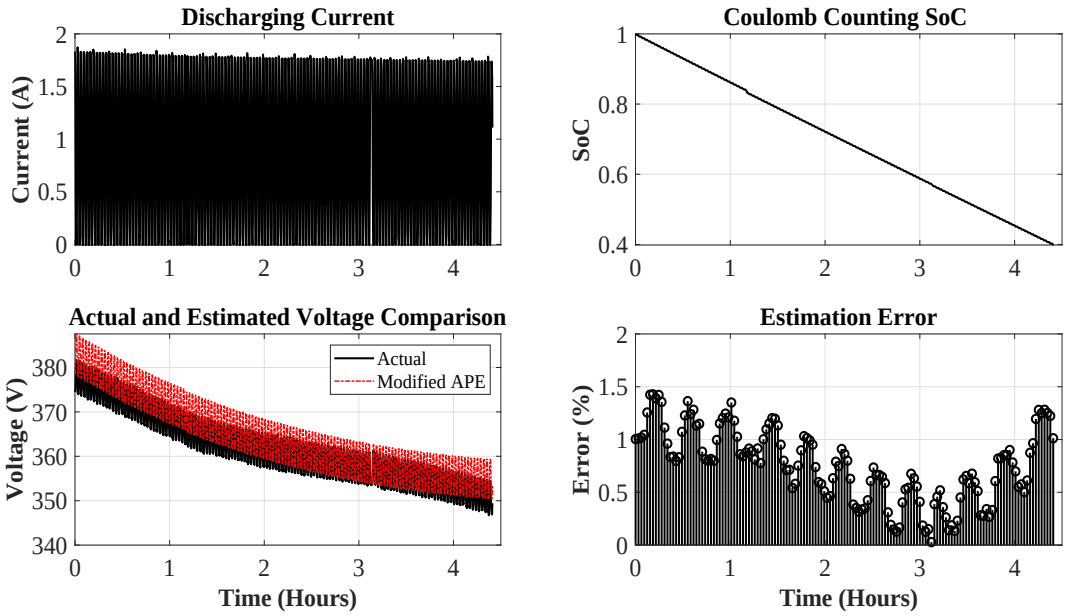

Figure 4.11: Terminal voltage estimation and absolute error $|e(t)|$ comparison for resistive load of 230 ohms, 1000 W, with 1 minutes ON and 1 minute OFF times.

The statistical analysis of terminal voltage estimation error is performed, and the details have been shared in Section 2.3 and Section 4.1. Note that the total number of samples collected in the estimation error array during the discharging test are 73,529. The mean, median, mode, and standard deviation analysis of the error array for modified APE are provided in Table 4.6. Moreover, the histogram and cumulative distribution

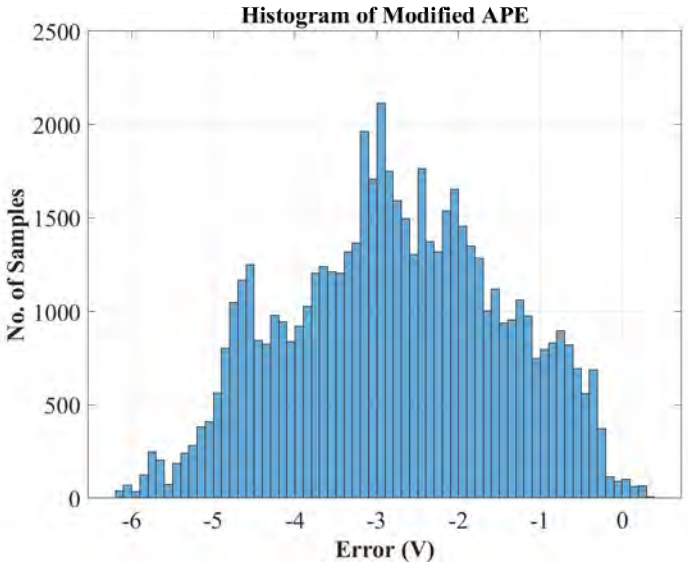

Figure 4.12: Histogram of terminal voltage estimation error for modified APE under Figure 4.11 battery bank discharge profile.

Table 4.6: Terminal voltage estimation error statistics under Figure 4.11 battery bank discharge profile.

Parameters Estimation Methods	Mean of error (V)	Median of error (V)	Mode of error (V)	Standard deviation of error (V)
Modified APE	-2.7754	-2.7828	-6.1766	1.3199

graphs of terminal voltage estimation error are shown Figure 4.12 and Figure 4.13, respectively. The red vertical lines in Figure 4.13 indicate the $\pm$ 1.5% terminal voltage estimation error i.e. $\pm$ 6 V. The statistical analysis of terminal voltage estimation error shows the effectiveness of modified APE strategy for real-time parameters estimation of EV traction system.

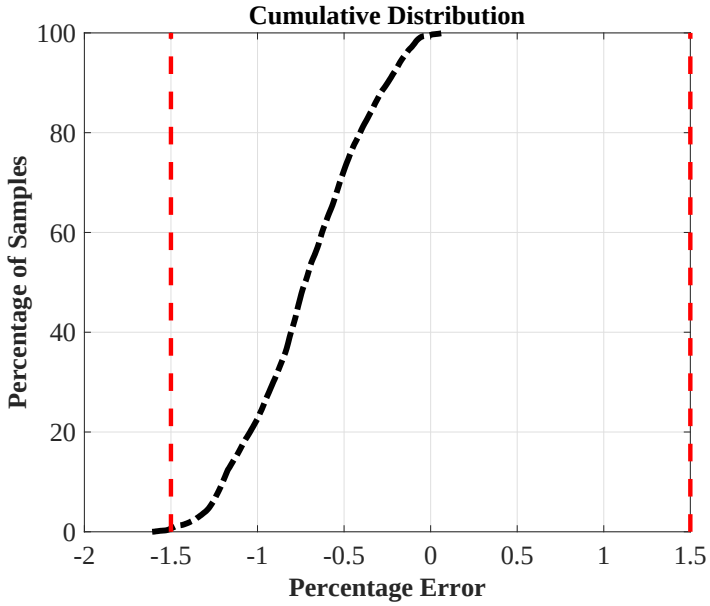

Figure 4.13: Cumulative distribution of terminal voltage estimation error for modified APE under Figure 4.11 battery bank discharge profile.

Chapter 5. Conclusions and Future Work

5.1. Conclusions

This thesis work is divided into three parts: accurate estimation of battery model parameters, reduction of experimental effort for battery parameters identification by proposing modified adaptive parameters estimation strategy, and real-time implementation of proposed parameters estimation strategy on a 400 V, 6.6 Ah Li-ion battery bank powered EV traction system.

The first part of this thesis demonstrated the effectiveness of our proposed two-stage technique for accurate estimation of Li-ion battery parameters. The parameters obtained from the first stage, i.e. adaptive parameters estimation (APE), are utilized to narrow the search space intervals for the second stage, i.e. optimization, for further refinement of the initially estimated parameters values. The narrowed search space interval when used with an optimization routine, requires less computation time, compared to an unguided or arbitrarily initialized optimization routine. The simulation study compares the estimated parameters and circuit elements values, with the results available in the literature. In the experimental study, the effectiveness of the proposed technique is evaluated by comparing the estimated and the actual voltage measured across the battery terminals, and by further performing a statistical analysis. The results show that the accuracy of the battery model parameters obtained by the optimization techniques alone is poor, and the required computation time is high. The accuracy of parameters obtained by UAS-based APE is good with very low computation time, while it is best when UAS based APE is used in combination with the PSO, or hybrid PSO optimization techniques while requiring an intermediate amount of computation time.

The existing APE strategy requires prior offline experimentation for open voltage estimation, and some post-processing for series resistance estimation. Therefore, the second part of this thesis proposes the modified APE strategy which estimates the open circuit voltage and series resistance along with the other circuit elements in a single adaptation run. Numerical simulations are performed on a 4.1 V, 270 mAh Li-ion battery model to quantify the accuracy of estimated parameters by comparing them

against well-known results obtained experimentally by Chen and Mora. The terminal voltage estimation error is less than 1%, which illustrates the effectiveness of the proposed modified APE strategy. Moreover, mathematical proofs are provided to support the modified APE strategy.

The third part of this thesis deals with the rigorous experimental validation of modified APE strategy and real-time implementation on a 400 V, 6.6 Ah Li-ion battery bank powered EV traction system. First, the results of modified APE strategy are compared with the existing APE technique and with the measured terminal voltage across 22.2 V, 6.6 Ah Li-ion battery. A comprehensive statistical analysis of terminal voltage estimation error is presented for sixteen different discharging and sixteen constant charging protocols. It can be inferred from the results that the modified APE strategy produces similar results compared to the existing APE strategy while minimizing the experimental effort and parameters estimation process time required by the existing APE scheme. The existing APE strategy requires eight experiments to estimate all battery model parameters. However, the proposed modified APE scheme needs just two experiments to be performed, i.e. one for open circuit voltage measurement before the adaptation process and one adaptive estimation experiment for battery model parameters. Second, the modified APE strategy is implemented for real-time parameters estimation of a 400 V, 6.6 Ah Li-ion battery bank, which powers a field-orientation controlled EV traction system. The real-time results are validated against an offline and fast periodic discharging battery bank voltage profile. The terminal voltage estimation error is around 1%, which shows the accuracy of the proposed modified APE strategy for real-time battery bank parameters estimation of EV traction systems.

5.2. Future Work

The modified APE strategy can be utilized for quick and accurate battery parameters estimation with minimal experimental effort and may be employed for numerous applications of a battery bank powered EV traction system. Some future directions related to battery parameters estimation work, especially for EV traction system, are as follows:

- An accurate Li-ion battery bank model can be used to develop an effective battery management system that optimizes the charging and discharging of a Li-ion battery to reduce the degradation of battery state-of-health (SoH).
- The operation of a Li-ion battery bank at higher temperature may deteriorate the battery capacity and thus causes inaccurate estimation of SoC and SoH. This event may degrade the overall performance of an EV traction system. Therefore, future efforts also include the incorporation of temperature effects in the adaptive parameters estimation process.
- Several control strategies are available in the literature for speed/torque control of an induction motor driven EV traction system, such as direct/indirect field orientation, direct torque control, model predictive control, model reference adaptive control, sliding mode control, to name a few. However, accurate SoC and SoH information may also be incorporated in the above control strategies for optimum EV performance in terms of EV drive time, Li-ion battery bank depth of discharge, and maximum allowed EV speed.

References

[1] M. A. Hannan, M. M. Hoque, A. Hussain, Y. Yusof, and P. J. Ker, "State-of-the-art and energy management system of Lithium-ion batteries in electric vehicle applications: Issues and recommendations," *IEEE Access*, vol. 6, pp. 19 362–19 378, 2018.

[2] D. Ali, S. Mukhopadhyay, H. Rehman, and A. Khurram, "UAS based Li-ion battery model parameters estimation," *Control Engineering Practice*, vol. 66, pp. 126–145, Sep 2017.

[3] H. M. Usman, S. Mukhopadhyay, and H. Rehman, "Universal adaptive stabilizer based optimization for Li-ion battery model parameters estimation: An experimental study," *IEEE Access*, vol. 6, pp. 49 546–49 562, 2018.

[4] L. Lu, X. Han, J. Li, J. Hua, and M. Ouyang, "A review on the key issues for Lithium-ion battery management in electric vehicles," *Journal of power sources*, vol. 226, pp. 272–288, 2013.

[5] R. Xiong, J. Cao, Q. Yu, H. He, and F. Sun, "Critical review on the battery state of charge estimation methods for electric vehicles," *IEEE Access*, vol. 6, pp. 1832–1843, 2018.

[6] S. Mukhopadhyay and F. Zhang, "A High-Gain Adaptive Observer for Detecting Li-ion Battery Terminal Voltage Collapse," *Automatica*, vol. 50, no. 3, pp. 896–902, Mar 2014.

[7] L. Liu, L. Y. Wang, Z. Chen, C. Wang, F. Lin, and H. Wang, "Integrated system identification and state-of-charge estimation of battery systems," *IEEE Transactions on Energy conversion*, vol. 28, no. 1, pp. 12–23, 2013.

[8] M. Hannan, M. Lipu, A. Hussain, and A. Mohamed, "A review of Lithium-ion battery state of charge estimation and management system in electric vehicle applications: Challenges and recommendations," *Renewable and Sustainable Energy Reviews*, vol. 78, pp. 834–854, Oct 2017.

[9] X. Chen, W. Shen, M. Dai, Z. Cao, J. Jin, and A. Kapoor, "Robust adaptive sliding-mode observer using RBF neural network for lithium-ion battery state of charge estimation in electric vehicles," *IEEE Transactions on Vehicular Technology*, vol. 65, no. 4, pp. 1936–1947, 2016.

[10] J. Yang, B. Xia, Y. Shang, W. Huang, and C. C. Mi, "Adaptive state-of-charge estimation based on a split battery model for electric vehicle applications," *IEEE Transactions on Vehicular Technology*, vol. 66, no. 12, pp. 10 889–10 898, 2017.

[11] S. Tang, Y. Wang, Z. Sahinoglu, T. Wada, S. Hara, and M. Krstic, "State-of-charge estimation for Lithium-ion batteries via a coupled thermal-electrochemical model," in *American Control Conference (ACC)*, Chicago, IL, USA, 2015, pp. 5871–5877.

[12] D. A. Pola, H. F. Navarrete, M. E. Orchard, R. S. Rabie, M. A. Cerda, B. E. Olivares, J. F. Silva, P. A. Espinoza, and A. Perez, "Particle-Filtering-Based Discharge Time Prognosis for Lithium-ion Batteries With a Statistical Characterization of Use Profiles," *IEEE Transactions on Reliability*, vol. 64, no. 2, pp. 710–720, Jun 2015.

[13] M. Chen and G. Rincon-Mora, "Accurate Electrical Battery Model Capable of Predicting Runtime and I-V Performance," *IEEE Transactions on Energy Conversion*, vol. 21, no. 2, pp. 504–511, Jun 2006.

[14] W.-J. Shen and H.-X. Li, "A sensitivity-based group-wise parameter identification algorithm for the electric model of Li-ion battery," *IEEE Access*, vol. 5, pp. 4377–4387, 2017.

[15] Y. Wang and L. Li, "Li-ion battery dynamics model parameter estimation using datasheets and particle swarm optimization," *International Journal of Energy Research*, vol. 40, no. 8, pp. 1050–1061, 2016.

[16] C. S. Huang, T. W.-S. Chow, and M.-Y. Chow, "Li-ion battery parameter identification with low pass filter for measurement noise rejection," in *26th IEEE International Symposium on Industrial Electronics (ISIE)*, Edinburgh, UK, 2017, pp. 2075–2080.

[17] D. Dvorak, T. Bäuml, A. Holzinger, and H. Popp, "A comprehensive algorithm for estimating Lithium-ion battery parameters from measurements," *IEEE Transactions on Sustainable Energy*, vol. 9, no. 2, pp. 771–779, 2018.

[18] K. Mueller, E. Schwiederik, and D. Tittel, "Analysis of parameter identification methods for electrical Li-ion battery modelling," in *World Electric Vehicle Symposium and Exhibition (EVS27)*, Barcelona, Spain, Nov 2013, pp. 1–9.

[19] P. Kumar and P. Bauer, "Parameter extraction of battery models using multiobjective optimization genetic algorithms," in *14th IEEE International Power Electronics and Motion Control Conference (EPE/PEMC)*, Ohrid, Macedonia, 2010, pp. 106–110.

[20] D. Kapoor, P. Sodhi, and A. Keyhani, "Estimation of parameters for battery storage models," in *IEEE Conference on Energy Conversion (CENCON)*, Johor Bahru, Malaysia, Oct 2014, pp. 406–411.

[21] J. C. Forman, S. J. Moura, J. L. Stein, and H. K. Fathy, "Genetic identification and fisher identifiability analysis of the Doyle–Fuller–Newman model from experimental cycling of a $LiFePO_4$ cell," *Journal of Power Sources*, vol. 210, pp. 263–275, 2012.

[22] Z. Yu, L. Xiao, H. Li, X. Zhu, and R. Huai, "Model Parameter Identification for Lithium Batteries Using the Coevolutionary Particle Swarm Optimization Method," *IEEE Transactions on Industrial Electronics*, vol. 64, no. 7, pp. 5690–5700, Jul 2017.

[23] M. A. Rahman, S. Anwar, and A. Izadian, "Electrochemical model parameter identification of a Lithium-ion battery using particle swarm optimization method," *Journal of Power Sources*, vol. 307, pp. 86–97, 2016.

[24] M. Clerc and J. Kennedy, "The particle swarm-explosion, stability, and convergence in a multidimensional complex space," *IEEE transactions on Evolutionary Computation*, vol. 6, no. 1, pp. 58–73, 2002.

[25] N. Omar, D. Widanage, M. Abdel Monem, Y. Firouz, O. Hegazy, P. Van den Bossche, T. Coosemans, and J. Van Mierlo, "Optimization of an advanced battery model parameter minimization tool and development of a novel electrical model for Lithium-ion batteries," *International Transactions on Electrical Energy Systems*, no. 12, pp. 1747–1767, Dec 2014.

[26] G. Giordano, V. Klass, M. Behm, G. Lindbergh, and J. Sjöberg, "Model-based Lithium-ion battery resistance estimation from electric vehicle operating data," *IEEE Transactions on Vehicular Technology*, vol. 67, no. 5, pp. 3720–3728, 2018.

[27] Q. Wang, J. Kang, Z. Tan, and M. Luo, "An online method to simultaneously identify the parameters and estimate states for Lithium ion batteries," *Electrochimica Acta*, vol. 289, pp. 376–388, 2018.

[28] L. Zhao, Z. Liu, and G. Ji, "Lithium-ion battery state of charge estimation with model parameters adaptation using H_∞ extended Kalman filter," *Control Engineering Practice*, vol. 81, pp. 114–128, 2018.

[29] M. Hu, Y. Li, S. Li, C. Fu, D. Qin, and Z. Li, "Lithium-ion battery modeling and parameter identification based on fractional theory," *Energy*, vol. 165, pp. 153–163, 2018.

[30] H. Rahimi-Eichi, F. Baronti, and M.-Y. Chow, "Online adaptive parameter identification and state-of-charge coestimation for Lithium-polymer battery cells," *IEEE Transactions on Industrial Electronics*, vol. 61, no. 4, pp. 2053–2061, 2014.

[31] A. Hentunen, T. Lehmuspelto, and J. Suomela, "Time-domain parameter extraction method for Thévenin-equivalent circuit battery models," *IEEE Transactions on Energy Conversion*, vol. 29, no. 3, pp. 558–566, 2014.

[32] F. Guo, G. Hu, and R. Hong, "A parameter adaptive method with dead zone for state of charge and parameter estimation of Lithium-ion batteries," *Journal of Power Sources*, vol. 402, pp. 174–182, 2018.

[33] J. Kennedy and R. Eberhart., "Particle Swarm Optimization," in *Proceedings of the IEEE International Conference on Neural Networks (ICNN)*, Perth, Australia, 1995, pp. 1942–1945.

[34] S. Mukhopadhyay and F. Zhang, "Adaptive detection of terminal voltage collapses for Li-ion batteries," in *51st IEEE Annual Conference on Decision and Control (CDC)*, Maui, HI, USA, 2012, pp. 4799–4804.

[35] D. Ali, S. Mukhopadhyay, and H. Rehman, "A novel adaptive technique for Li-ion battery model parameters estimation," in *IEEE National Aerospace and Electronics Conference (NAECON) and Ohio Innovation Summit (OIS)*, Dayton, OH, USA, 2016, pp. 23–26.

[36] "Mittag-Leffler Functions and Fractional Calculus," in *Special Functions for Applied Scientists*. New York, NY: Springer New York, 2008, pp. 79–134.

[37] S. Mukhopadhyay and F. Zhang, "A High-Gain Adaptive Observer for Detecting Li-ion Battery Terminal Voltage Collapse," *Automatica*, vol. 50, no. 3, pp. 896–902, Mar 2014.

[38] A. Ilchmann, *Non-identifier-based high-gain adaptive control*. Lecture Notes in Control and Information Sciences 189. Springer-Verlag, 1993.

[39] Shayok Mukhopadhyay, "Mittag-Leffler function, M-file, cmex DLL, and S-function - File Exchange - MATLAB Central," [online]. Availale: https://www.mathworks.com/matlabcentral/fileexchange/20731, last accessed on April 29, 2019.

[40] Y. Li and Y. Chen, "When is a Mittag–Leffler function a Nussbaum function?" *Automatica*, vol. 45, no. 8, pp. 1957–1959, 2009.

[41] "MATLAB *fmincon* Optimization Toolbox," [online]. Available: https://www.mathworks.com/help/optim/ug/fmincon.html, last accessed on April 29, 2019.

Vita

Hafiz M. Usman was born in Lahore, Pakistan. He received his B.Sc. in Electrical Engineering from the University of Engineering and Technology (U.E.T) Lahore, Pakistan, in 2016. Usman joined the master's program in Electrical Engineering at the American University of Sharjah (AUS), UAE, in 2017, where he worked as a graduate research assistant. During his M.Sc. studies at AUS, he published two journals papers including one in IEEE Access, and also published five conference papers. Usman has also served as a reviewer for IEEE and IET journals. His research interests include adaptive control systems, optimization, power electronics and electric drives.